AD-A190 962 PERFORMANCE AND LONG DURATION TEST OF A 30 KW THERMAL ARCJET ENGINE(U) JET PROPULSION LAB PASADENA CA T J PIVIROTTO ET AL. NOV 87 JPL-D-4643 AFAL-TR-87-010 1/2

UNCLASSIFIED F/G 21/3 NL

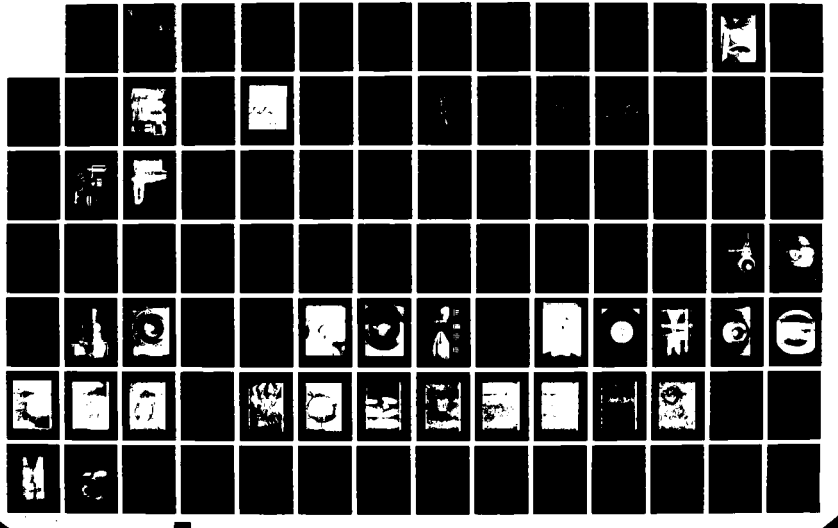

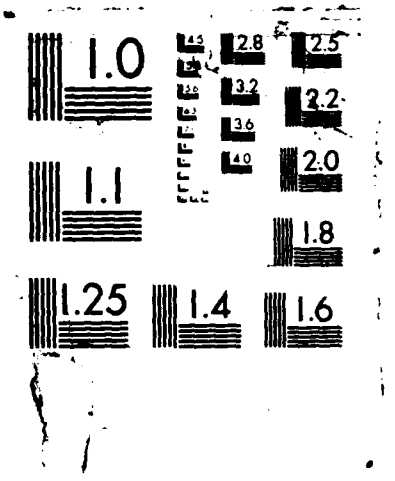
1.0
1.1
1.25
1.4
1.6
1.8
2.0
2.2
2.5
2.8
3.2
3.6
4.0
4.5

AD-A190 962

AFAL-TR-87-010

AD:

DTIC FILE COPY

Final Report
for the period
28 December 1984 to
30 November 1986

Performance and Long Duration Test of a 30 kw Thermal Arcjet Engine

SELECTED
JAN 25 1988
D

November 1987

Authors:
T. J. Pivirotto
D. Q. King
J. R. Brophy
W. D. Deininger

Jet Propulsion Laboratory
4800 Oak Grove Drive
Pasadena, CA 91109

JPL D-4643
RPL 60021

Approved for Public Release

Distribution is unlimited. The AFAL Technical Services Office has reviewed this report, and it is releasable to the National Technical Information Service, where it will be available to the general public, including foreign nationals.

This document has been approved for public release and sale; its distribution is unlimited.

Prepared for the: **Air Force Astronautics Laboratory**

Air Force Space Technology Center
Space Division, Air Force Systems Command
Edwards Air Force Base,
California 93523-5000

88 1 21 026

SECURITY CLASSIFICATION OF THIS PAGE

REPORT DOCUMENTATION PAGE

1a. REPORT SECURITY CLASSIFICATION UNCLASSIFIED	1b. RESTRICTIVE MARKINGS
2a. SECURITY CLASSIFICATION AUTHORITY	3. DISTRIBUTION/AVAILABILITY OF REPORT Approved for public release; distribution is unlimited.
2b. DECLASSIFICATION/DOWNGRADING SCHEDULE	
4. PERFORMING ORGANIZATION REPORT NUMBER(S) JPL D-4643	5. MONITORING ORGANIZATION REPORT NUMBER(S) AFAL-TR-87-010
6a. NAME OF PERFORMING ORGANIZATION Jet Propulsion Labratory 6b. OFFICE SYMBOL (If applicable)	7a. NAME OF MONITORING ORGANIZATION Air Force Astronautics Laboratory
6c. ADDRESS (City, State and ZIP Code) 4800 Oak Grove Drive Pasadena, CA 91109	7b. ADDRESS (City, State and ZIP Code) LKCJ Edwards AFB CA 93523-5000
8a. NAME OF FUNDING/SPONSORING ORGANIZATION Air Force Astronautics Laboratory 8b. OFFICE SYMBOL (If applicable) LKCJ	9. PROCUREMENT INSTRUMENT IDENTIFICATION NUMBER MIPR RPL 60021
8c. ADDRESS (City, State and ZIP Code) Edwards AFB CA 93523-5000	10. SOURCE OF FUNDING NOS. PROGRAM ELEMENT NO.: 62302F; PROJECT NO.: 3058; TASK NO.: 00; WORK UNIT NO.: IA
11. TITLE (Include Security Classification) Performance and Long Duration Test of a 30-kW thermal Arcjet Engine (U)	
12. PERSONAL AUTHOR(S) T.J. Pivirotto; D.Q. King; J.R. Brophy; W.D. Deininger	
13a. TYPE OF REPORT Final	13b. TIME COVERED FROM 84/12/28 TO 86/11/30
14. DATE OF REPORT (Yr., Mo., Day) 87/11	15. PAGE COUNT 99
16. SUPPLEMENTARY NOTATION	

17. COSATI CODES		
FIELD	GROUP	SUB. GR.
21	03	

18. SUBJECT TERMS (Continue on reverse if necessary and identify by block number)
Electric Propulsion, ~~Arcjet~~ Electrothermal Arcjet, Space Propulsion

19. ABSTRACT (Continue on reverse if necessary and identify by block number)

The objective of this effort was to evaluate the lifetime and performance of a 30-kWe constricted arc ammonia arcjet. This engine was based on a design developed by Avco Corporation in 1963 that delivered 978 seconds of specific impulse with ammonia during a 50-hour test. After 573 hours of operation, a short circuit between the cathode and anode of JPL's thruster forced the life test to end. Throughout the 573-hour test, the thruster operated at 24.9 kWe, delivering 2.29 N (0.15 lbs) of thrust, 865 seconds of specific impulse, and 37% efficiency. Although the lifetime of JPL's thruster fell short of AFAL's original 1500-hour goal for the effort, the arcjet demonstrated a duration of over eleven times the lifetime of the 1963 Avco arcjet. Further, the demonstrated lifetime of 576 hours is adequate for many orbit raising missions.

20. DISTRIBUTION/AVAILABILITY OF ABSTRACT UNCLASSIFIED/UNLIMITED ☒ SAME AS RPT. ☐ DTIC USERS ☐	21. ABSTRACT SECURITY CLASSIFICATION UNCLASSIFIED
22a. NAME OF RESPONSIBLE INDIVIDUAL Robert D. Meya, 1Lt, USAF	22b. TELEPHONE NUMBER (Include Area Code) (805)275-5473 22c. OFFICE SYMBOL LKCJ

DD FORM 1473, 83 APR EDITION OF 1 JAN 73 IS OBSOLETE.

SECURITY CLASSIFICATION OF THIS PAGE

TABLE OF CONTENTS

DTIC COPY INSPECTED

Accession For
NTIS GRA&I
DTIC TAB
Unannounced
Justification
By
Distribution/
Availability Codes
Dist | Avail and/or Special
A-1

FIGURES

FIGURES (Continued)

FIGURES (Continued)

FIGURES (Continued)

TABLES

Section 1

INTRODUCTION

Advanced space propulsion systems are required to meet projected Air Force needs through the year 2000. Most of these missions require a large, on-orbit impulse capability. High specific impulse (I_{sp}) electric engines can provide this impulse while consuming relatively little propellant. An arcjet engine system which operates in the I_{sp} range of 600 - 2000 sec is a promising candidate to meet these projected Air Force missions needs. This electric propulsion system is ideally suited to missions currently under consideration, such as the Space-based Radar and other space platforms, because sufficient power will already be installed on the spacecraft for other functions. This power can be used for propulsion when not required by the primary functions.

Development of the arcjet engine was an Air Force- and NASA-sponsored activity that proceeded vigorously from its inception during the late 1950s, when the plasma exhaust was used in wind tunnels to study re-entry ablation, up to the mid-1960s when the programs were terminated. During that time period, arcjet engines were being developed for propulsion systems powered by large space nuclear reactors. Their simplicity, high I_{sp} and good thrust efficiency made these engines very attractive where on-board spacecraft power levels of tens of kilowatts and greater were planned. As a means of re-establishing arcjet engine technology, Jet Propulsion Laboratory (JPL) is currently developing an arcjet engine, in which the most promising features and insights from the previous efforts, together with the most modern fabrication and sealing techniques, are being incorporated.

A facility was needed to advance the technology of thermal arcjet engines. This facility was required to be capable of supplying and disposing of the required amount of electrical and thermal power, be compatible with propellants of various kinds, and operate under simulated conditions of space. This facility needed to be instrumented such that engine performance, and performance degradation with time, could be measured accurately. The facility was completely automated so that very long-term tests of continuous engine operation could be conducted efficiently.

This report describes a facility built around a water-cooled, 1.2 m diameter by 2.1 m long vacuum tank and a 13,400 CFM vacuum pumping plant which meets those requirements. A heat exchanger between the vacuum tank and pumps removes the heat added to the propellant by the arcjet engine. The DC power supply used to power the engines is capable of supplying 400 A at 215 V (86 kW) steady-state, and up to 500 A at 200 V (100 kW) with a 50% duty cycle. This facility is instrumented to measure engine power, internal pressure, outer surface temperatures and thrust. The vacuum tank pressure and propellant mass flow rate are also monitored. The entire facility is monitored and controlled by a Hewlett-Packard 3421A Data Acquisition/Control Unit and a Hewlett-Packard 9836 computer, allowing for 24 hour per day, 7 days per week, hands-off operation.

This report describes the design and fabrication of an arcjet engine and its characterization at power levels between 10 and 30 kW and at ammonia mass flow rates of 0.25 and 0.30 g/s. This same engine was used for a long duration test of 573 hours. During the long duration test the power level varied between 24 and 29 kW with ammonia mass flow rates between 0.25 and 0.27 g/s. The performance of the facility and engine, during the test, are also presented, together with an analysis of the effects of accumulated run time on the engine structure.

Section 2

FACILITY

2.1 Vacuum Tank

A cylindrical stainless steel vacuum tank (Fig. 1) with an internal diameter of 1.2 m and a centerline length of 2.1 m was used. The cylindrical wall, one end flange and the window ports were cooled with water flowing through copper tubing soldered to the external surfaces. An epoxy heat transfer material was used to improve the thermal contact between tubes and tank surfaces. This tank has eleven ports, of from 20 to 30 cm diameter, for access to and viewing of the experiment.

2.2 Diffuser

Since the vacuum tank pressure can have an effect on thrust, a diffuser was developed to reduce this pressure to a minimum for the mass flow rates used during the tests described herein. Tank pressure can affect thrust by influencing the nozzle expansion process. This effect can be particularly large for arcjets because the nozzle Reynolds Number is very low (<1000); hence, the boundary layers are very thick. A second effect can come from the impingement of gas currents on various parts of the thrust stand and engine. Because of these impingement effects, shields were used to cover as much of the thrust stand as possible (see Fig. 2).

A review of the literature indicated that diffuser design data and methods for ambient pressures below one torr did not exist. Extrapolations from the existing data were used as a starting point and the performance of a straight pipe diffuser with an internal diameter of 14.9 cm and a length of 53.7 cm was examined. The results are shown in Fig. 3 as vacuum tank pressure vs. arc power. As can be seen, this diffuser reduced the tank pressure from 0.158 torr to 0.109 torr at a power of 20 kW. The mouth of this diffuser was 6.4 cm from the engine exit plane. Next, the length of this diffuser was extended to the engine exit plane and a second test performed. The tank pressure was reduced to 0.096 torr at 20 kW. The reason for this curve rolling over at higher power is not understood. A larger diameter diffuser (16.1 cm), extending to the nozzle exit plane (60 cm long) was next installed and tested. This diffuser dropped the tank pressure to 0.070 torr at 20 kW and still shows a tendency to roll over at high power. All of these

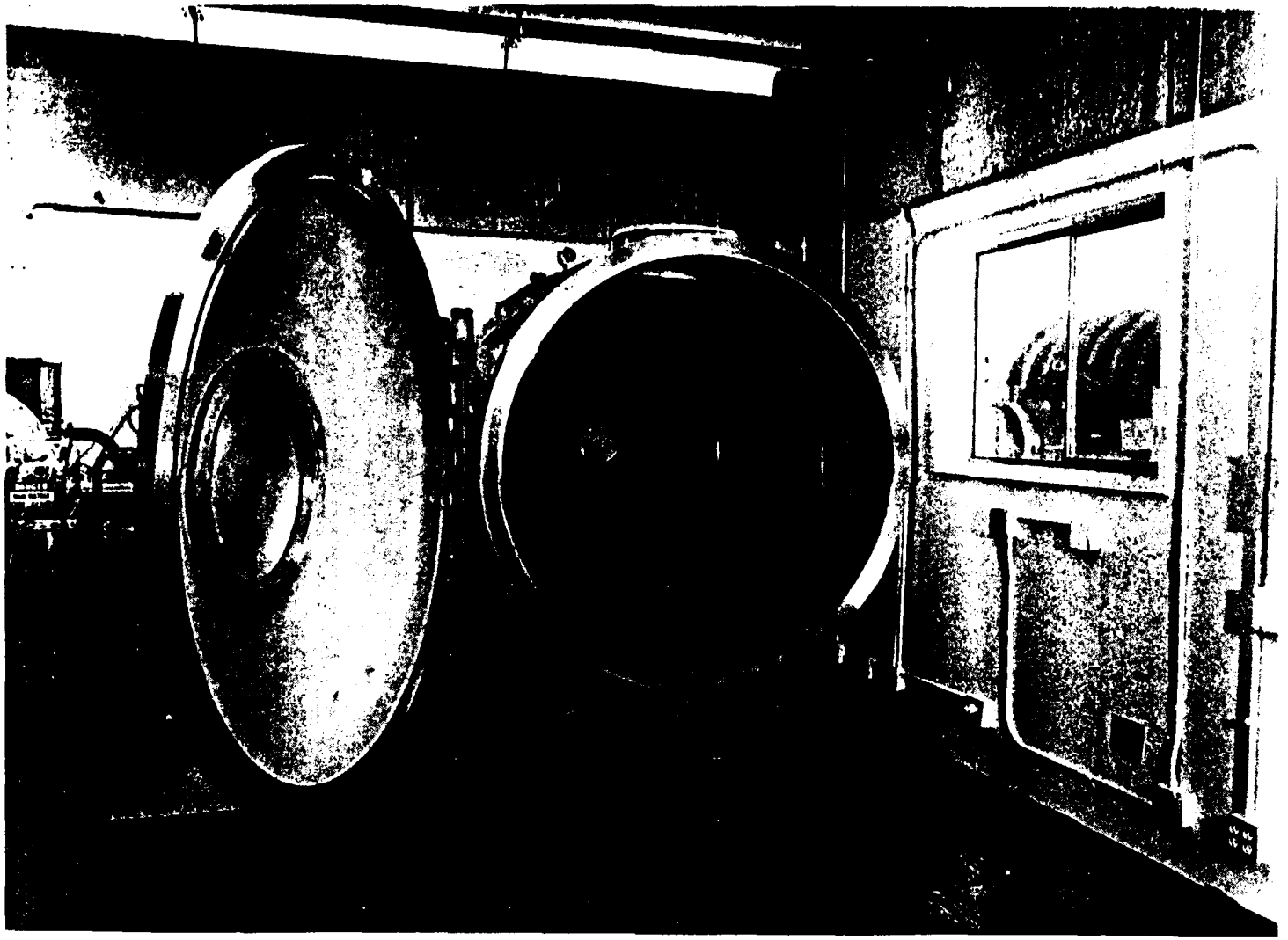

Figure 1. Arcjet Facility Vacuum Tank

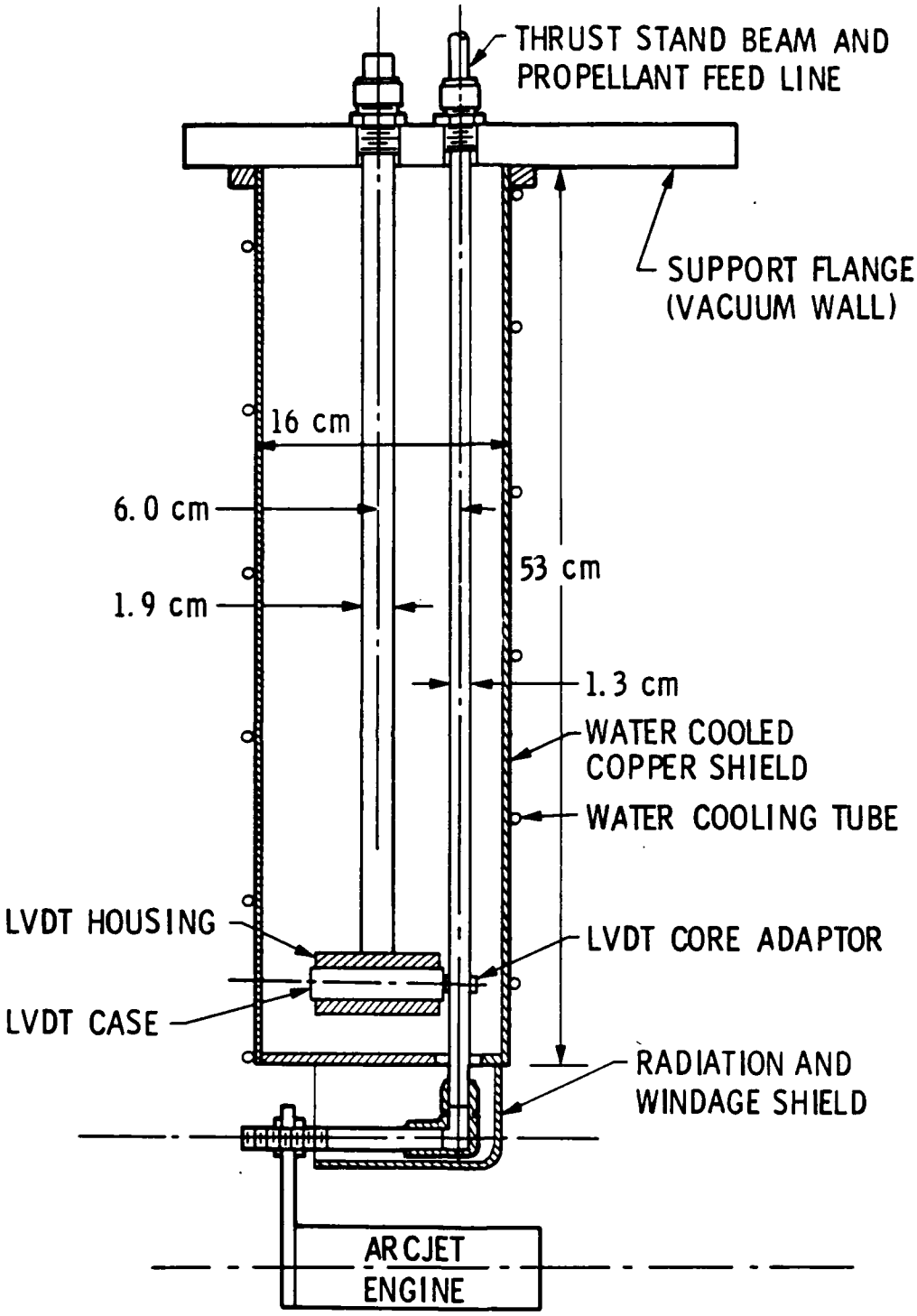

Figure 2. Schematic of Arcjet Engine Thrust Stand

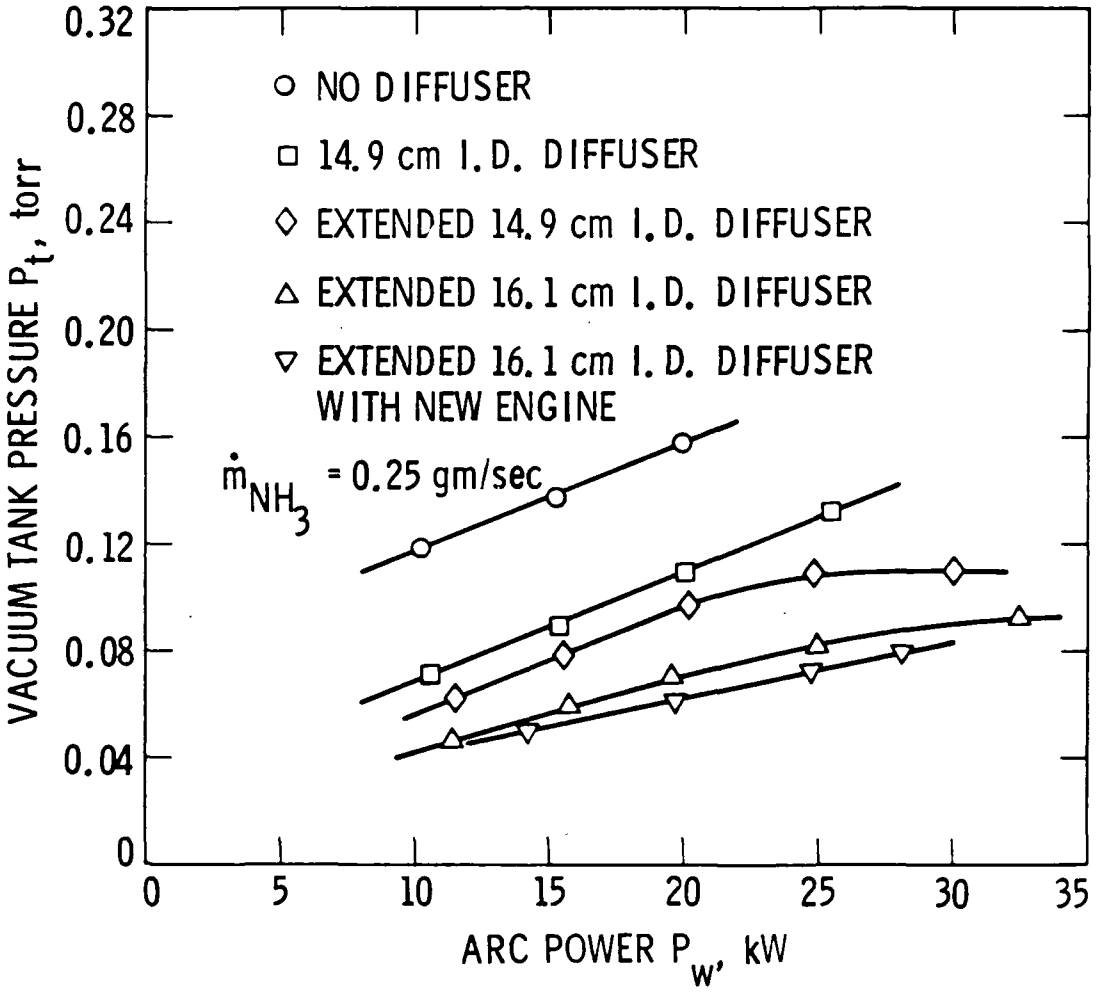

Figure 3. Vacuum Tank Pressure at Various Power Levels for Several Diffuser Designs

tests were performed with an engine that had been damaged in an earlier test. The damage was a 3 mm pit in the nozzle wall. When this last diffuser was tested with a new engine, the vacuum tank pressure was further reduced to 0.062 torr. This final diffuser design was made from stock stainless steel pipe and had a 0.95 cm diameter copper tube wrapped around the outside, in a helix, for water cooling. The copper tube was silver-soldered to the diffuser. By measuring the flow rate and temperature rise of this cooling water, it was found that the power absorbed by the diffuser was about 70% of the total arc power at 10 kW and this increased to about 80% at 30 kW. Since the engine radiates away about 10% of the arc power (Ref. 1), this result suggests that most of the remaining power, in the exhaust plume, is transferred to the diffuser walls. Most of the remaining power must be transferred to the facility heat exchanger located in the vacuum line between the vacuum tank and the vacuum pumps. The fact that the tank pressure increases with arc power for all of the curves of Fig. 3, including the one for no diffuser, indicates that the exhaust gas temperature, at the vacuum pump inlet, increases with arc power and/or that the degree of dissociation increases with power. The pump inlet pressure must affect the vacuum tank pressure through the boundary layer in the diffuser.

2.3 Heat Exchanger

A heat exchanger is needed to remove the power from the propellant flow stream before the gases enter the vacuum pumps. This heat exchanger was constructed by forming coils of finned copper tubes and placing them in a 30 cm diameter vacuum pipe which connects the vacuum tank to the vacuum pumping plant. To keep the conductance as high as possible, the tank and vacuum pumps were set only 1.75 m apart. In addition to the heat exchanger, a vacuum blade valve, a debris-catching screen and a 30 cm diameter stainless steel bellows were inserted in the vacuum line between the tank and pump inlet. The bellows effectively isolates the tank from any pump vibration.

2.4 Vacuum Pumping Plant

The high-capacity vacuum pumping plant (Fig. 4) consists of a 13,400 CFM Roots blower as a first stage, followed in turn by a 1300 CFM Roots blower and a 300 CFM mechanical vacuum pump (Stokes Microvac Pump, Model 412H-10). The first stage is powered by a 50-horsepower motor and is capable of continuous operation with an inlet pressure as high as 0.5 torr. This stage can also operate safely, for short periods, with an inlet pressure of 2 torr. All the pumps are water-cooled. Since these are constant speed pumps, the achieved tank pressure is a linear function of the injected mass flow rate. With a zero propellant mass flow rate, the vacuum tank can be taken down to about 0.002 torr. With an ammonia mass flow rate of 0.25 g/s, the tank pressure increases to about 0.067 torr.

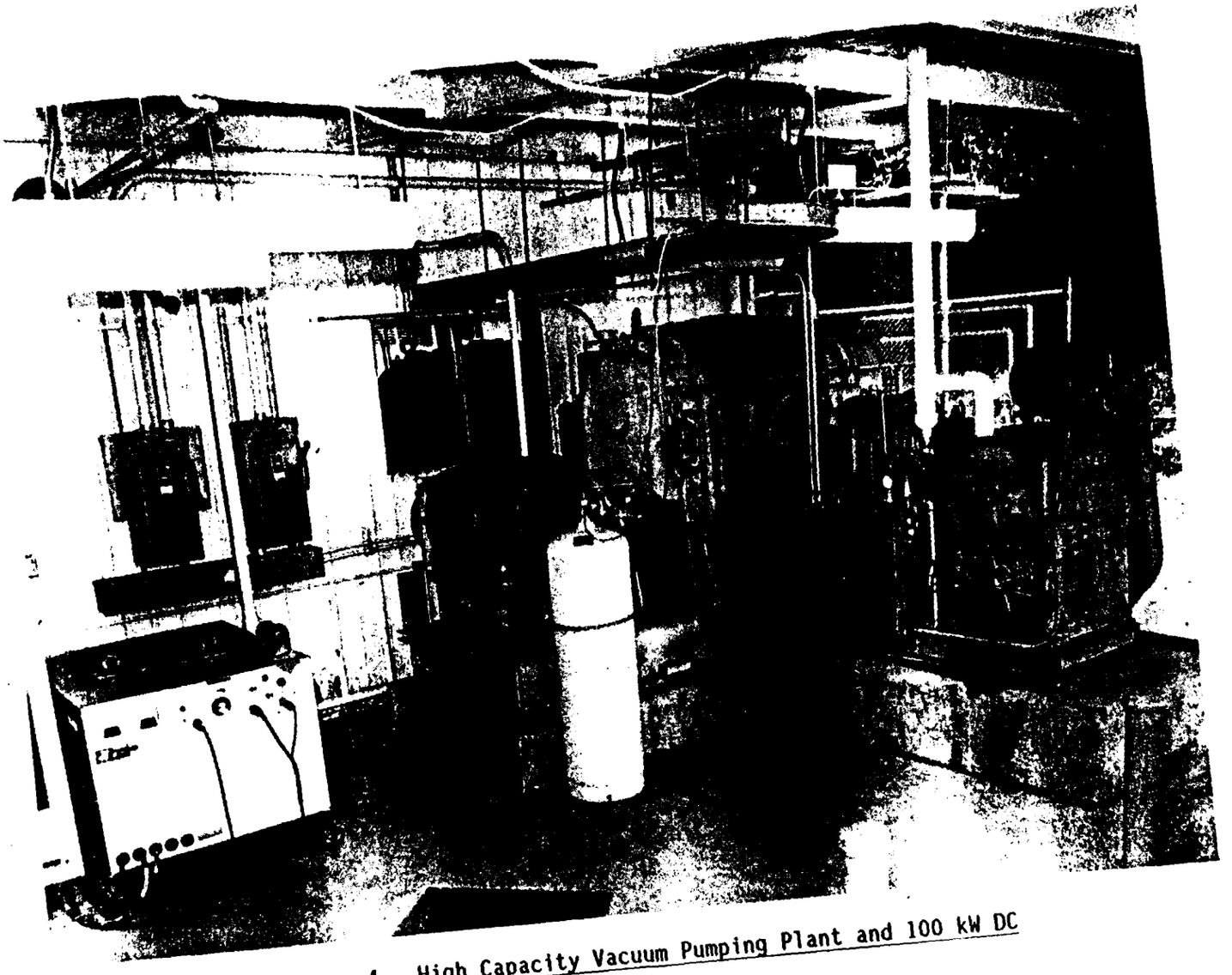

Figure 4. High Capacity Vacuum Pumping Plant and 100 kW DC Power Supply

2.5 Power Supply

The arcjet engines are powered by a Linde PHC-402 DC power supply, which can be seen next to the vacuum pumps in Fig. 4. This supply has a continuous duty capacity of 400 A at a load voltage of 215 V (86 kW) and a 50% duty capacity of 500 A at 200 V (100 kW). A 0.3 ohm forced air cooled ballast resistor is used to reduce the power supply ripple to about 3% and to protect the power supply from a short circuit at the arcjet engine. Also, the PCH-402 has an electronically-controlled, saturable core for current control. This feature allows for power supply control at either constant current or constant power with a relatively simple feedback control circuit.

2.6 Propellant Storage and Handling

A 1000-kg ammonia storage tank has been installed for long duration testing of arcjet engines. This tank has a large heat-absorbing area so that no additional heat is required to supply the vapor at the required rate. For typical test conditions, this tank alone can supply vapor for 45 days of continuous testing. It can also be refilled without interrupting a test in progress. The vapor pressure of ammonia is 130 psia at 72^{o}F and 215 psia at 100^{o}F. This pressure must be reduced to about 30 psia for the flow controller and this was accomplished with a stainless steel regulator. Stainless steel pressure gauges are used to monitor all system pressures and all propellant lines are also stainless steel. The mass flow rate of ammonia vapor was controlled and measured with a Sierra Instruments, Inc. Series 830 Side-Trak mass flow controller which has a range of 0 to 30 standard liters per minute. For higher flow rates, a second identical controller can be installed in parallel to the first one.

2.7 Instrumentation

Constricted arcjets have a sawtooth voltage wave form (Fig. 5) superimposed on the DC voltage level (Ref. 2). This wave form is caused by the anode spot being blown downstream, thereby increasing the voltage until the voltage drop is high enough to extinguish the arc. A new anode attachment point is then established upstream and the arcjet voltage drop is then reduced by several tens of volts in less than a few hundred nanoseconds. Because of this rapidly fluctuating voltage, a low inductance, coaxial shunt must be used to accurately measure the arc current. The arc voltage was measured with separate leads to the anode and cathode, thus avoiding errors due to line losses.

The propellant mass flow rate was measured and controlled with a Sierra Instruments Side-Trak Model No. 830 flow controller. This flow controller has been calibrated for ammonia vapor and can measure flow rates from 0 to 30.0 standard liters per minute or 0 to 0.36 g/s with a probable error of less than 1% of full-scale.

The thrust was determined by measuring the amount of deflection of the cantilevered hollow beam that supports the arcjet engine (see

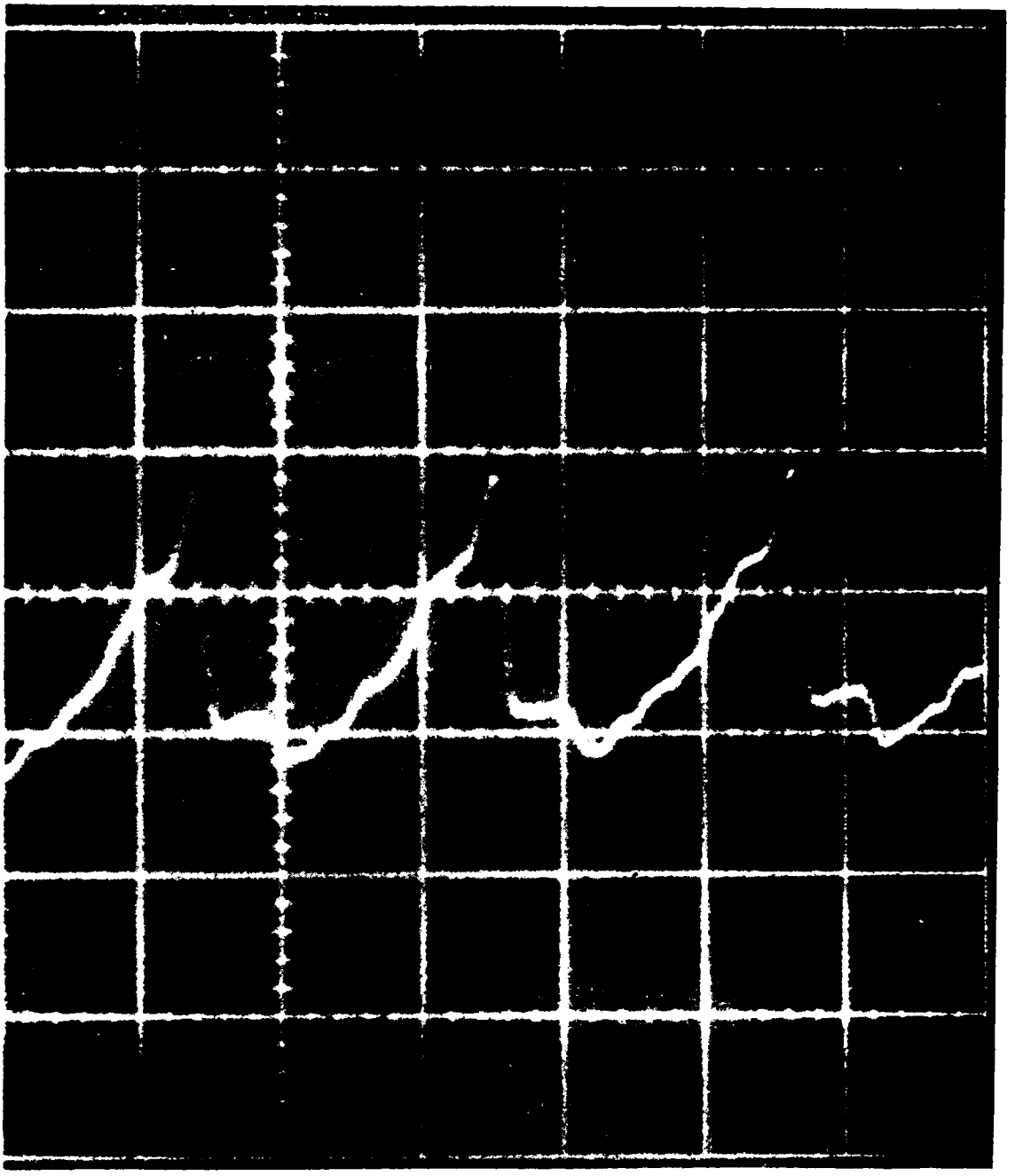

Figure 5. AC Component of Arcjet Voltage, Ordinate is 20 V Per Division, Abscissa is 5 μs Per Division, Mean DC Voltage was 72V

Fig. 2). This beam, which is part of the propellant feed system, was made of 321 stainless steel, has a 1.27 cm outside diameter, a wall thickness of 0.17 cm and deflects about 1 mm for a thrust of 200 g. The amount of deflection was measured with a Linear-Variable-Differential-Transformer (LVDT) that has an operating range of $\pm$0.25 cm. The body of the LVDT was held in a housing located at the bottom end of a second, 1.91 cm diameter, cantilevered rod made of 321 stainless steel. Both pieces of steel are fully annealed. The LVDT core was attached to the hollow beam with an adapter. The housing for the LVDT body has six adjusting screws so that the attitude of the body relative to the core could be adjusted in three translational and three rotational degrees of freedom. This fine degree of adjustment was necessary to keep the LVDT body and core from touching throughout the range of movement of the thrust beam. Hence, this method of measurement of beam deflection does not affect the stiffness of the thrust beam nor does it add hysteresis to the measuring system. Both beams are attached to a 321 stainless steel plate with feed-through fittings. The plate fits into a window port at the top of the vacuum tank. The thrust stand and engine attachment fixture are shielded from the hot engine and low-density circulating gases by a water-cooled copper jacket as is shown in Fig. 2. The engine attachment fixture was designed so that engines with various mass distributions could be mounted with their center-of-gravity underneath the thrust beam. The thrust stand was calibrated with a dead-weight technique and the sensitivity was found to be 9.44 mV/g_f (see Appendix A). The propellant pressure was measured, at the top end of the thrust beam, with a strain gauge type pressure transducer. The range of this gauge was 0 to 500 cm-Hg and its accuracy was better than 1% of full scale (see Appendix A). Water-cooled pools of mercury are used to transfer power to the engine while maintaining mechanical isolation between the engine and heavy power leads so that thrust can be measured (see Appendix B).

The vacuum tank pressure was measured with a variable-capacitance type gauge. This transducer is capable of measuring the pressure of any gas and/or vapor mixtures with an accuracy of $\pm$0.5% of the reading and has a 0 to 10 torr range.

The temperature of the LVDT case, and various stationary parts of the thrust stand, were measured with Chromel/Constantan thermocouples. The outer surface temperature of the engine nozzle, which was of order 2000^{o}C, was measured with a Raytek infrared remote sensing pyrometer. The pyrometer was located outside of the vacuum tank and viewed the engine through a 1.9 cm thick glass window. A General Electric Company ribbon filament standard lamp was used to calibrate this system. The lamp was located inside the vacuum tank at the position occupied by the engine during engine testing. The known lamp brightness temperature was then used to correct the pyrometer data with a systematic uncertainty of $\pm$6^{o}C.

2.8 Autonomous Control

The entire test facility was monitored and controlled by a Hewlett-Packard 3421A Data Acquisition/Control Unit and a Hewlett-Pack-

ard 9836 Computer. The data acquisition/control unit has 16 input data channels and 4 output actuators (relays) for active facility control. It has a built-in digital voltmeter with automatic range and zeroing features, a maximum sensitivity of 1 μV, a maximum DC input voltage of 300 V and an input impedance of 10 M Ω or greater. For temperature measurements, it has an internal (electronic) reference junction. The data reading rates vary from 1 to 38 readings per second, depending on type of data, resolution required and number of channels being monitored. The accuracy, over a period of 1 year, is equal to or better than 0.095% of reading plus 6 counts.

For the development and endurance testing of arcjet engines, the input data was:

a. Propellant flow rates.
b. Arcjet current.
c. Arcjet voltage.
d. LVDT input voltage.
e. LVDT output voltage.
f. Vacuum tank pressure.
g. Propellant pressure.
h. Radiometer signal.
i. Various thermocouple signals.

The several channels that were susceptible to voltage spikes were protected with metal-oxide varistors and fuses. The one used to measure arc voltage used a 10 to 1 divider made with precision metal film resistors.

The raw data, stored on floppy disks, was used to calculate arcjet input power, thrust, specific impulse and overall efficiency in real time. This autonomous control system was also used to monitor the operation, including itself, and when it found that something critical was out of tolerance, it shut down the operation in an orderly fashion and notified an operator (see Appendix C).

Section 3

ENGINE DEVELOPMENT

An important part of this task was to select an example of the best performing ammonia arcjet technology from previous efforts, duplicate the essential features and then test and measure its performance and reliability over a long duration run. After reviewing all literature obtainable, the AVCO Corporation R-3 arcjet engine was selected for duplication because this engine was specifically designed for ammonia and it had been successfully run for 50 hours with good and reliable performance. This engine design and its performance measurements can be found in Reference 3. A schematic of an equivalent hydrogen engine, taken from Ref. 3, is shown in Fig. 6 and the essential dimensions for an ammonia engine, also taken from Ref. 3, are given in Table 1.

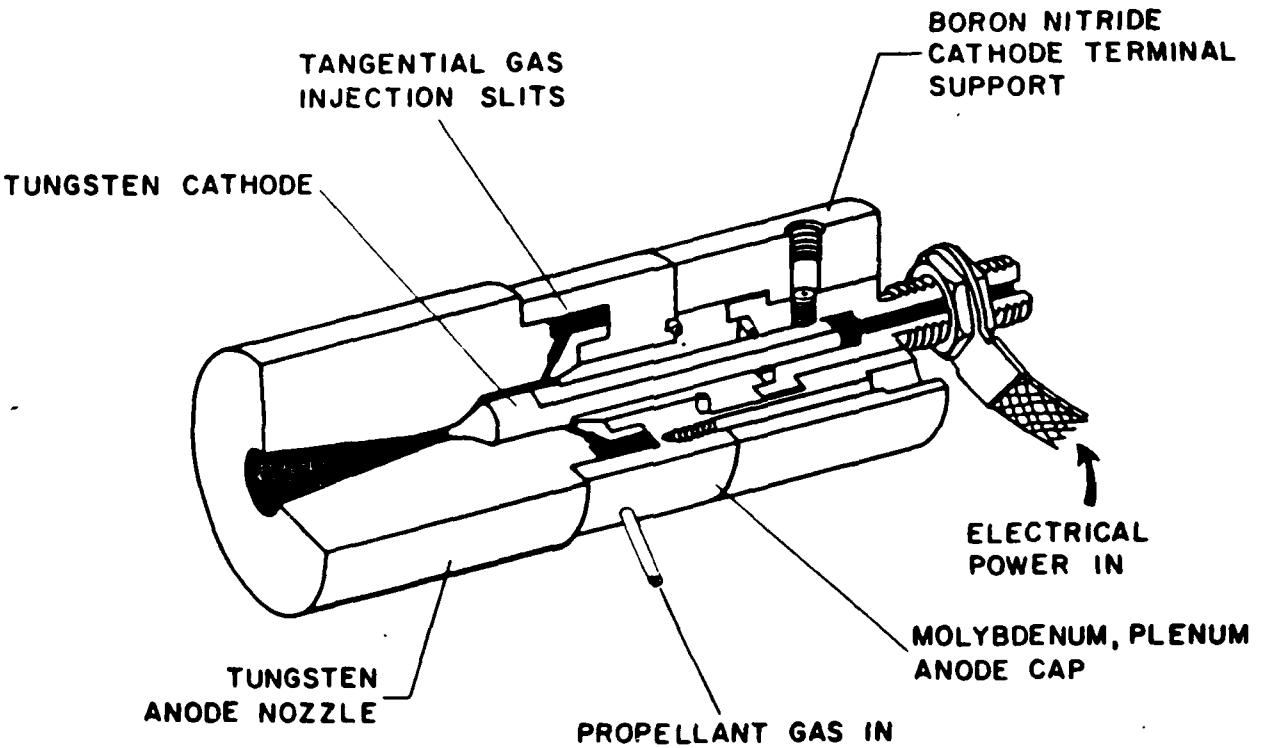

Figure 6. 30 kW Thermal Arcjet Engine Designed for Hydrogen Propellant by Avco Corporation

Table 1. Dimensions of the AVCO R-3 Ammonia Engine.

Constrictor Length l, cm	1.066
Constrictor Diameter dc, cm	0.508
Nozzle Exit Diameter de, cm	2.41
Nozzle Area Ratio A/A*	23
Nozzle Angle, deg	38
Electrode Gap X, cm	0.21
Gas Injection Angle, deg	30
Nominal Engine Diameter D, cm	5.08
Nominal Engine Length L, cm	14.0
Nominal Engine Weight W, kg	2.6

The anode-nozzle and cathode of the engine were made of 2% thoriated tungsten while the body was made of molybdenum and the electrical insulators of boron nitride.

After carefully reviewing all the available literature on previous arcjet engine developments it became clear that most engine failures were caused by failures of the high temperature sealing techniques being used. In the AVCO effort the selected technique was brazing, and various brazing techniques and materials were studied in a parallel effort. Electron beam welding was also tried. These efforts did result in successful high temperature seals, as demonstrated in a 50-hour endurance test with ammonia and a 723-hour endurance test with hydrogen. However, this success did require complicating the hydrogen engine design by providing for cooling of the braze joint with the propellant, as can be seen in Fig. 7, also taken from Ref. 3.

A different approach to the high temperature seal problem was taken by the Giannini Scientific Corporation in their effort to develop radiation-cooled, 30-kW class, thermal arcjet engines. Their approach was to use metal-to-metal lapped joints, thereby eliminating all low melting-point braze material. This technique worked well when the joints were carefully made. A schematic of an engine design using lapped joints for high temperature seals is shown in Fig. 8 and was taken from References 4 and 5.

Based on these considerations, insights gained from reviewing the literature and experience gained from preliminary design, fabrication and testing at JPL, a design was developed and is shown schematically in Fig. 9.

The plenum chamber, constrictor and supersonic nozzle were turned from a single piece of 2% thoriated tungsten. The nozzle had a 38° total expansion angle and an exit diameter of 2.41 cm. The constrictor had a diameter of 0.51 cm and a length of 1.07 cm and the plenum chamber had a diameter of 2.03 cm and a 50° half angle taper at the constrictor end. This nozzle block was fitted into a cylindrical molybdenum body with a 7° taper as shown in Fig. 9. A gas tight seal was effected between the tungsten and molybdenum by carefully lapping the parts

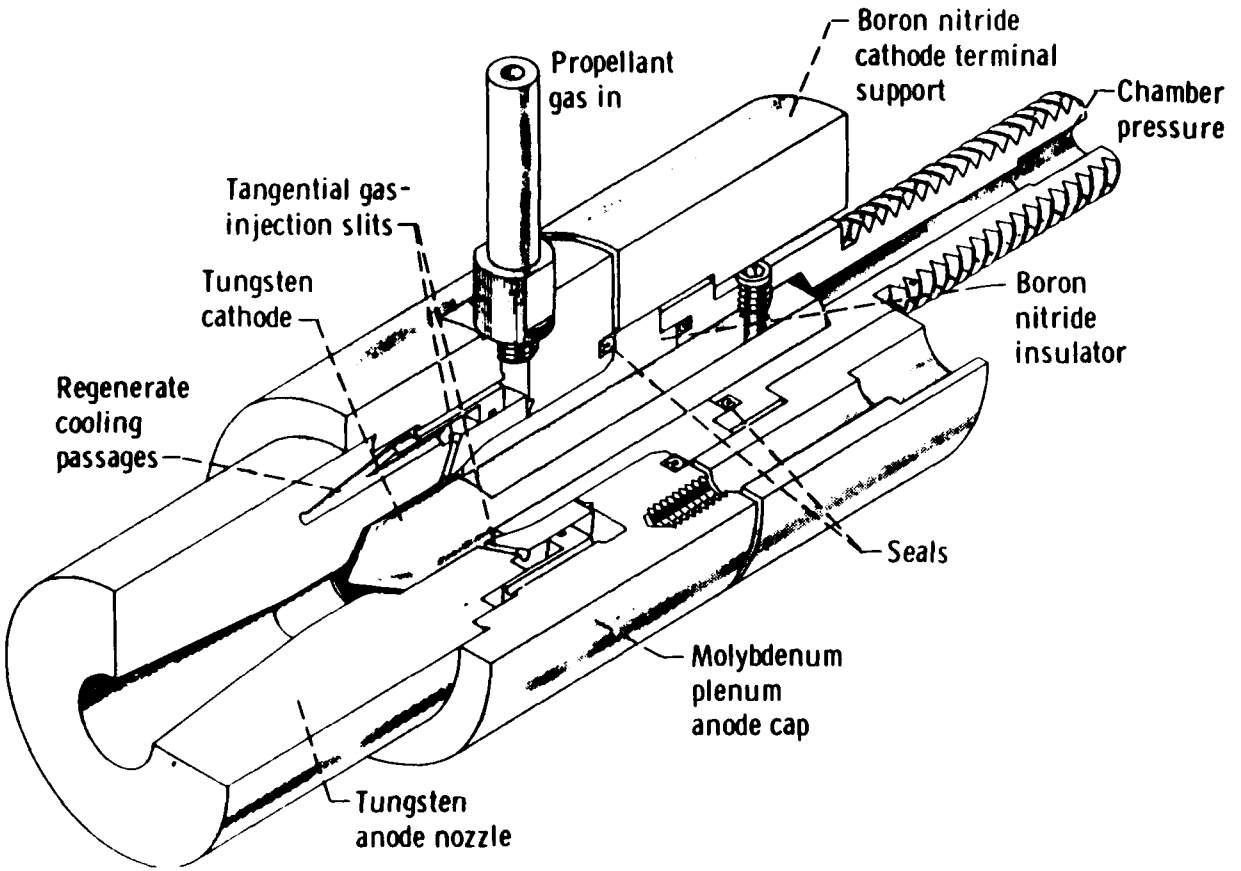

Figure 7. 30 kW Thermal Arcjet Engine Designed for Hydrogen Propellant by Avco Corporation

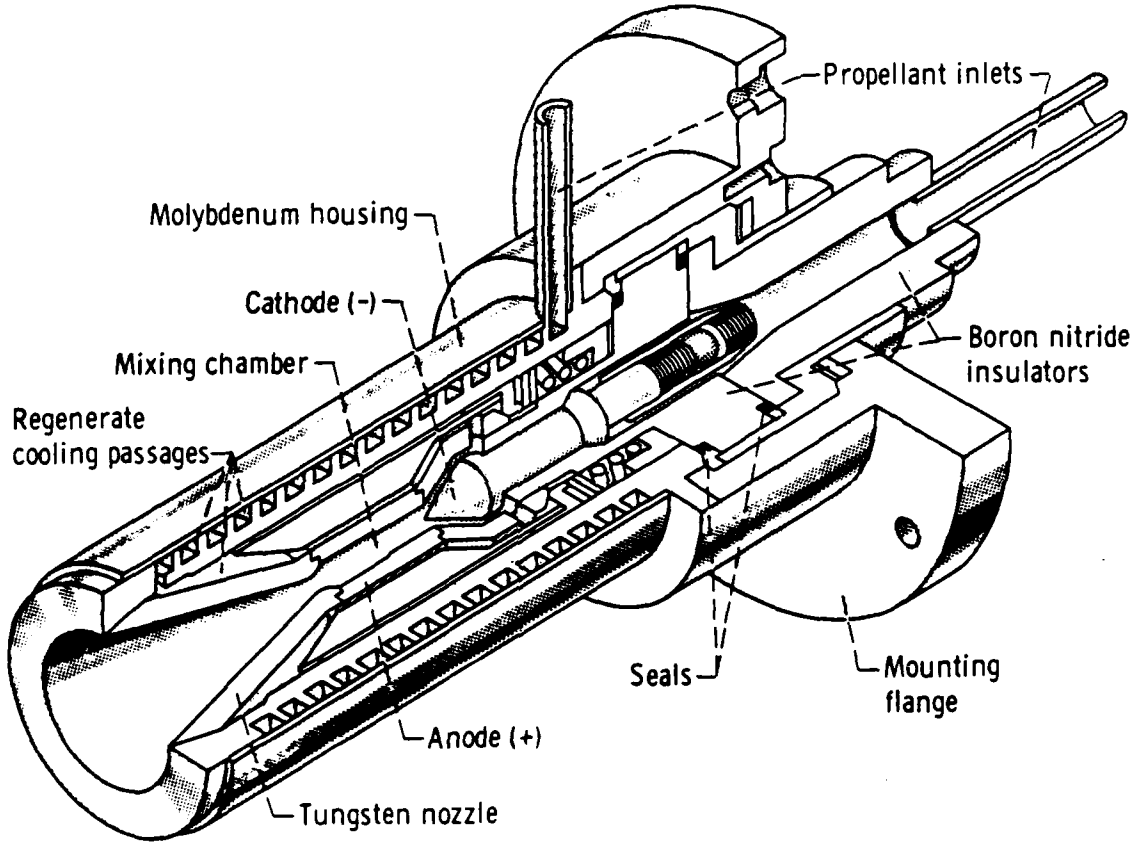

Figure 8. 30 kW Thermal Arcjet Engine Designed for Hydrogen Propellant by Giannini Scientific Corporation

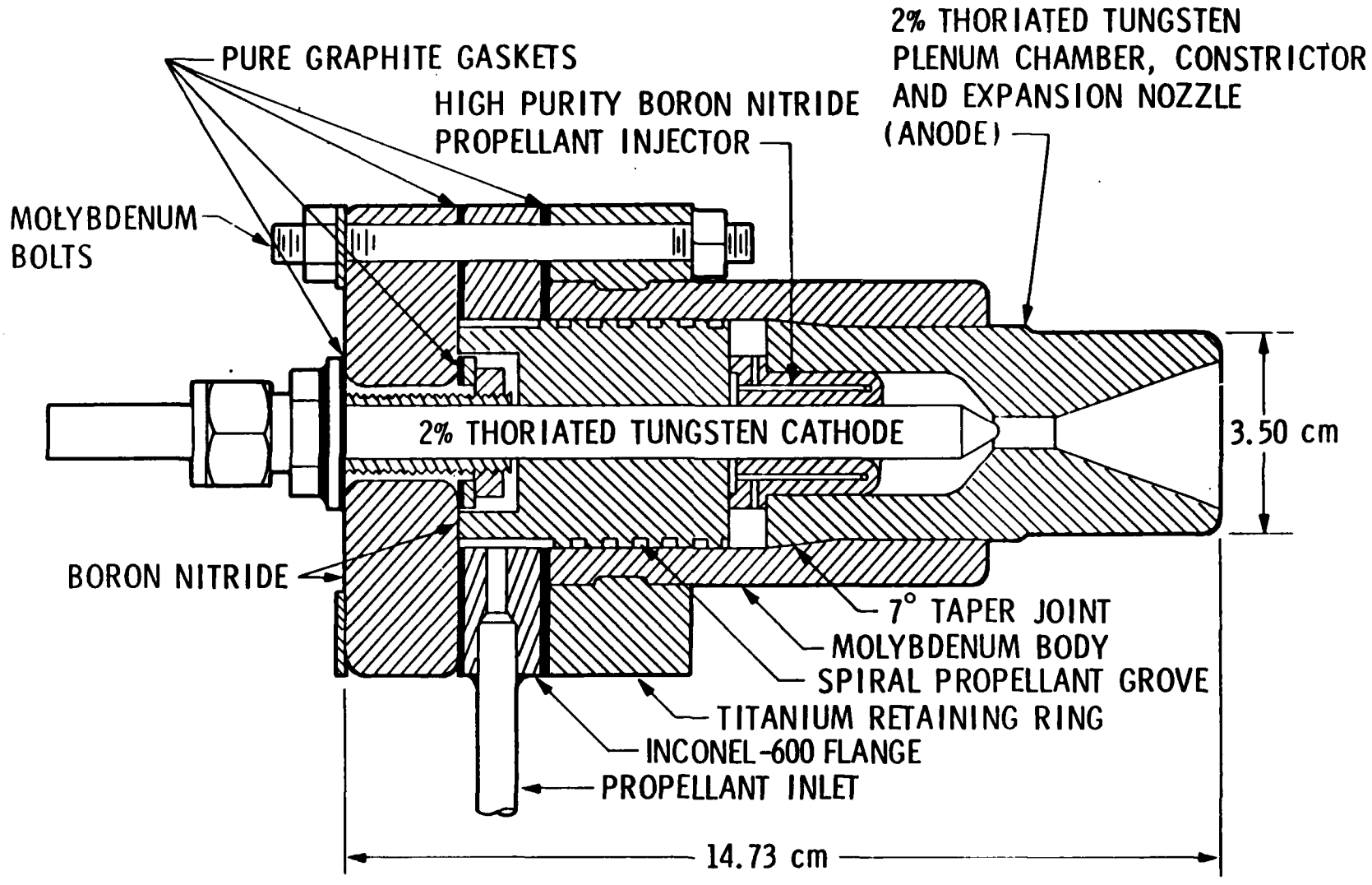

Figure 9. Schematic of High Temperature Radiation-Cooled Arcjet Engine Design

together. High pressure nitrogen was used to test for and assure a gas tight seal after assembly of the engine.

The cathode was also made of 2% thoriated tungsten and was 0.95 cm in diameter, 18 cm long and had a 60^{o} included angle tip and a 0.15 cm radius point. The axial gap between the cathode cone and the constrictor entrance was set to 0.21 cm. The cathode was held concentric to the constrictor and plenum chamber with a cylindrical insulator made of high purity (high temperature) boron nitride as shown in Fig. 9. The propellant was injected into the plenum chamber through four 0.15 cm diameter holes drilled through the boron nitride. The downstream ends of these four blind holes were met by four 0.15 cm diameter holes drilled into the end surface of the boron nitride cylinder at an angle of 30^{o} to a line normal to the plane for the figure, as is shown schematically in Fig. 10. In this way the propellant was injected tangentially into the plenum chamber at a radius of 0.75 cm and with a downstream inclination of 30^{o}.

The ammonia propellant was fed into the engine through a stainless steel tube welded into a flange made of Inconel 600 as shown in Fig. 9. The back end of the engine was closed with a 1.91 cm thick disk of boron nitride. All corners of this disk had to be well-rounded to prevent cracking. A standard swaglock bulkhead fitting was used to seal the cathode at the boron nitride disk. A 2.54 cm diameter by 0.25 cm thick stainless steel washer was welded to the fitting, as shown, in order to increase the bearing surface area on the boron nitride. A cylinder of boron nitride with a square, helical groove machined in its outer surface was used to help force most of the incoming propellant to flow along the hot inner surface of the molybdenum body to reduce the heat flow back to the graphite seals. Some propellant also flows between the boron nitride cylinder and the cathode to help cool the cathode.

A split ring of titanium was used to engage the molybdenum body through a matching groove machined into the molybdenum as is shown in Fig. 9. The back end of the engine was held together by eight 0.64 cm diameter molybdenum bolts that ran through the boron nitride disk, inconel flange and titanium retaining ring.

Spaces between the swaglock fitting and the boron nitride disk, between the boron nitride disk and the inconel flange and between the flange and the molybdenum body were sealed with 0.08 cm thick pure graphite gaskets. This gasket material was obtained from Union Carbide Corporation and is marketed under the trade name of Grafoil. This material is capable of sealing up to a temperature of $3316^{o}C$ in an inert atmosphere. The eight bolts were torqued to 2.82 N-m and the seals leak checked with high pressure nitrogen. No leaking was evident. However, after operating the engine at high temperature and then allowing it to cool to room temperature, the torque was found to be greatly decreased. This result indicates that during high temperature operation the boron nitride, inconel and titanium expand more than the molybdenum bolts, thus further compressing the graphite gaskets, and possibly stretching the bolts and/or nuts.

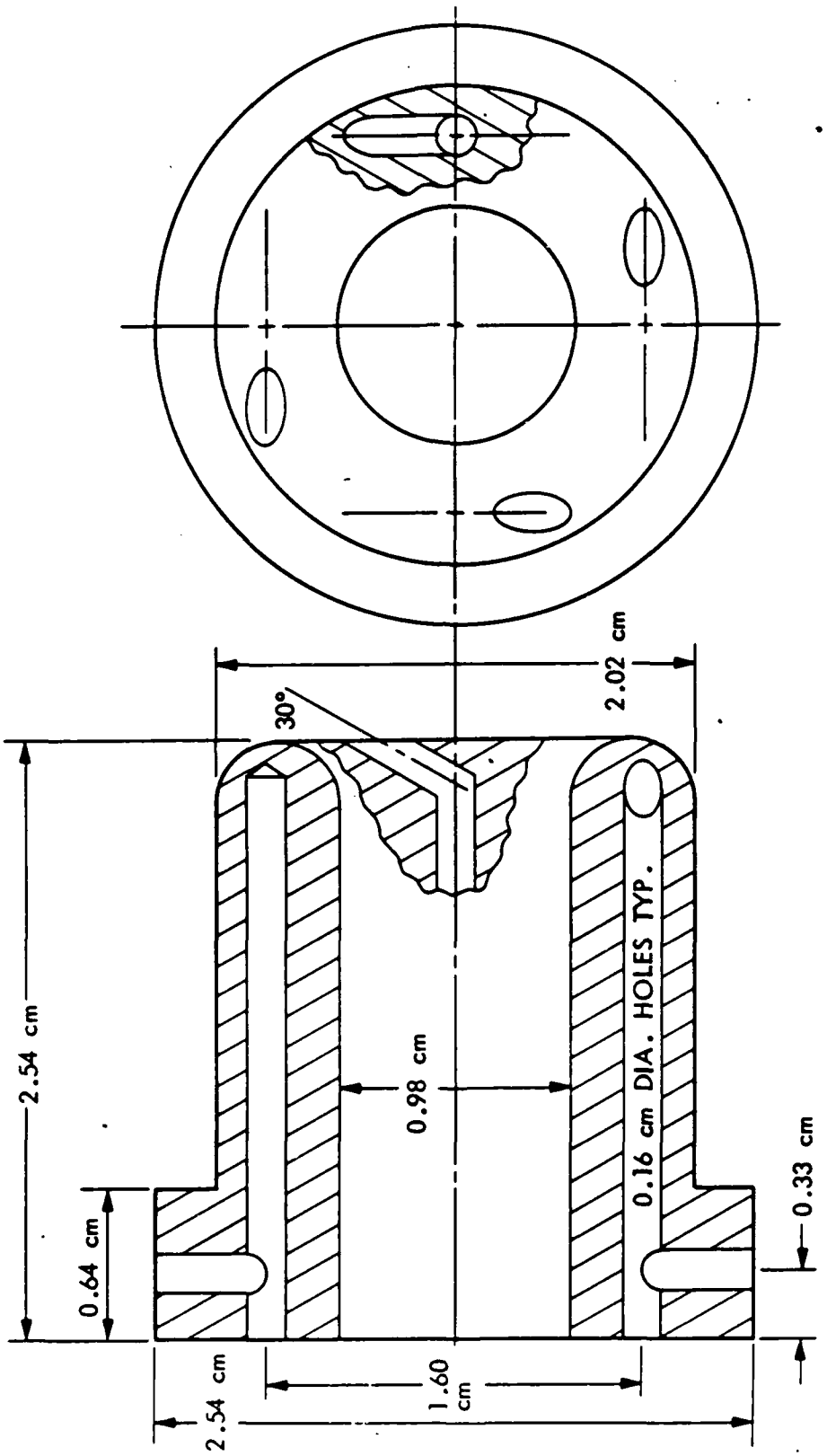

Figure 10. Dimensional Drawing of Propellant Injector

Figure 11 is a composite picture of the arcjet engine, including a picture of the coaxial current feed assembly. The bottom end of this assembly is submerged into two concentric pools of mercury (see Appendix B). In this way, power can be fed to the engine without having heavy power cables affecting the thrust measurements. The coaxial arrangement was necessary to prevent magnetic effects due to the high currents. Also shown in Fig. 11 is the fixture used to attach the engine to the thrust stand. The ammonia propellant flows through the thrust beam, to which this fixture is attached, and through the fixture to the engine. Again, this was done to eliminate any possible effects of propellant lines on the thrust measurement. Figure 12 is a picture of the assembled engine, including the coaxial current feed and thrust stand attachment fixture.

In the process of developing the arcjet engine design shown in Fig. 9, two other configurations were experimented with. The first of these is shown schematically in Fig. 13 and the second in Fig. 14. The first design, Fig. 13, was used to study problems associated with (1) the machining of refractory metals, (2) high temperature seals, and (3) starting the arcjet engine. The machining was successfully accomplished with a lubricant composed mainly of the chlorinated hydrocarbon 1,1,1-trichloroethane (95%) and Neat's foot oil (4%), manufactured by the Relton Corporation, Arcadia, California. Very sharp tungsten carbide tools were used with light cuts and slow feed. The piece was held near room temperature and the rotational cutting speed was generally between 4 and 40 in/sec.

Various gasket materials were investigated and Union Carbide Corporation pure graphite gasket material (Grafoil) was found to be the most satisfactory.

The technique developed to start the arcjet involved establishing a glow discharge at a voltage of 250 to 300 V and a current of 5 to 10 mA. This was done with a separate, high voltage, start power supply. During this phase, a small amount of argon or neon was used to support the discharge. Next, the gas flow was slowly increased, thereby increasing the gas pressure in the discharge. The discharge current would slowly increase with pressure and so would the cathode temperature. When the discharge current reached 2 to 4 A, the main, high current power supply could be turned on and the start power supply turned off. For a description of these power supplies, see the section of this report on facilities. When the current reached 2 to 4 A, the gas flow rate was typically between 5 and 10 standard liters per minute. Once the main power supply was on and the current between 50 and 100 A, power between 1 and 2 kW, the ammonia could be turned on and the argon or neon turned off with no adverse effects on the engine.

The main problem with the simple engine design shown in Fig. 13 was that at high temperature the tie rods that held pressure on the gasket relaxed, causing propellant leaks at the gaskets and arc starvation. This problem, and the desire to regeneratively cool the back end of the engine body and cathode, led to the design shown in Fig. 14. Here, eight molybdenum bolts were used to hold the engine together. These bolts, initially torqued to 2.82 N-m, prevented all leaks from occurring

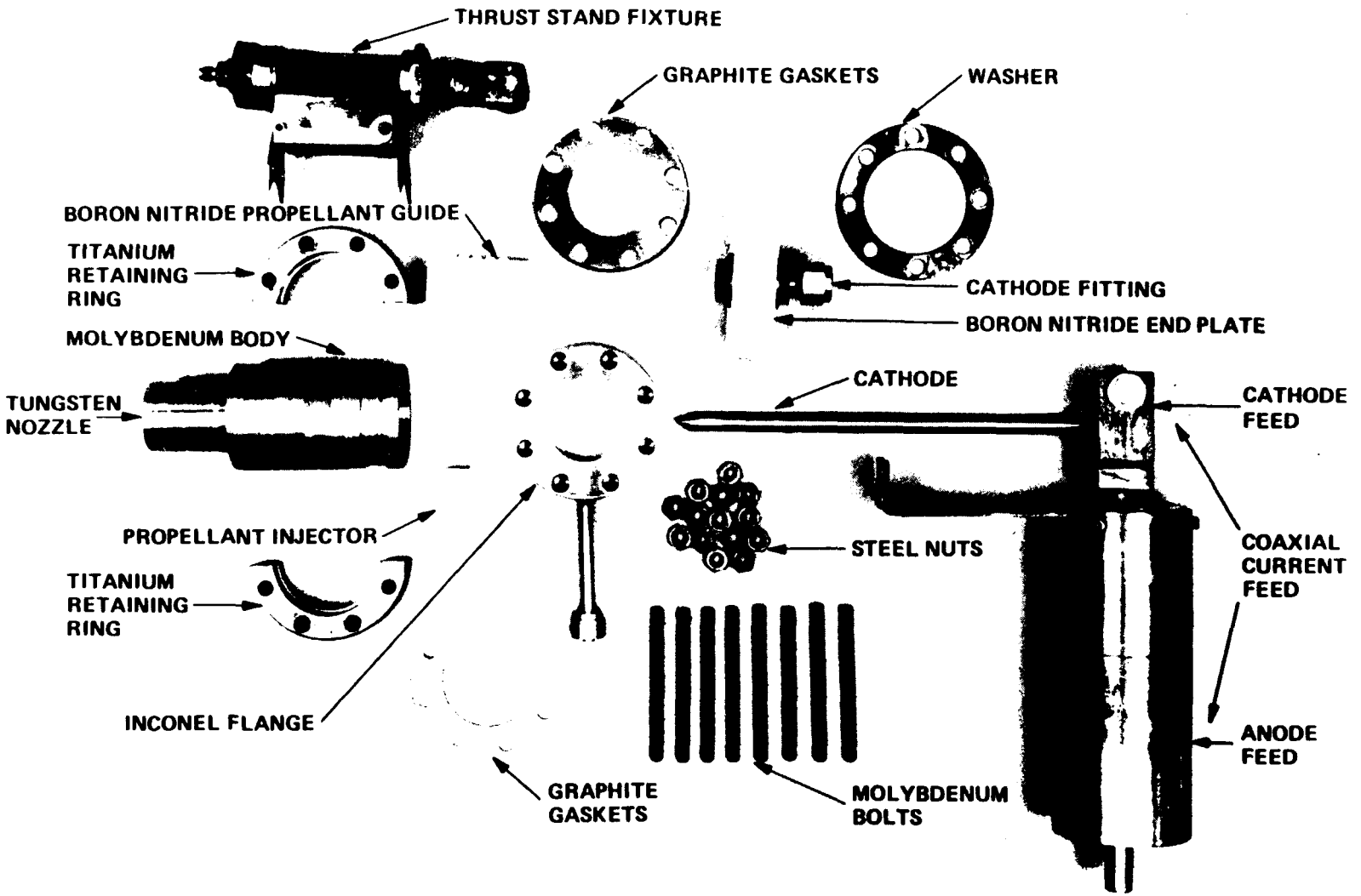

Figure 11. Parts Breakdown of Radiation-Cooled Arcjet Engine

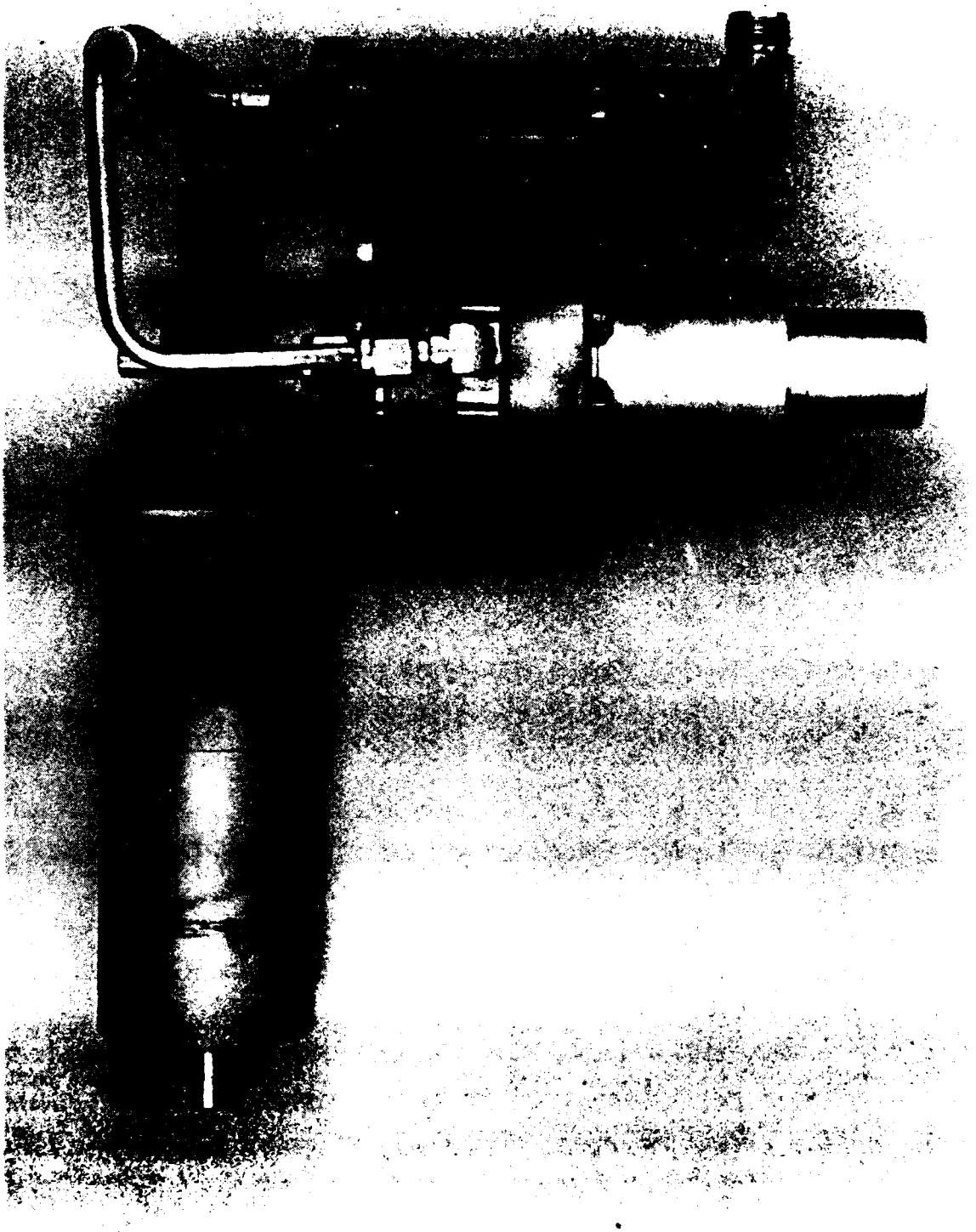

Figure 12. Assembled Arcjet Engine with Coaxial Current Feed Electrodes and Thrust Stand Fixture

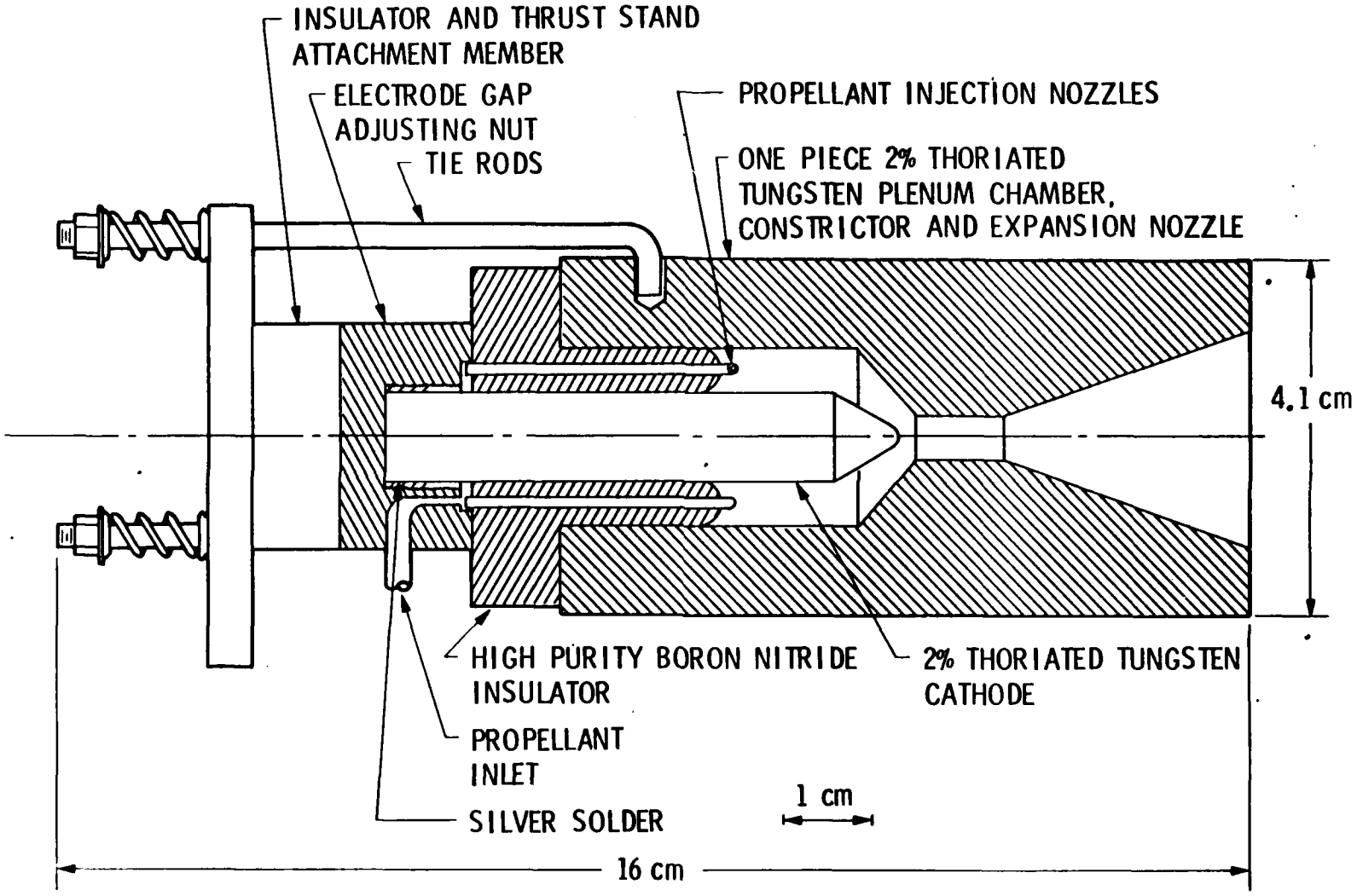

Figure 13. Schematic Diagram of Initial Arcjet Design

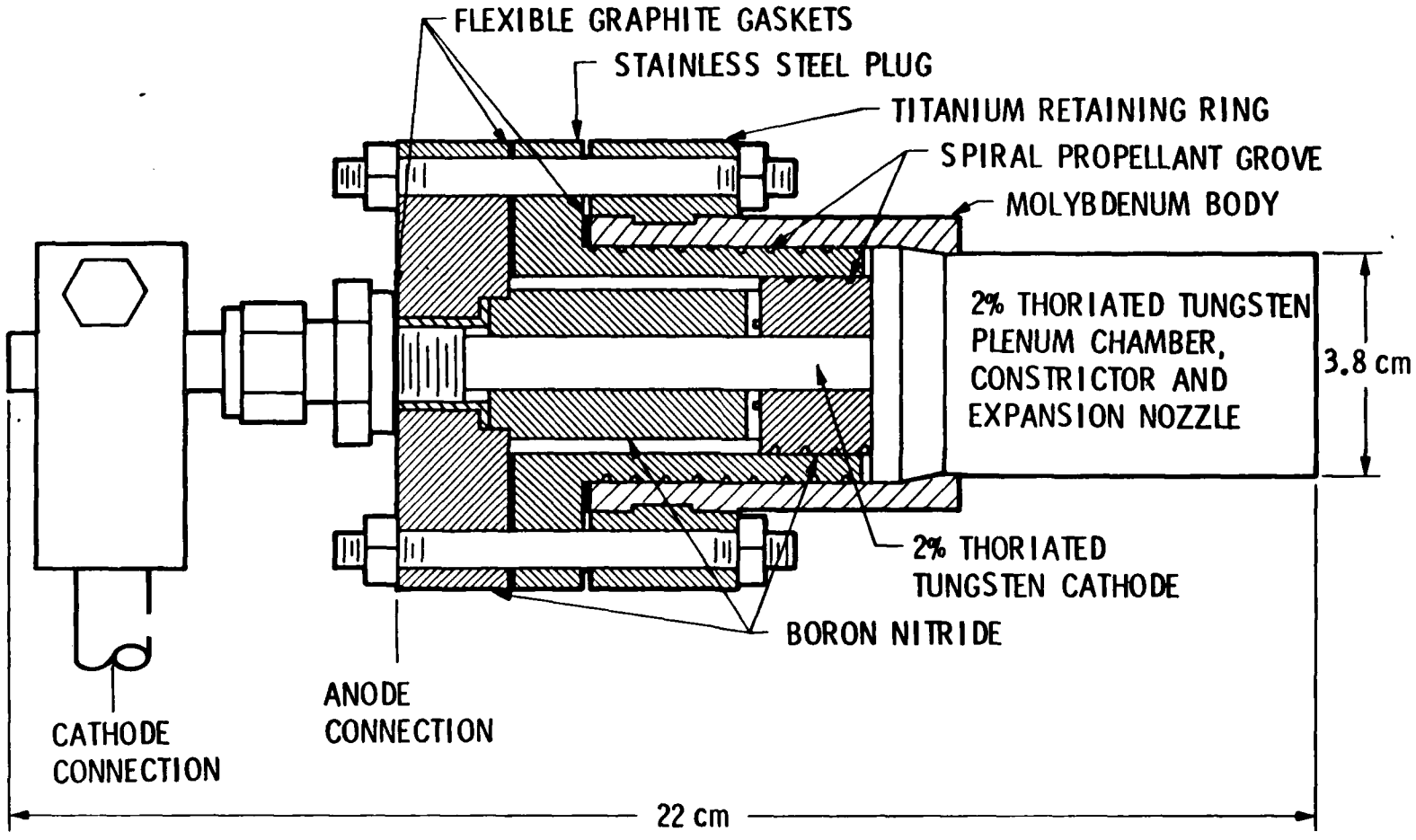

Figure 14. Schematic Diagram of High-Temperature Arcjet Design

during engine operation. However, either because of creep in the bolts or nuts or compressing of the flange, insulator, retaining ring and/or gaskets, the bolts had to be re-torqued before each test. Also, to help cool the body and increase engine efficiency and to intercept some of the heat flowing back from the nozzle toward the seals, the propellant was forced to flow in a spiral groove machined into the stainless steel plug as shown in Fig. 9. After operating this design for a continuous 168 hours, it was found that the spiral groove walls were badly nitrided. Because of this problem, the spiral grooved propellant guide was changed to boron nitride and the flange to Inconel-600 as shown in Fig. 9.

Section 4

PERFORMANCE TEST RESULTS

The engine shown in Fig. 12 has been started and run for periods at least long enough to reach thermal equilibrium several times. In each case, a glow discharge was established between anode and cathode with neon as the propellant and at a flow rate of about 1 SLM. The applied voltage was from 250 to 300 VDC. By slowly increasing the neon mass flow rate the discharge current could be increased until a more or less stable discharge of 2 to 4 A could be established. This was sufficient to heat the cathode to incandescence. The main power supply could then be turned on and a discharge of 100 A and about 20 V quickly established. The neon mass flow rate was between 5 and 10 SLM at this point. After operating at this power level (approximately 2 kW) for several minutes, the nozzle would become red hot. At this point the ammonia was turned on and then the neon turned off. The current would then drop by about a factor of two and the voltage would increase to about 100 V. The current was then brought back up to 100 A. From this point on the power could be varied between 10 and 30 kW without extinguishing the arc. Figures 15 through 20 show the results of such a starting procedure at two ammonia mass flow rates. Each data point was obtained after the engine had operated at that power level for at least 15 minutes. It was previously established that this period was more than long enough for the engine to reach a stable temperature and pressure.

Figure 15 shows the engine thrust as a function of engine power and ammonia mass flow rate. The thrust values were obtained from the measured LVDT output and the LVDT calibration. Corrections were applied for variation of LVDT temperature and for variation of the temperature of the flange that supports the thrust stand (see Fig. 2). These corrections were of order one gram or less for the data presented. Corrections for magnetic effects and for the effects of propellant pressure inside the thrust beam (Bourdon tube effect) were not made because they were previously determined to be insignificant. The power was obtained from separate measurements of current and voltage. The current measurement was made with the aid of a low inductance coaxial shunt which was calibrated prior to these tests. The voltage was measured at the mercury cups in order to eliminate the need to have leads attached to the engine directly. These voltage measurements were corrected for the

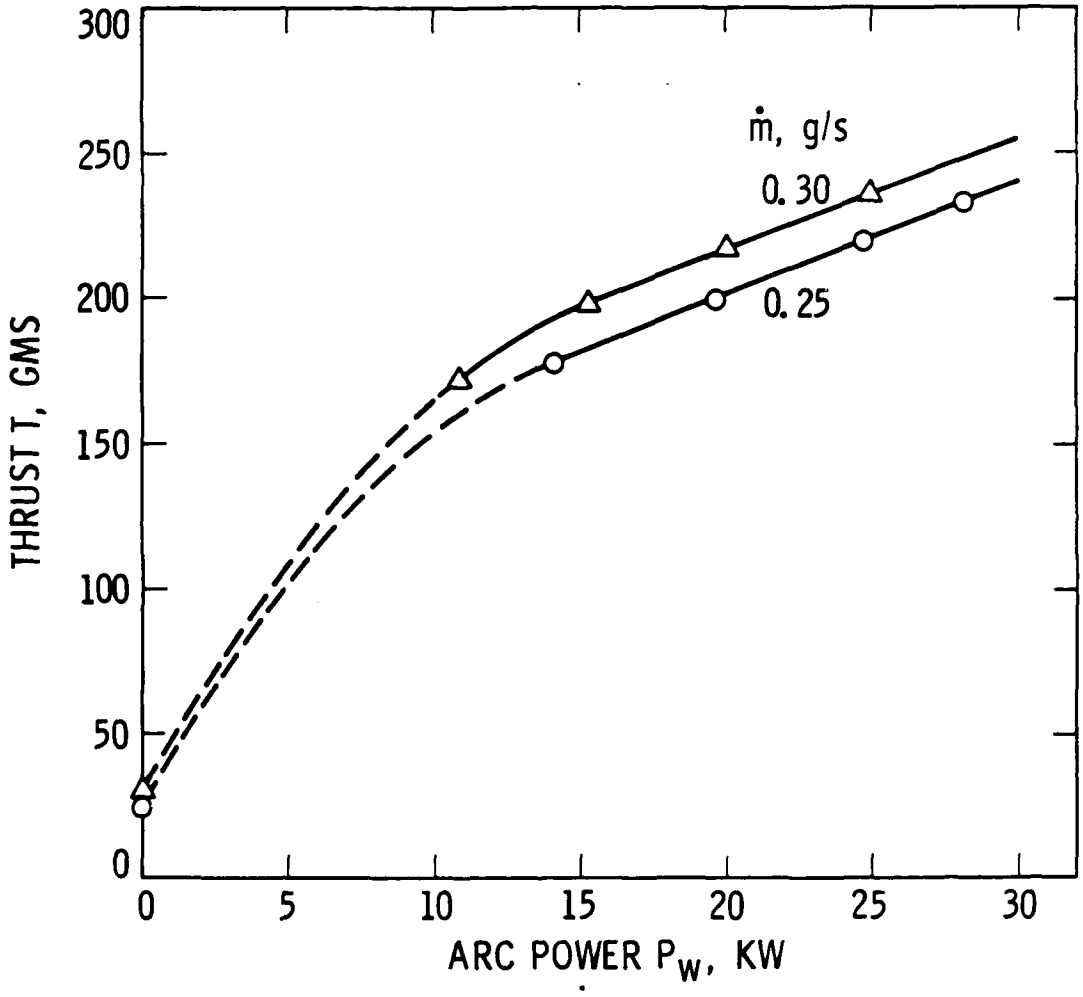

Figure 15. Effect of Arc Power and Ammonia Mass Flow Rate on Thrust

voltage drop across the mercury pools and coaxial current feed. This correction was at most 0.75 V. The corrected current and voltage measurements are shown in Figs. 16a and 16b, respectively, as functions of arc power and ammonia mass flow rate, and in Fig. 17a as the voltage/current characteristic of this arc load at both mass flow rates. The load impedance, or voltage to current ratio, is shown in Fig. 17b as a function of arc power and ammonia mass flow rate. The ammonia mass flow rate was taken directly from the Sierra Instruments mass flow meter/controller since this instruments calibration indicated that the measurement was within 1% of the true value. This instrument was calibrated with nitrogen instead of ammonia and the results converted to ammonia by applying a correction (K factor) of 0.73.

The specific impulse (I_{sp}) and thrust efficiency (η_T) were calculated from the measured input power, ammonia mass flow rate and thrust. These results are shown in Figs. 18a and 18b, respectively, as functions of the two independent variables, power and mass flow rate. The I_{sp} and η_T were computed using

$$I_{sp} = T/g_o\dot{m} \tag{1}$$

$$\eta_T = T^2/2\dot{m}P_w, \tag{2}$$

where:

T = Thrust, N

$\dot{m}$ = mass flow, kg/s

g_o = mass to force conversion constant, N/kg

P_w = total applied arc power, J/s

The nozzle outer surface temperature, at a point 1 cm from the nozzle exit plane, was continuously measured with an infrared optical pyrometer. These corrected temperature measurements are shown in Fig. 19 as a function of engine power and ammonia mass flow rate.

The propellant pressure was measured in the thrust stand beam at a point just outside of the vacuum tank; see Fig. 2. These measurements were made with a strain gauge type pressure transducer. The engine chamber pressure would be less than these measurements by the pressure drop in the thrust stand beam, thrust stand fixture and propellant injector. These measured pressures are shown in Fig. 20a as a function of engine power and ammonia mass flow rate.

The vacuum tank pressure was measured, at a point just above the engine, with a capacitor-type pressure transducer rated for pressure between 10^{-3} and 1 torr. The output of this transducer was not dependent on gas composition. This transducer was zeroed both electronically and with reference to an ion gauge in a second vacuum system pumped by

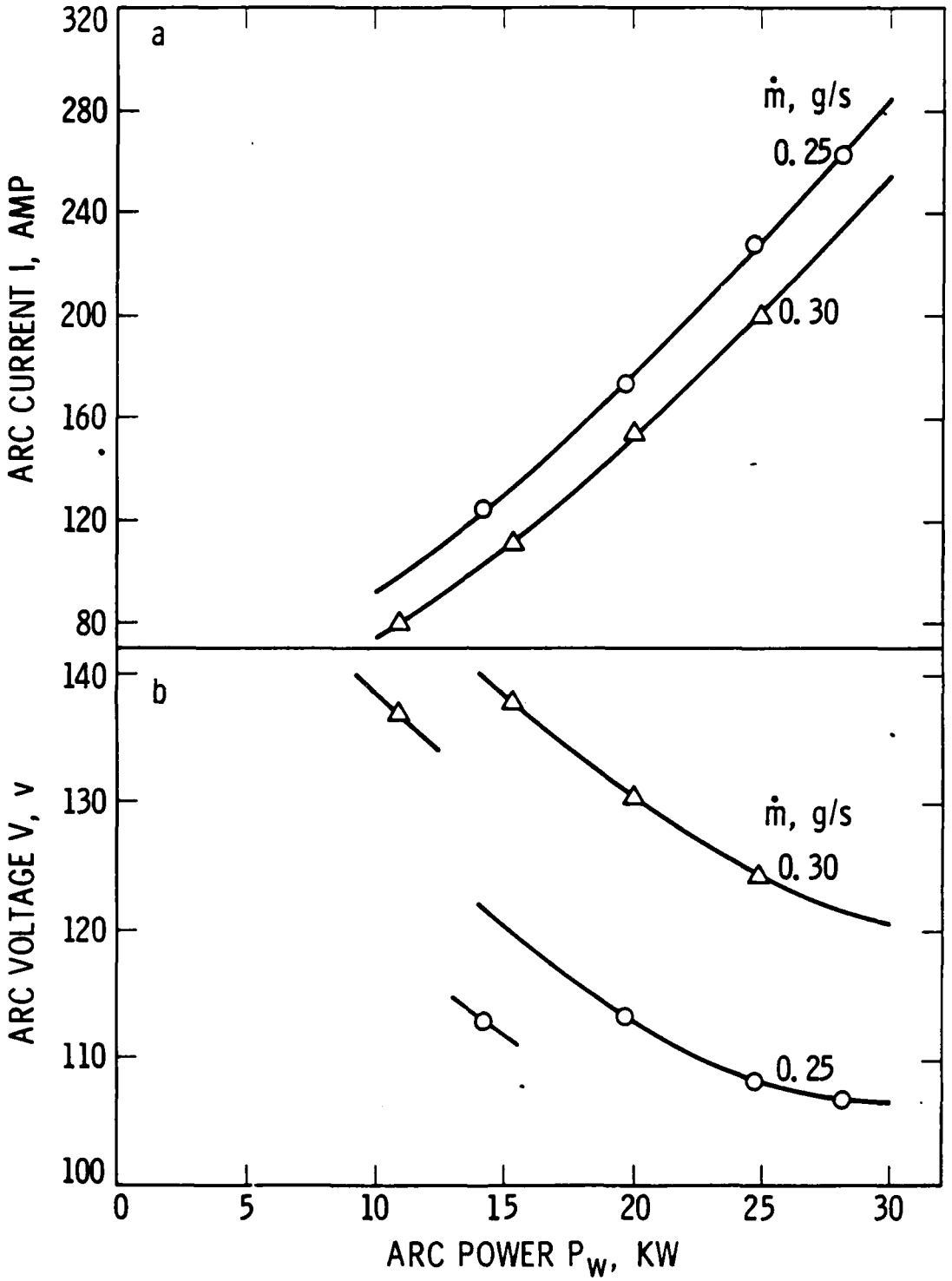

Figure 16 Effect of Arc Power and Ammonia Mass Flow Rate on Arc Current (a), and Arc Voltage (b)

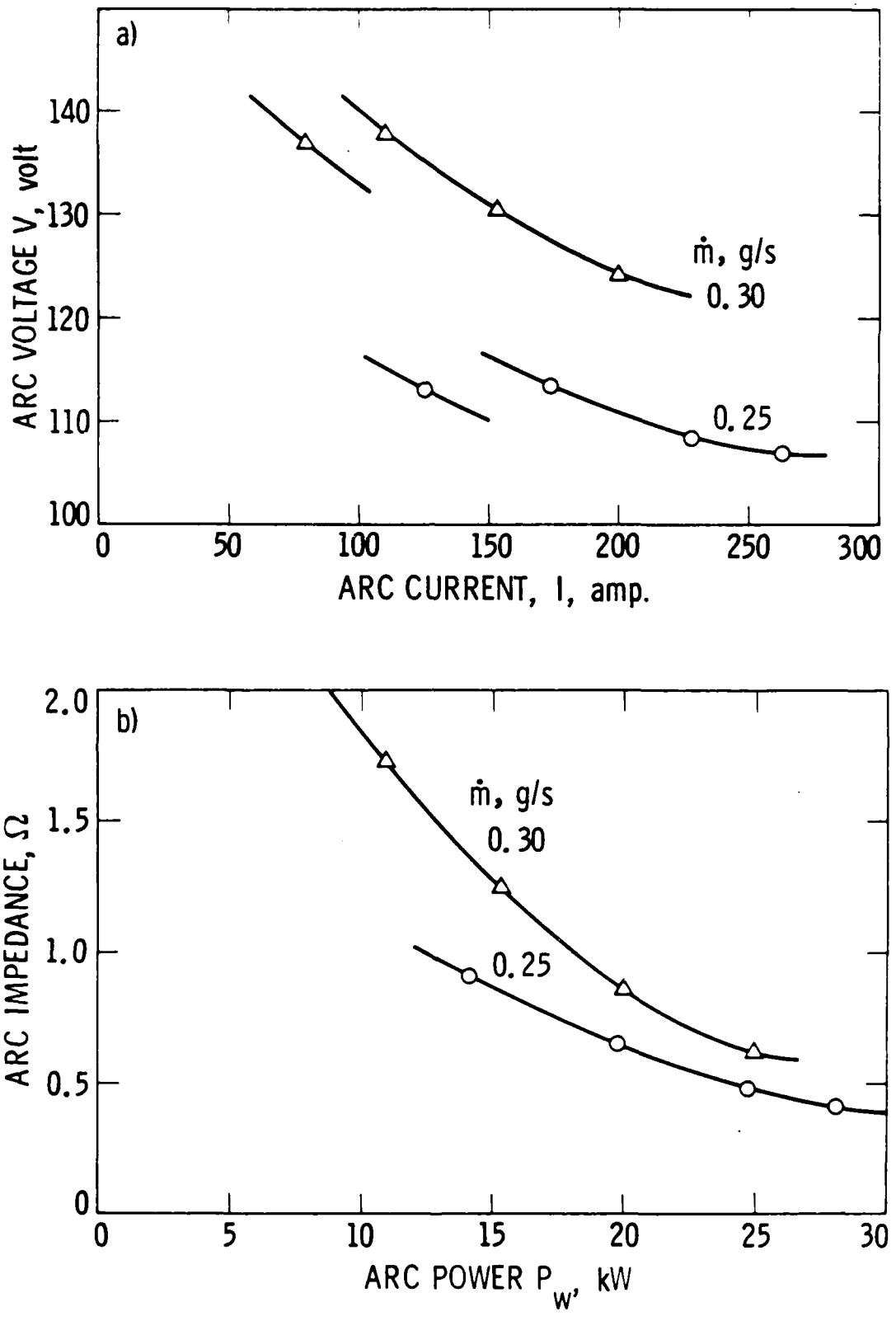

Figure 17. Arc Voltage/Current Characteristic at Two Ammonia Mass Flow Rates (a), Effect of Arc Power and Ammonia Mass Flow Rate on Arc Impedance (b)

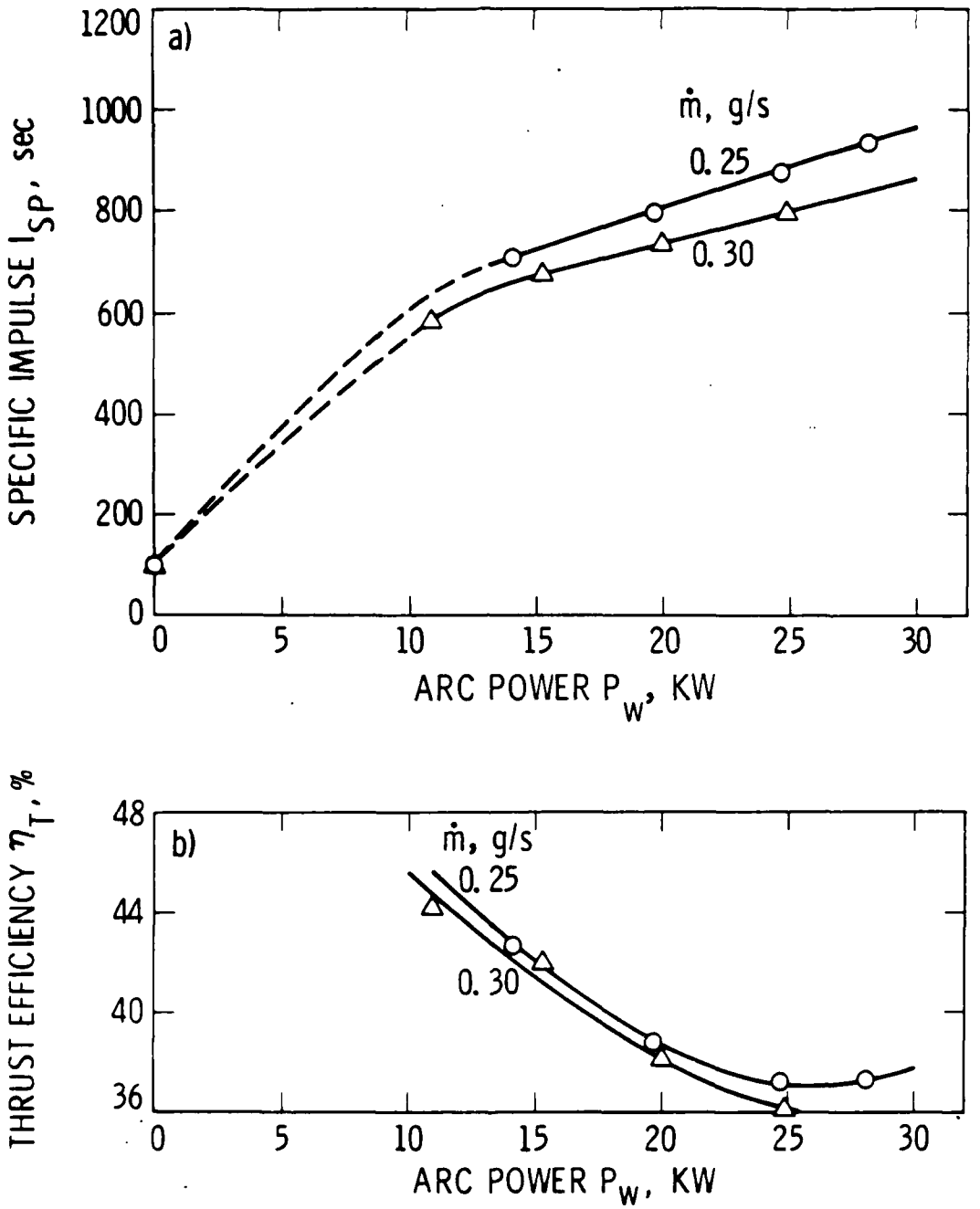

Figure 18. Effect of Arc Power and Ammonia Mass Flow Rate on Engine Specific Impulse (a), and on Engine Thrust Efficiency (b)

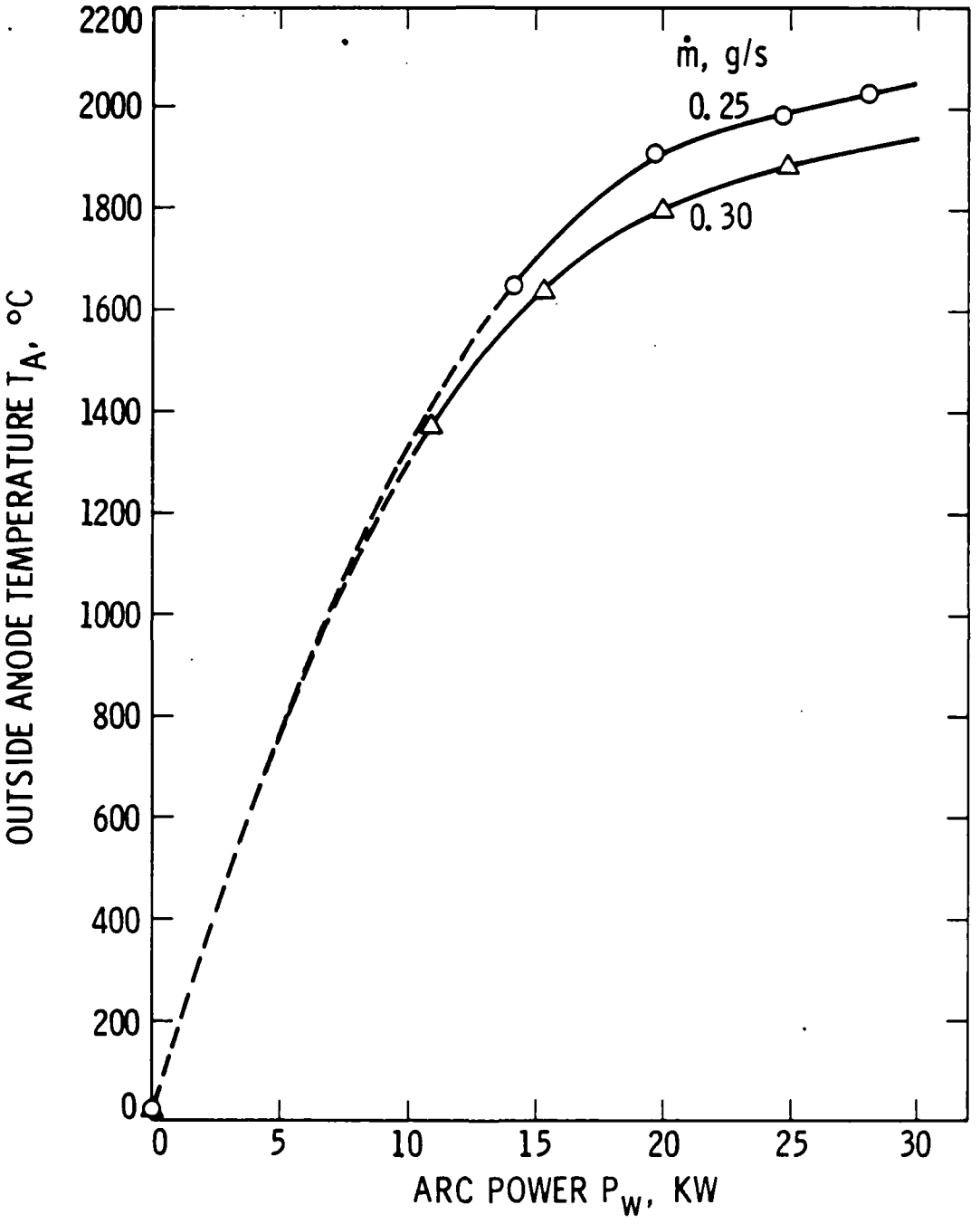

Figure 19. Effect of Arc Power and Ammonia Mass Flow Rate On Anode Outer Surface Temperature

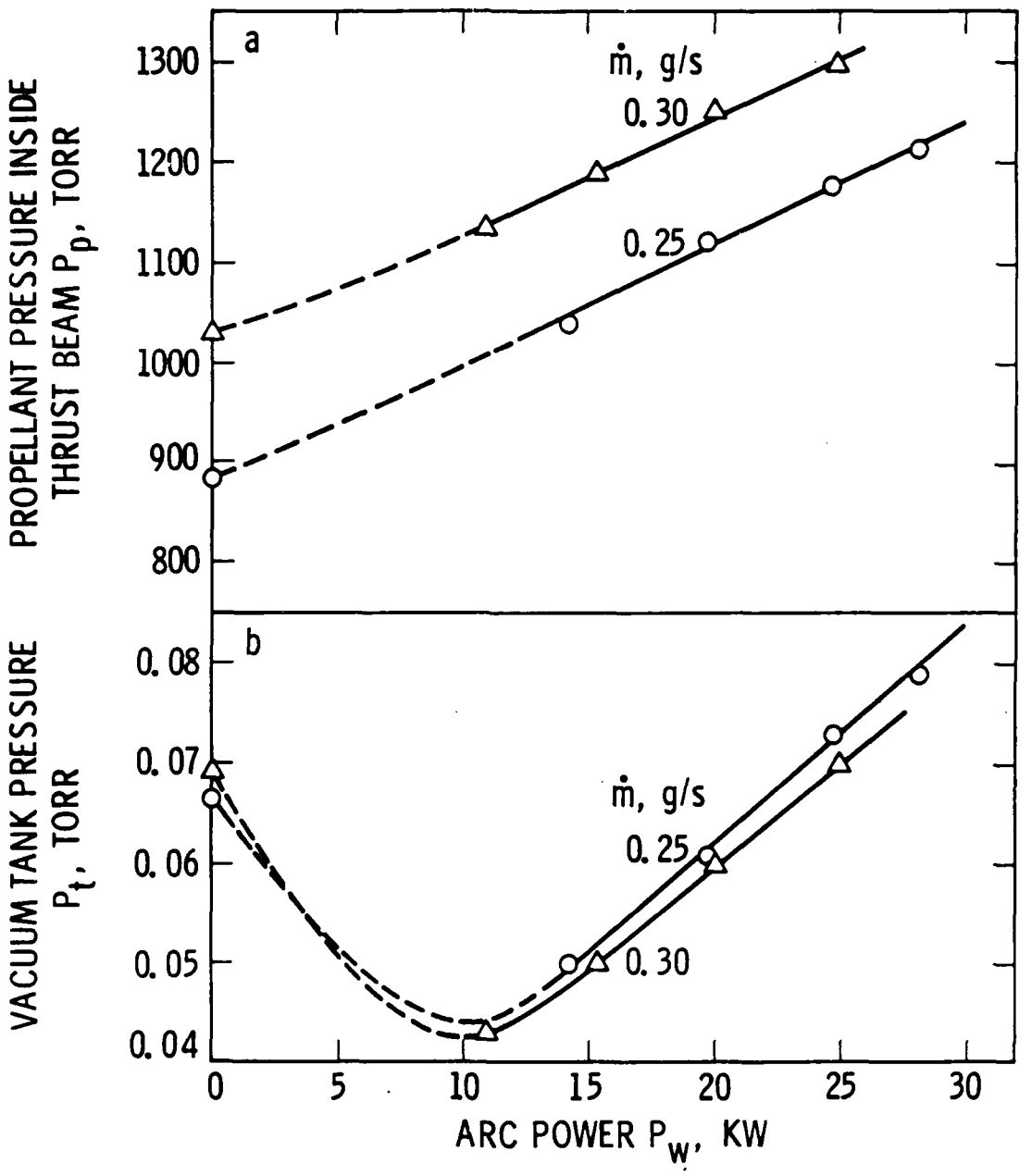

Figure 20. Effect of Arc Power and Ammonia Mass Flow Rate on Propellant Pressure (a), and Vacuum Tank Pressure (b)

diffusion pumps. The transducer output was also checked against a McCloud type pressure gauge. The measurements of vacuum tank pressure as a function of engine power and ammonia mass for rate are shown in Fig. 20b.

Section 5

LONG-DURATION TEST RESULTS

The arcjet engine and parts shown in Figs. 9, 10, 11 and 12 were tested for a period of 573 hours at power levels between 24 and 29 kW and ammonia mass flow rate of 0.25 and 0.27 g/s. The performance results of this long-duration test are given in Figs. 21 through 29. The overall performance of this arcjet engine are shown in terms of thrust efficiency and specific impulse vs. accumulated test time in Fig. 21. During this test a data point per minute was recorded. Out of this mass of data a data point every six hours was arbitrarily selected for the presentation shown in Fig. 21. Each data point was corrected for the same temperature effects and voltage drops discussed in the section of this report on "Performance Test Results."

In order to show how the efficiency and specific impulse varied with time in more detail, a block of data covering a 24-hour period was selected and a data point every 0.25 hours plotted vs. time for the presentation of Fig. 22. This block of data represents the test results between the 502nd and 526th hour of the test, as is indicated in Fig. 21. During this 24-hour period, the arc power was constant at 24.5 $\pm$ 0.5 kW and the ammonia mass flow rate was 0.271 $\pm$ 0.001 g/s.

Again, to show how the engine performance varied, in fine detail, a one hour block of data was selected and each recorded data point (one per minute) plotted vs. time in Fig. 23. This data was from the period 521st to 522nd hour of the test as is indicated in Figs. 21 and 22. During this period the power was 24.2 $\pm$ 0.1 kW and the ammonia mass flow rate was again 0.271 $\pm$ 0.001 g/s.

The same sequence of time periods and data frequency was used to illustrate the time variations of arc voltage and current, arc impedance (ratio of voltage to current), arc power, anode temperature, vacuum tank pressure and propellant pressure. In Fig. 24 the arc properties, voltage, current, impedance and power are shown at six-hour intervals for the entire test period. The voltage and power were corrected for the voltage drop in the coaxial current feed system. These same parameters are shown in more detail in Figs. 25 and 26 at 15- and 1-minute intervals, respectively.

Again, the anode temperature, vacuum tank pressure and propellant pressure at the thrust beam inlet are shown at six-hour intervals, Fig. 27, fifteen minute intervals, Fig. 28, and one-minute intervals, Fig. 29. The anode temperature data was corrected for window effect as discussed in the section of the report on "Performance Test Results." The pressure data required no corrections and is shown as recorded.

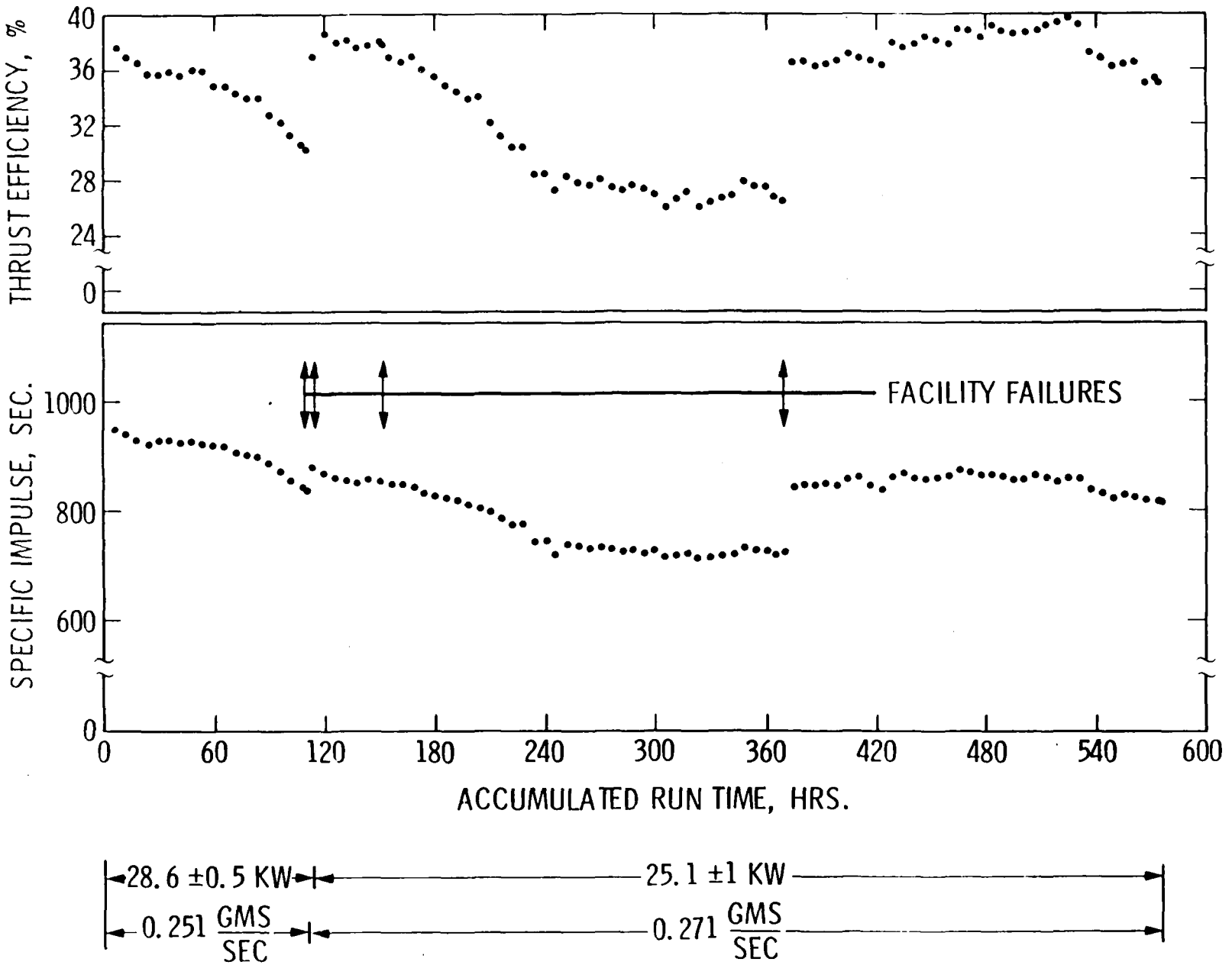

Figure 21. Thrust Efficiency and Specific Impulse vs. Accumulated Run Time with One Data Point Per Six Hours

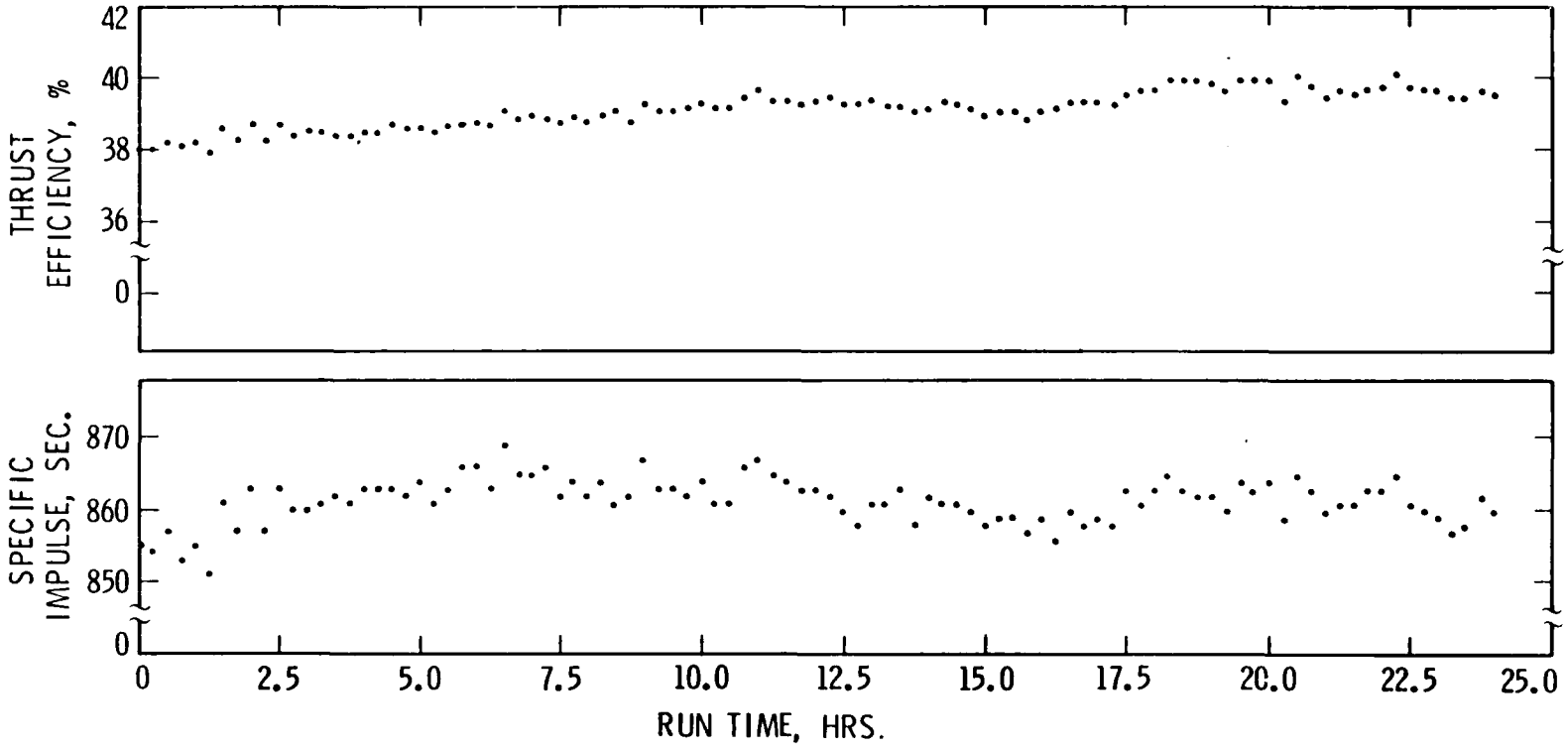

Figure 22. Thrust Efficiency and Specific Impulse vs. Time for a Specific Twenty-Four Hour Period with One Data Point Per Quarter Hour

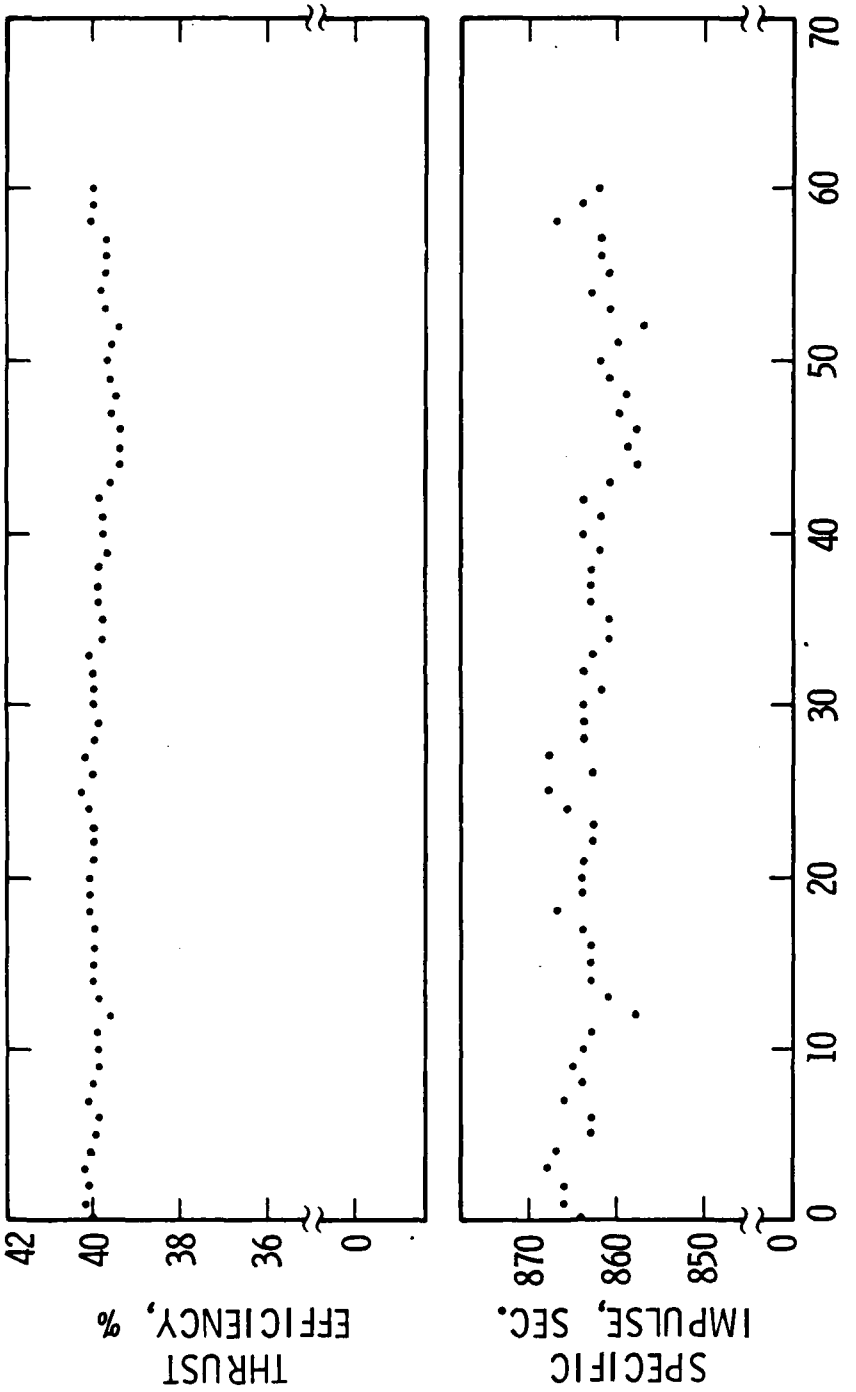

Figure 23. Thrust Efficiency and Specific Impulse vs. Time for a Specific One-Hour Period with One Data Point Per Minute

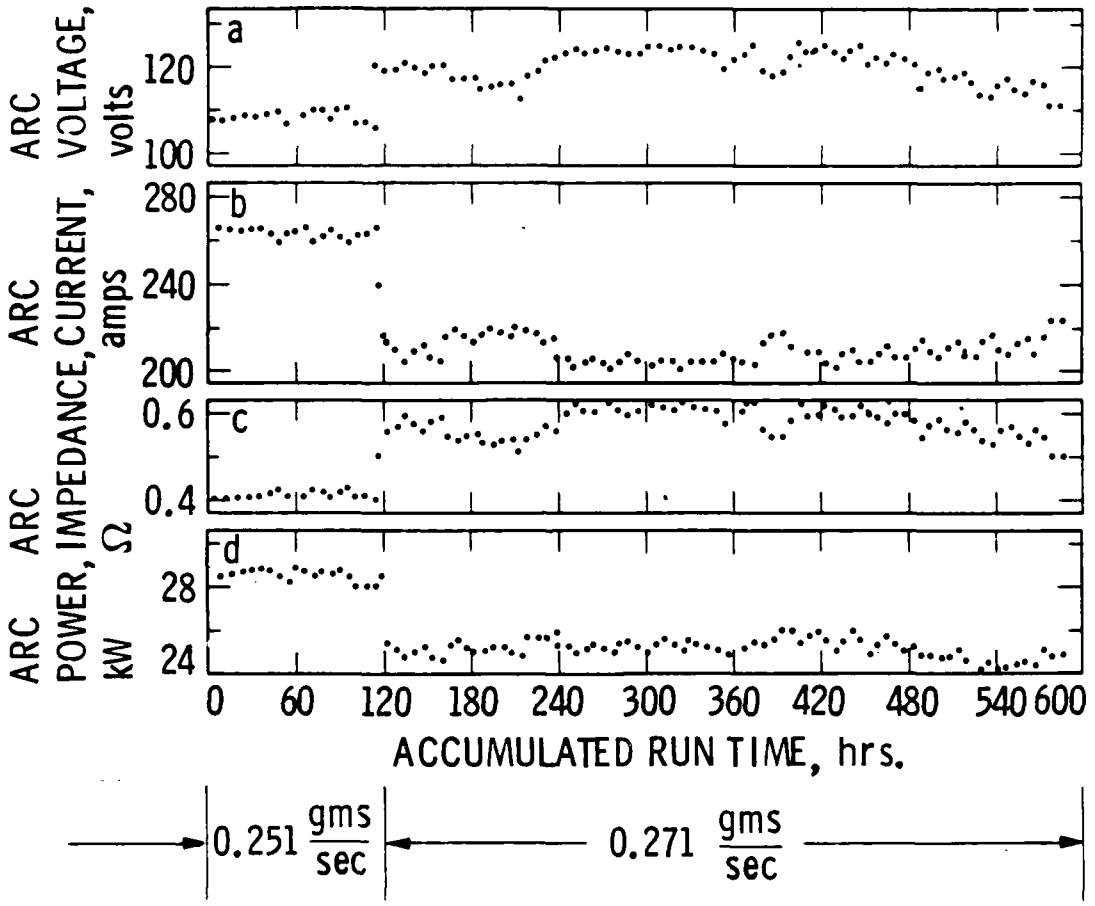

Figure 24. Arc Voltage (a), Current (b), Impedance (c), and Power (d) vs. Accumulated Run Time with One Data Point Per Six Hours

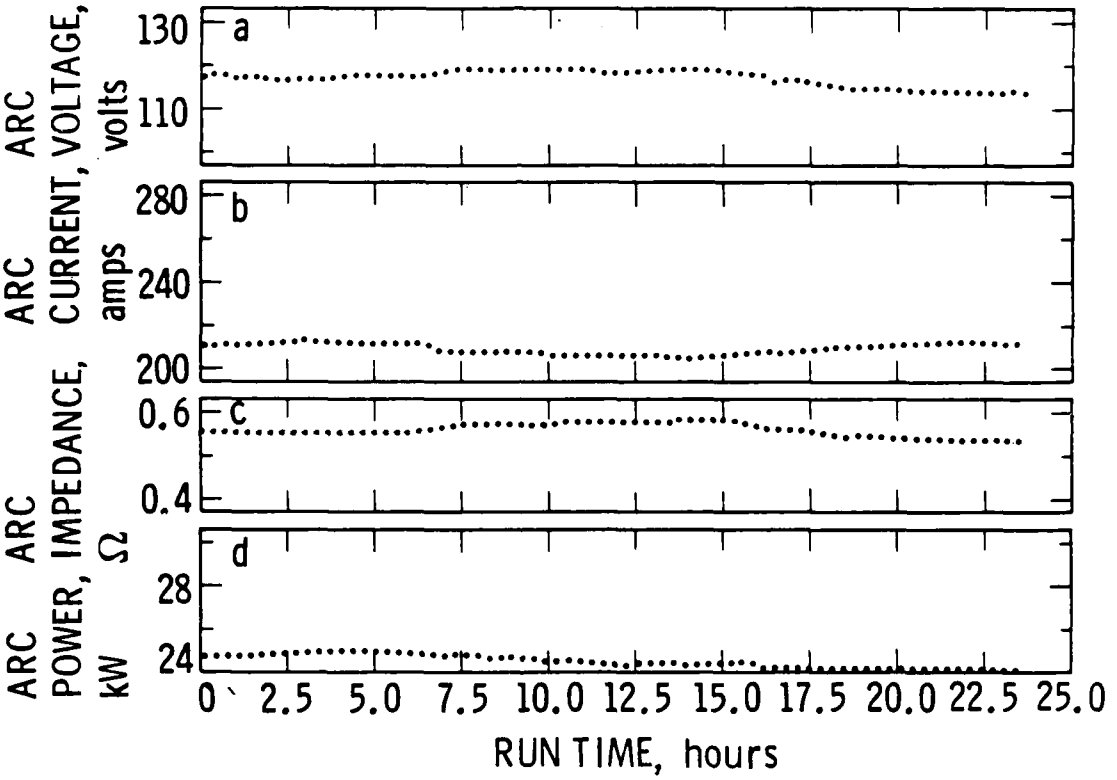

Figure 25. Arc Voltage (a), Current (b), Impedance (c), and Power (d) vs. Time for a Specific Twenty-Four-Hour Period with One Data Point Per Quarter Hour

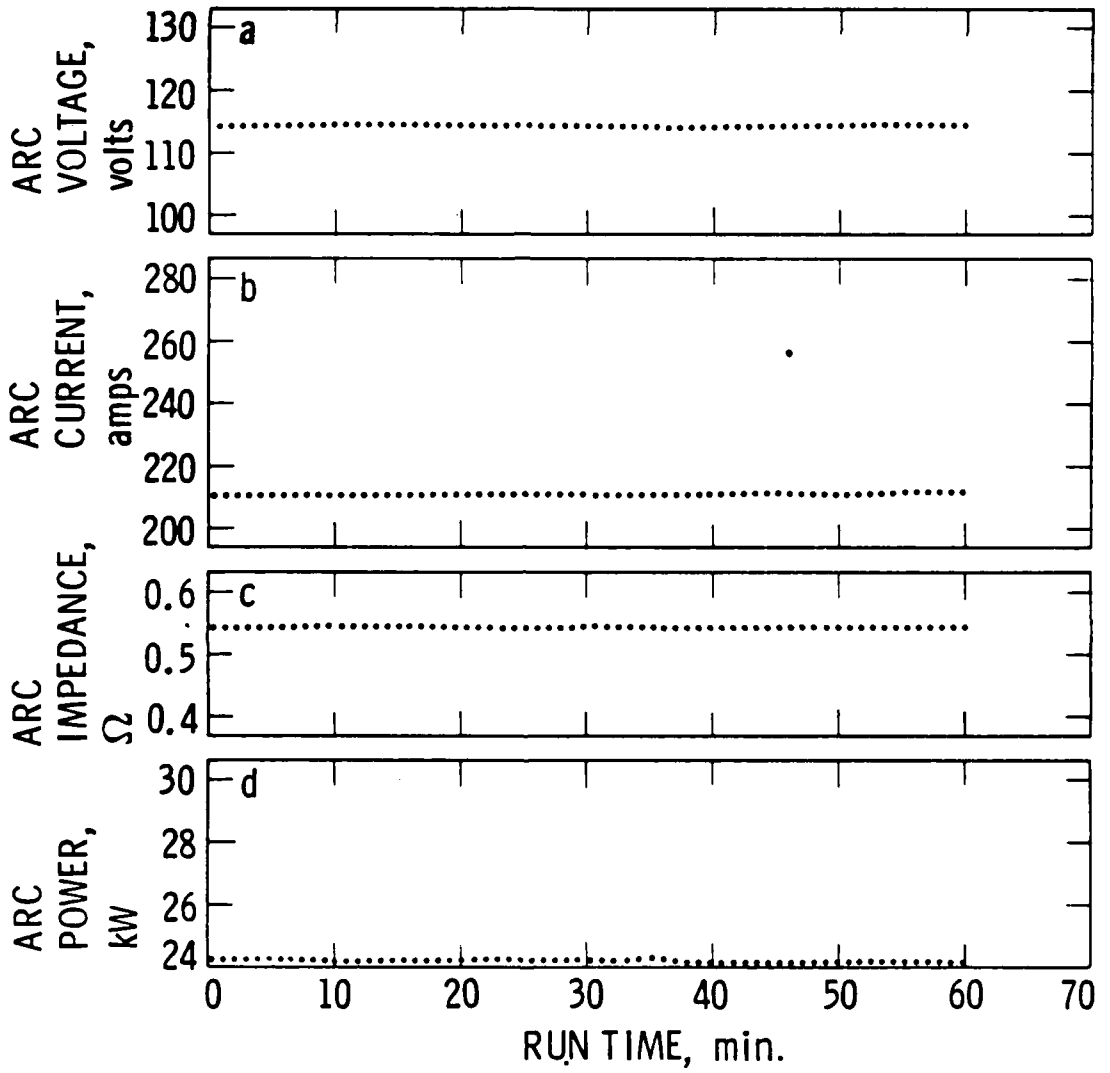

Figure 26. Arc Voltage (a), Current (b), Impedance (c), and Power (d) vs. Time for a Specific One-Hour Period with One Data Point Per Minute

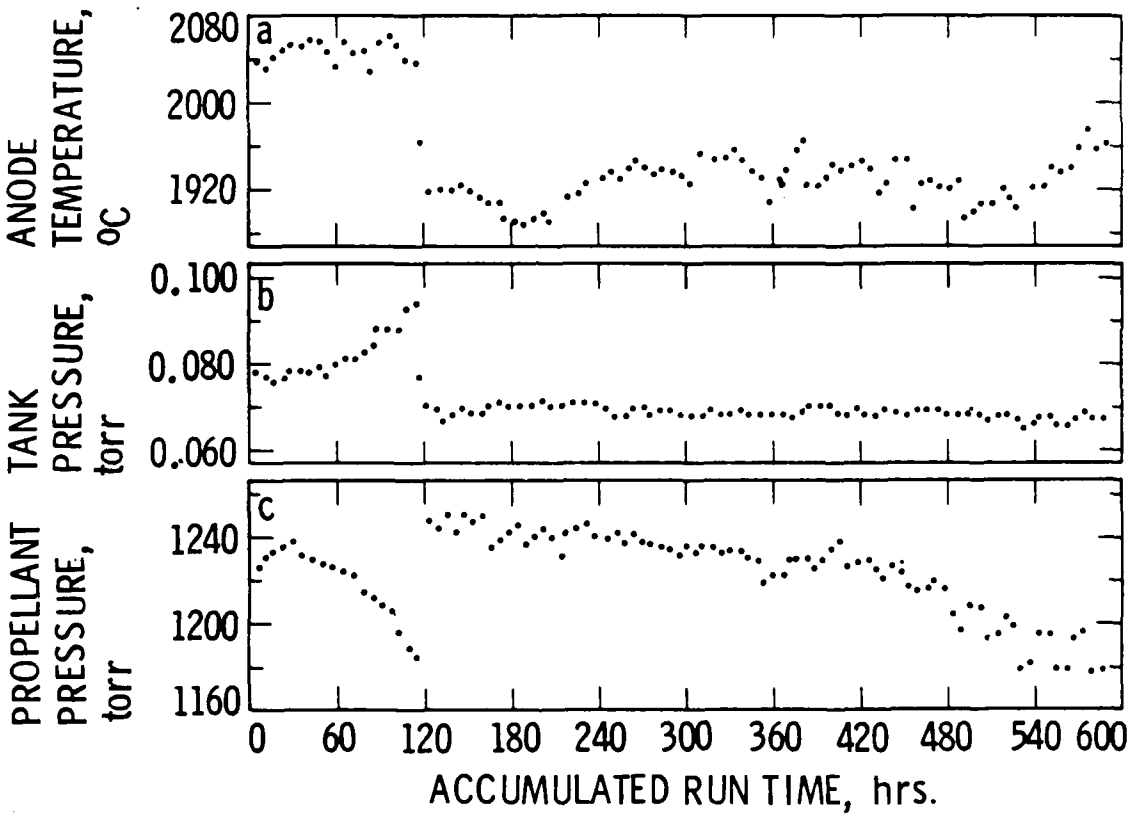

Figure 27. Anode Temperature (a), Vacuum Tank Pressure (b), and Propellant Pressure (c) vs. Accumulated Run Time with One Data Point Per Six Hours

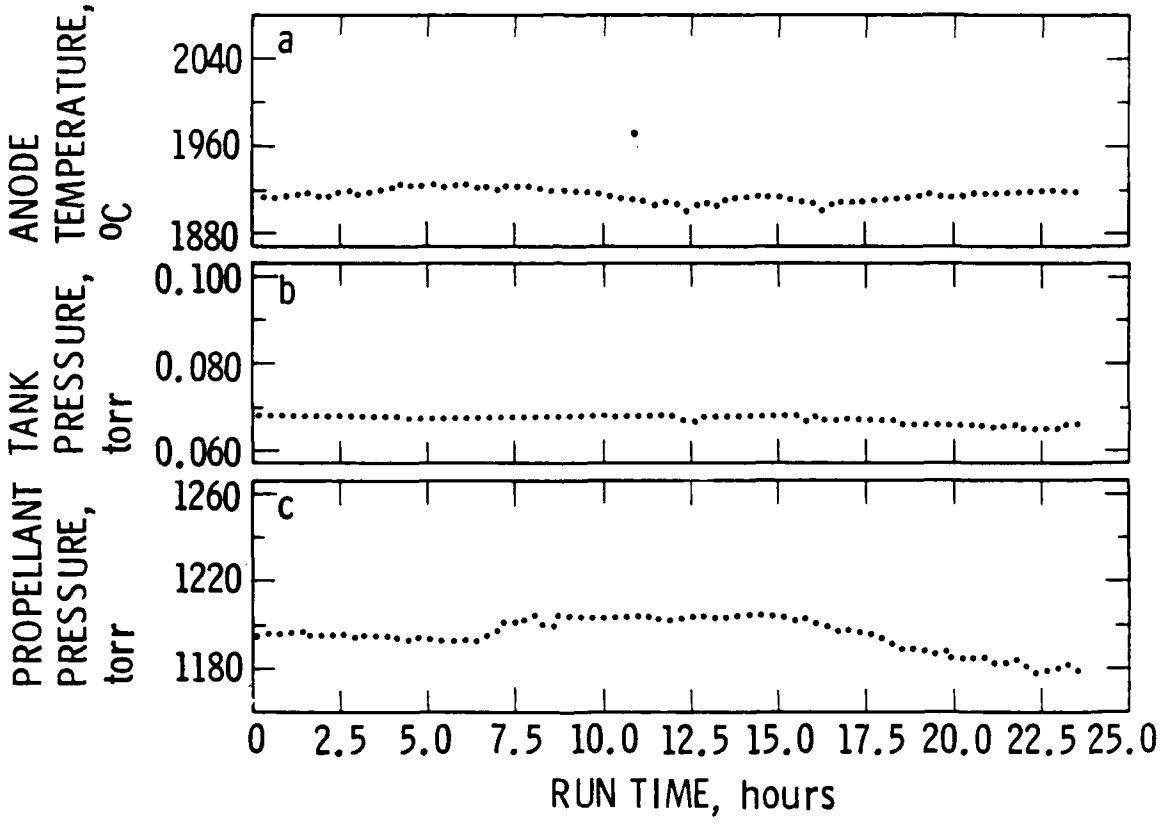

Figure 28. Anode Temperature (a), Vacuum Tank Pressure (b), and Propellant Pressure (c) vs. Time for a Specific Twenty-Four Hour Period with One Data Point Per Quarter Hour

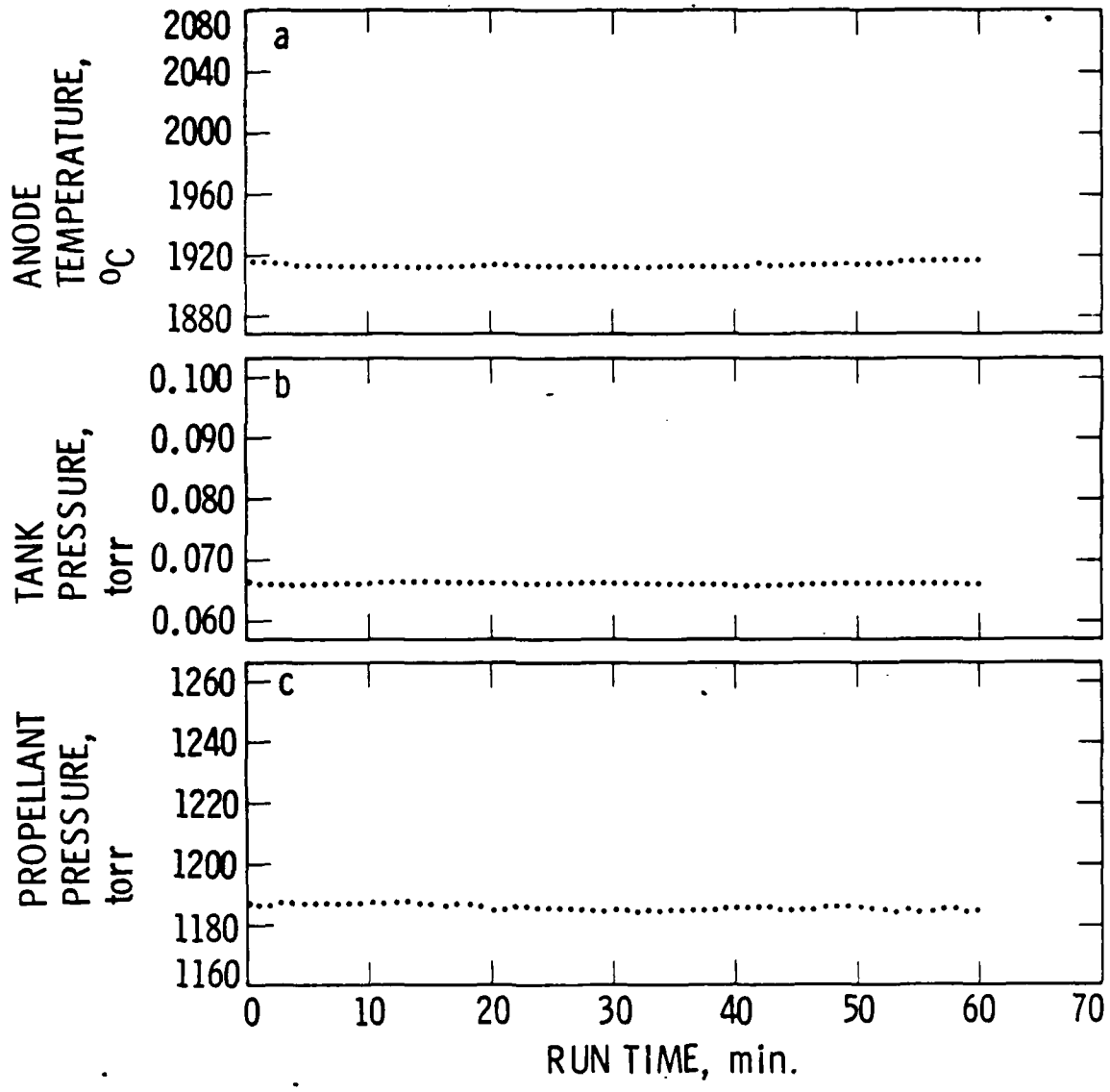

Figure 29. Anode Temperature (a), Vacuum Tank Pressure (b), and Propellant Pressure (c) vs. Time for a Specific One-Hour Period with One Data Point Per Minute

Section 6

DISCUSSION

6.1 Performance Test Results

For a device like an arcjet engine the thrust is proportional to the square root of the product of propellant mass flow rate and power available for producing thrust. This power is the difference between the power given to the propellant by the arc and the power lost the walls, to frozen flow losses, nozzle losses and incomplete expansion or

$$T = (2\dot{m}[\eta_a P_w - P_l])^{1/2} \qquad (3)$$

where η_a is the arc efficiency, and has been found to be 90 to 95% in a high pressure gas (Ref. 6) and P_l represents the sum of all other power losses. The data of Fig. 15 generally follows Equation 1. We show a finite thrust at zero power because of the power represented by the plenum chamber pressure. This power is not included in Equation 1 since P_w is just the electrical power dissipated by the engine.

The arc current and voltage are shown in Figs. 16a and 16b, respectively. The voltage decreases with increasing power because the plasma temperature, and therefore its electrical conductivity, increases as the power is increased. It is believed that at low power, for each mass flow rate, the arc was operating in a different mode. Perhaps this is due to a different, more upstream anode attachment point for the arc. The arc voltage increases with mass flow rate because the fluid pressure in the constrictor increases with mass flow rate (see Fig. 20a), and an increased pressure causes the electrical conductivity to decrease. Since, in these experiments, we are using a current-controlled power supply, the voltage will follow the current inversely as the mass flow and power level are changed. As shown in Fig. 16a, this results in the current increasing faster than linear with power and current decreasing with an increasing mass flow rate.

The arc voltage/current characteristic, for both mass flow rates, are shown in Fig. 17a. They both have a negative slope, which is expected of high pressure arcs, and again show the mode jump. The arc impedance, or voltage/current ratio, is shown in Fig. 17b. This load impedance demonstrates a large change with power and mass flow rate. This, again, is characteristic of high pressure arcs because the fluid conductivity is a strong function of the electron temperature, and therefore, of arc power and gas pressure. Note that the mode jump is not evident when the data is plotted as impedance.

The calculated specific impulse (I_{sp}) and thrust efficiency (η_T) are shown in Fig. 18. Since I_{sp} is proportional to thrust for a constant ammonia mass flow rate (see Eq. 1), the data in Fig. 18a follows the thrust data of Fig. 15. The thrust efficiency, η_T goes as the thrust squared (see Eq. 2).

The thrust efficiency decreases as the input power increases because the electrode losses, convective heat transfer losses to the

nozzle wall and frozen flow losses all increase with input power. Hence, a smaller fraction of the increased input power goes toward increasing the thrust as P_w increases. The slight decrease in η_T with increasing mass flow rate is not understood at this time.

The anode (nozzle) outer surface temperature is shown as a function of input power and ammonia mass flow rate in Fig. 19. This temperature increases with power because more absolute power must be dissipated at higher input power. Since at these low vacuum tank pressures (see Fig. 20b) the largest heat dissipation mechanism is radiation, which goes like the fourth power of the temperature, the temperature increase slows down as P_w increases. The fact that the temperature decreases with increasing ammonia mass flow rate is due to a decreased current (see Fig. 16a) causing decreased arc-anode losses and a decreased enthalpy, causing a lower convective heat transfer loss to the nozzle wall.

The propellant pressure inside the thrust beam and the vacuum tank pressure are shown as functions of input power and mass flow rate in Figs. 20a and 20b. The propellant pressure increase with power is due to the heat input to the propellant as it flows in the thrust beam, the thrust stand fixture and the engine. This increase is simply a demonstration that these parts get hotter with input power. In these experiments the engine is exhausting directly into a 16.5 cm diameter, straight, water-cooled diffuser in order to decrease the vacuum tank pressure. At any given arc power and ammonia mass flow rate the vacuum tank pressure will be determined by the dynamic properties of the jet and how it interacts with the diffuser walls and on the temperature of the exhaust gases as they reach the constant volume vacuum pump inlet. About 75% of the plume power is removed in the first 60 cm of the water-cooled diffuser. Most, if not all, of the rest of the power is removed by a heat exchanger located between the diffuser exit and the pump inlet. The fact that the tank pressure drops significantly from zero to 10 kW suggests that the diffuser is effective. The fact that the pressure then increases with increased input power suggests that the jet-diffuser interaction is changing with power and possibly that the gas temperature at the pump inlet was also increasing with input power.

6.2 Long Duration Test Results

During the long duration arcjet engine test the engine was shut down five times. The first four interruptions were due to facility failures and the fifth and final shutdown was due to an engine failure. The times of the five shutdowns are marked in Fig. 21. The first, at 109 hours into the test, was caused by a short circuit inside the coaxial current feed. The autonomous control system detected the failure as a drop in voltage and minimized damage to the facility by immediately terminating the test. After cool down, the system was carefully inspected and it was found that the cause of the short circuit was a failure of the mercury-pot water cooling system. Deposits from the hard cooling water, on the inner walls of the cooling tubes, had broken free and had accumulated at a narrow fitting. This process caused the water flow rate to slowly decrease, allowing the mercury temperature to increase. It appears that the mercury reached its boiling point (80°C

at 0.094 torr., Ref. 7) and droplets were thrown up to bridge the 9 cm gap between exposed surfaces of the two electrodes (see Appendix B).

As the mercury slowly heated and evaporated the surface level dropped, causing the buoyancy force on the coaxial electrodes to decrease. The result of this effect was an apparent drop in measured thrust which shows up as the slow drop in efficiency and specific impulse seen in Fig. 21 during the first 109 hours of the test. This effect also shows up as a slow increase in vacuum tank pressure, due to the mercury vapor, seen in Fig. 27. A careful review of the data in Figs. 21 and 27 suggest that the mercury started heating up at about 60 hours into the test.

In order to repair the coaxial current feed system, the arcjet engine was removed from the thrust stand. The engine was not disassembled but it was photographed and the eight bolts tightened since they were found to be very loose. This loosening probably occurred during the engine cool-down since there is no noticeable voltage drop during the hot run, which would occur if a propellant leak had opened up. The thermal expansion of the boron nitride, Inconel 600 and titanium was greater than the molybdenum bolts (see Fig. 9), possibly causing further compression of the graphite gaskets and/or creep in the threads of the steel nuts.

A picture of the engine, after 109 hours of continuous testing, is shown in Fig. 30 and a close-up of the nozzle, constrictor and cathode tip in Fig. 31. Notice that the only apparent sign of change is an increase in constrictor diameter, from 0.51 to 0.58 cm., at the downstream end, estimated from the picture and known upstream diameter, and a very definite change to the cathode tip configuration. The cathode tip already appears to have a concave cavity forming, with a diameter of approximately 0.3 cm. An annular band or structure of crystals seems to be forming on the periphery of the cavity. More will be said about these changes in the section of this report on the results of material analysis.

The engine was re-installed on the thrust stand, the thrust stand re-calibrated and the test started for the second time. After an additional four hours of testing a vacuum tank window cracked and the test again had to be interrupted for facility repairs. This was accomplished quickly and the test restarted after an additional delay of about four hours. During this four-hour period it was decided that in order to reduce stress on the engine and facility, the remainder of the test would be at a reduced power and increased propellant mass flow rate. Therefore, when the test resumed, the power was set at 25kW and the ammonia mass flow rate at 0.271 g/s.

The test proceeded an additional 38 hours when the third facility failure occurred. This failure was detected by the autonomous control system as a sudden increase in vacuum tank pressure and it terminated the test successfully with no damage to the engine. This third facility failure was also caused by deposits in the diffuser water cooling lines

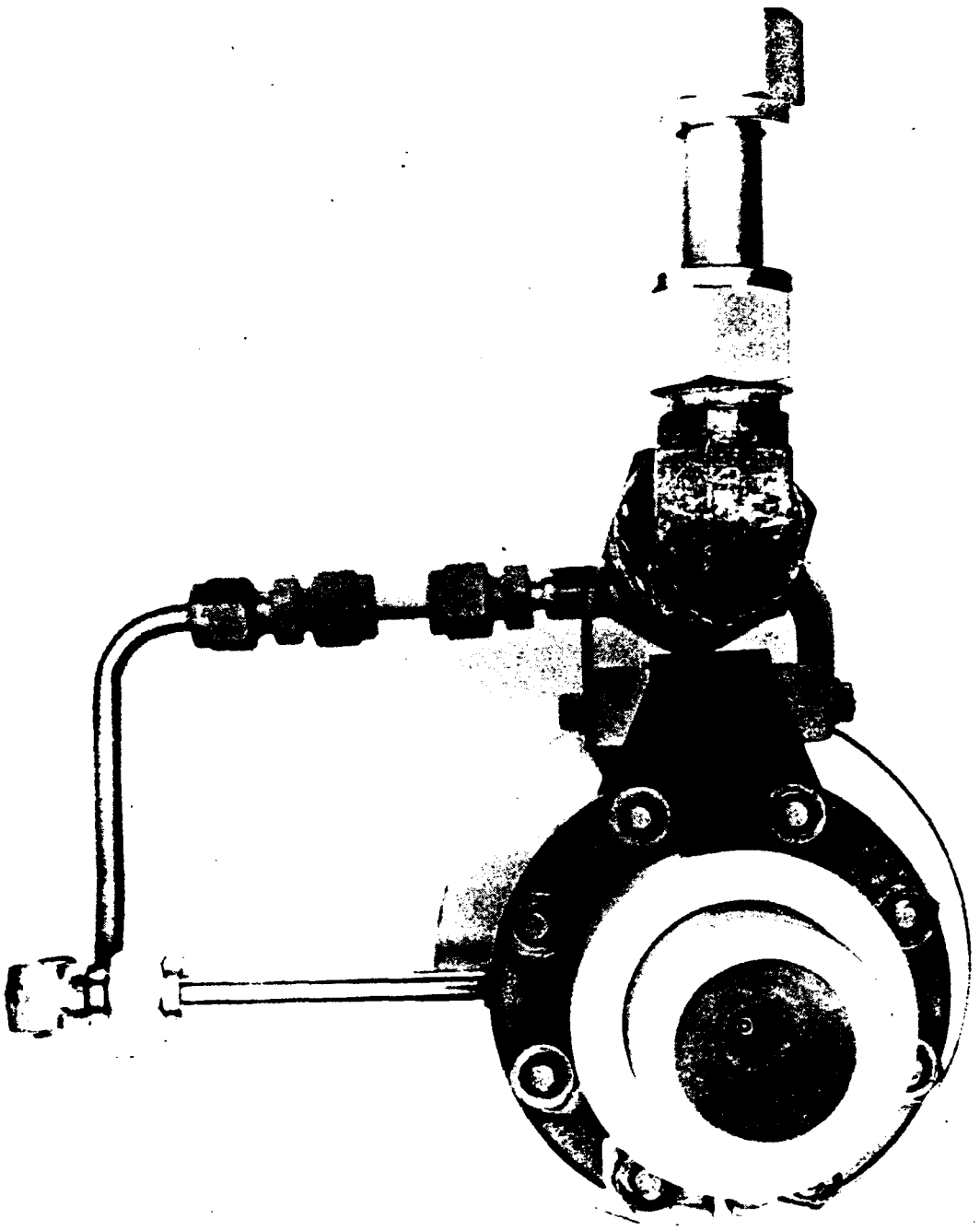

Figure 30. Photograph of Entire Engine After 109 Hours of Continuous Operation at 29 kW

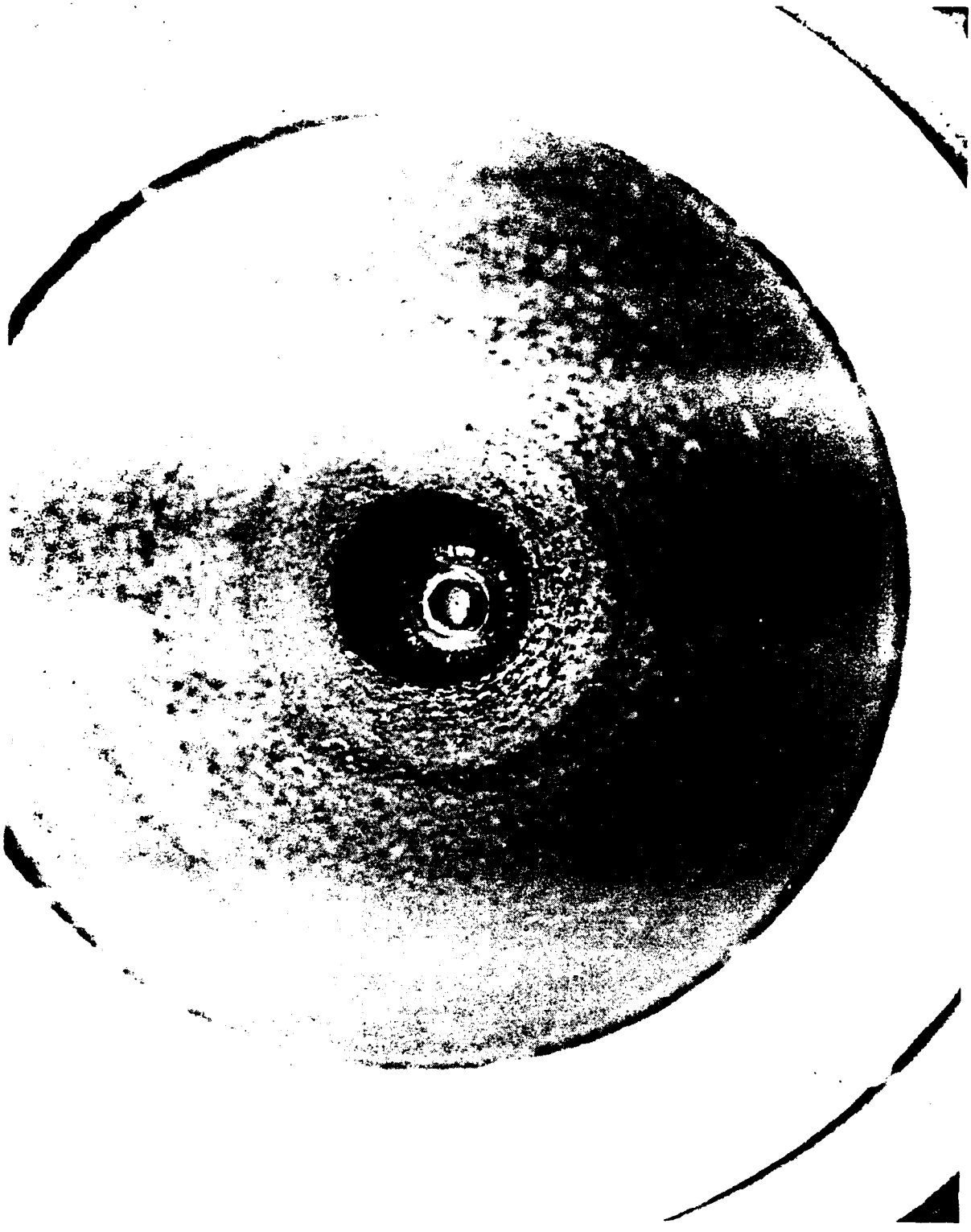

Figure 31. Photograph of Nozzle, Constrictor and Cathode after 109 Hours of Continuous Operation at 29 kW

reducing the water flow rate, resulting in a water leak, caused by overheating and rupturing of the coolant tube, and a sudden increase in vacuum tank pressure.

After repairing the diffuser the test was resumed and continued for 218 hours when the fourth and last facility failure occurred. The autonomous control system detected this failure as a voltage drop and again terminated the test with no damage to the engine. This failure was caused by an electrical breakdown between the bus bars that carry power to the mercury pots. They were insulated with silicone rubber tape and apparently the tape was punctured at a sharp corner. Only the rubber insulation was damaged and this was quickly repaired.

However, while the vacuum tank was opened, it was noticed that a layer of silicone diffuser pump oil on top of the mercury pools had solidified to a rubber-like consistency. Silicone oil had been floated onto the mercury to slow down mercury evaporation and apparently it solidified because of the heat and vacuum conditions. The effect of this solidification was to lock up the thrust stand and cause the apparent slow drop in thrust that can be seen in Fig. 21 from the 150th hour to about the 270th hour. This conclusion is confirmed by the fact that the thrust was again at the previous level after the silicone oil had been cleaned out of the mercury pools and the test restarted, as can clearly be seen in Fig. 21.

While the mercury pools were being cleaned the engine was again removed from the thrust stand, photographed and the eight nuts retightened. Fig. 32 shows a side-on view of the engine and indicates little effect of the 369 hours of accumulated run time. Fig. 33 is a picture of the nozzle, constrictor and cathode tip. It appears that the upstream end of the constrictor has not been eroded; however, the downstream diameter has increased from the original diameter of 0.51 cm to 0.68 cm. Also, the concave cavity forming in the cathode tip has increased in diameter to about 0.4 cm. The annular structure of crystals is still apparent on the periphery of the cavity.

After repairing the electrical insulation and cleaning out the silicone oil the engine was restarted and ran for an additional 204 hours with fairly constant performance, as can be seen in Fig. 21. The fact that the thrust efficiency increased from 36% to 40%, then back down to 35% during the period is not understood. The cause may be a similar but less obvious change in power and/or changes due to the erosion patterns of the cathode tip and constrictor. Note that as the efficiency dropped during the last 48 hours of the test the anode temperature increased. Since the anode temperature is a reflection of the amount of power flowing into the nozzle wall and since this power comes from the anode sheath drop and from heat transfer from the expanding gas stream, the increase in anode temperature implies an increase in sheath drop and/or an increase in heat transfer.

The remaining test parameters and calculations are shown in Figs. 24 and 27 for the entire test period. The scales have been greatly expanded in order to bring out detail that would otherwise be missed. The effect of changing power and ammonia mass flow rate at about 110 hours

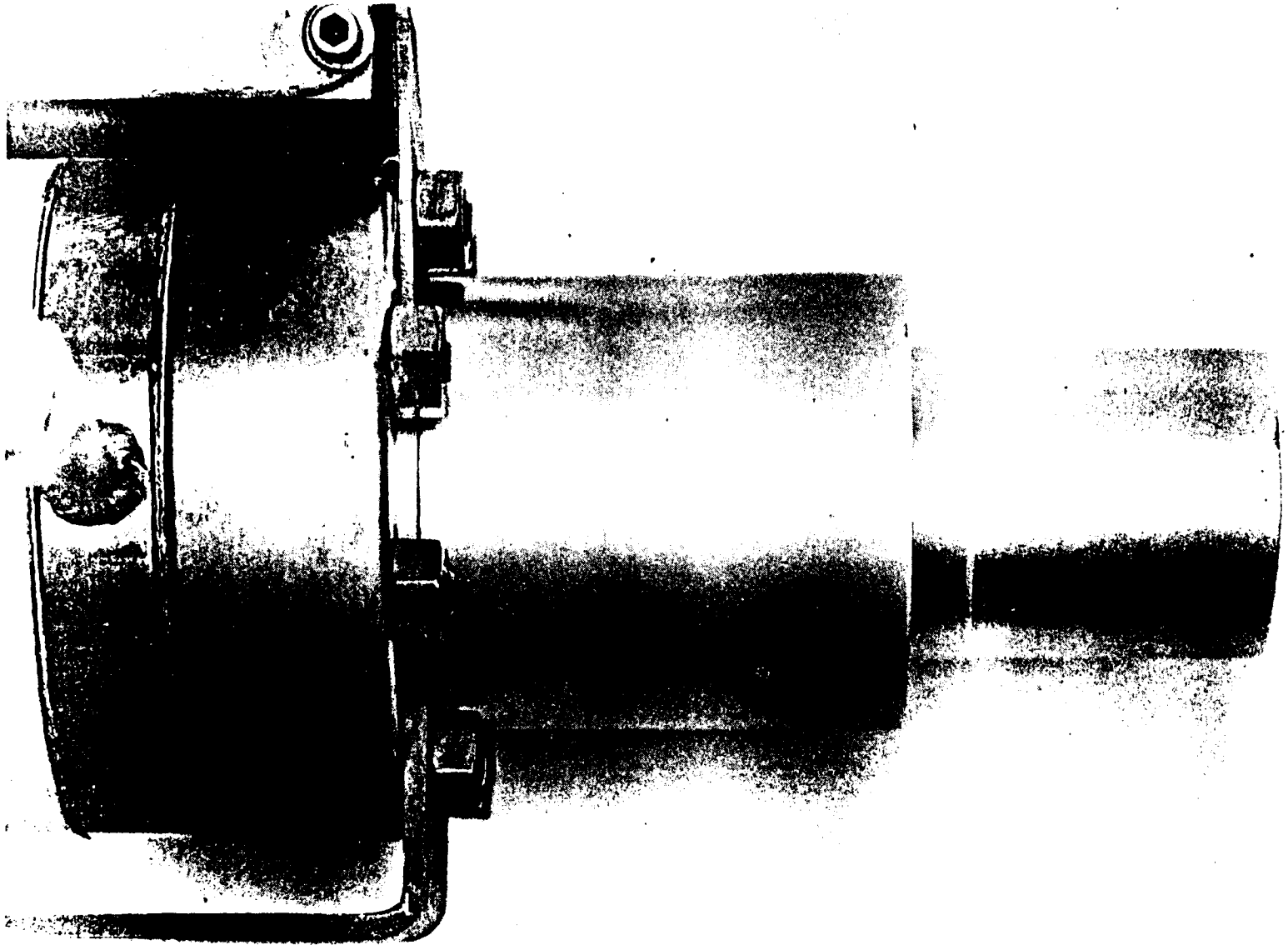

Figure 32. Photograph of Entire Engine After 369 Hours of Accumulated Run Time

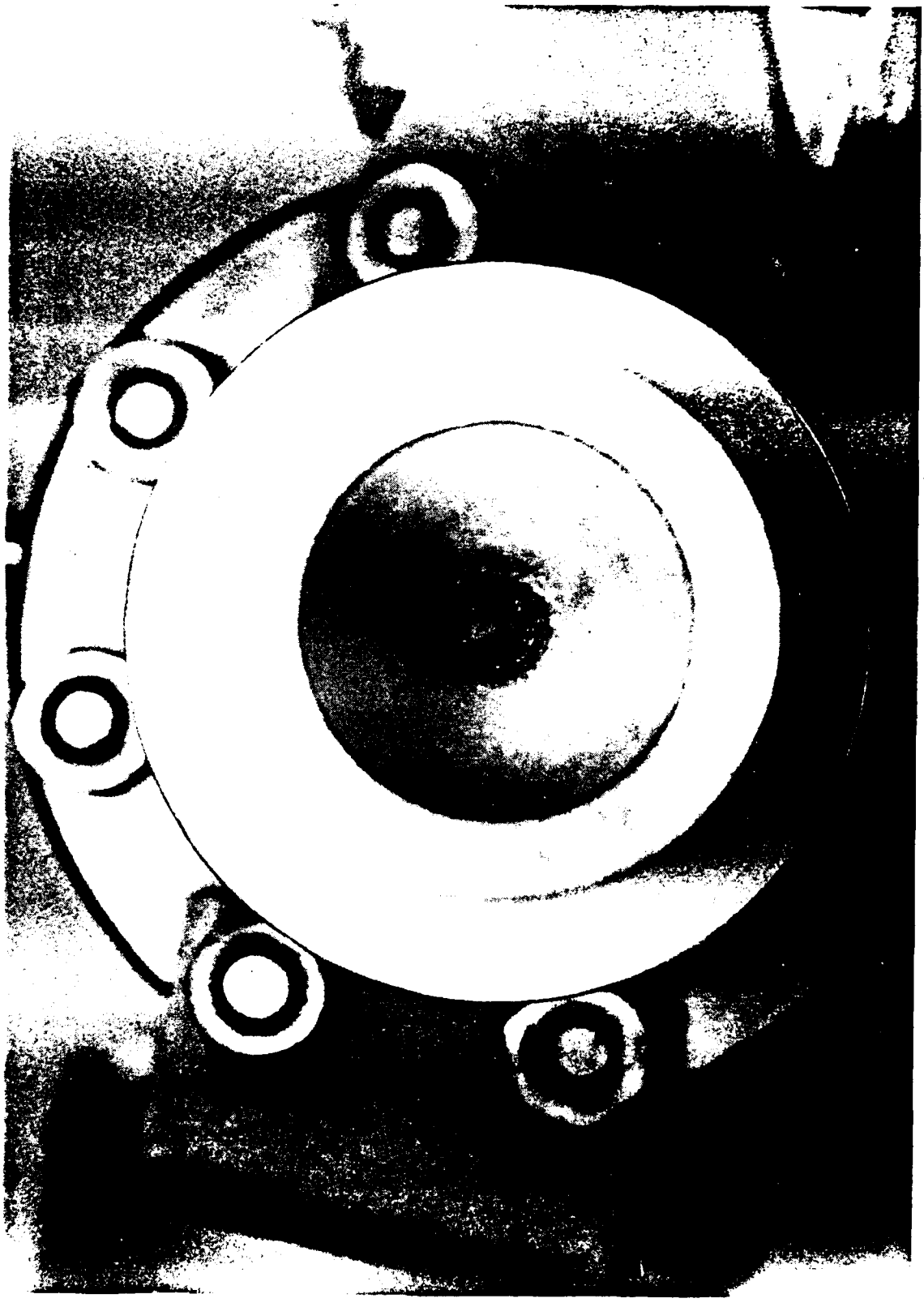

Figure 33. Photograph of Nozzle, Constrictor and Cathode after 369 Hours of Accumulated Run Time

into the test is apparent in each parameter. The amplitude of the fluctuations with time of each parameter, both before and after the power and mass flow rate change, are given in Table 2.

Table 2. Parameter Fluctuations During Long Duration Test

Parameter	% of mean, before	% of mean, after
Arc voltage	4	12
Arc current	3	11
Arc impedance	7	22
Arc power	3	8
Anode temperature	2	5
Vacuum tank pressure	21	9
Propellant pressure	4	6

Most of the variations are small and can be ascribed to a slow variation of the engine configuration due to erosion. There is also a periodic variation with a period of 24 hours. These can most easily be seen in the voltage, current, impedance and propellant pressure during the last 100 hours or so of the test. The cause of these fluctuations is not clear but it may be related to line voltage and ambient temperature fluctuations. The fluctuation of arc impedance is unusually high because the arc power supply is forced to operate on a negative characteristic so that as the voltage increases, the current must decrease. Also, the vacuum tank pressure, during the initial part of the test, shows a large increase because of the overheated mercury as was discussed above. A more detailed analysis of the entire body of data will be required to bring out all the correlations that are only hinted at in Figs. 21, 24 and 27.

To show the nature of these fluctuations with higher resolution, Figs. 22, 23, 25, 26, 28 and 29 have been prepared. In general, they indicate that this arcjet engine design is capable of very steady operation when the power, configuration and mass flow rate can be kept constant. The data in Figs. 22, 25 and 28 cover a 24-hour period from the 502nd to the 526th hour and one date point per 0.25 hour was arbitrarily selected. For Figs. 23, 26 and 29 a one-hour period (521st to 522nd hour) and one date point per minute are shown. The fluctuations of each parameter over both periods are given in Table 3.

Table 3. Parameter Fluctuations Over One and 24-Hour Periods

Parameter	% of mean for 24-hour period	% of mean for 1-hour period
Efficiency	6	2
Specific Impulse	2	1
Arc Voltage	5	1
Arc Current	4	1
Arc Impedance	8	1
Arc Power	4	1
Anode Temperature	1	<1
Vacuum Tank Pressure	5	<1
Propellant Pressure	2	<1

6.3 Engine Failure

At 573.14 hours into the test, the computer recorded the last line of normal data. The indicated voltage was 111.8 V and the power 24.92 kW. Thirty-nine seconds later it detected and reported a voltage drop to 99.9 V and power to 22.27 kW. Since the lower tolerance on voltage was set at 100 V at the time, the computer terminated the test. All other parameters looked normal when the test was terminated. Upon inspection, the only abnormalities that could be seen were two small tracks of tungsten, each terminated by a very small ball of tungsten, in the expansion nozzle. The engine was not removed from the thrust stand; however, a picture of the nozzle was taken with the aid of a mirror placed inside the diffuser inlet. This picture is shown in Fig. 34, with the tungsten tracts indicated.

The engine was restarted after the inspection and the start was normal, as was the transition from argon to ammonia with the power at about 10 kW. When the power was increased to about 16 kW a change in constrictor configuration occurred, as viewed from the diffuser, and the test was terminated. This time, on inspection, it was found that a great amount of damage was done to the constrictor wall. This damage can be seen in Fig. 35, taken after the engine was removed from the thrust stand. The engine was only then disassembled and carefully inspected and analyzed.

Beside the constrictor damage, which was sustained after termination of the long duration test, the only major effects of the test on the engine were erosion of the cathode tip, the constrictor wall, and of the propellant injection nozzle. A side view of the cathode tip before and after the long duration test is shown in Fig. 36. The before picture is of a second cathode machined to the same specification as was the used cathode. Note the crystal growth around the periphery of the central hemispherical cavity first noted at 109 hours and then again at 369 hours. It is surmised that one of those crystals grew long enough to either touch the anode near the constrictor entrance or got close

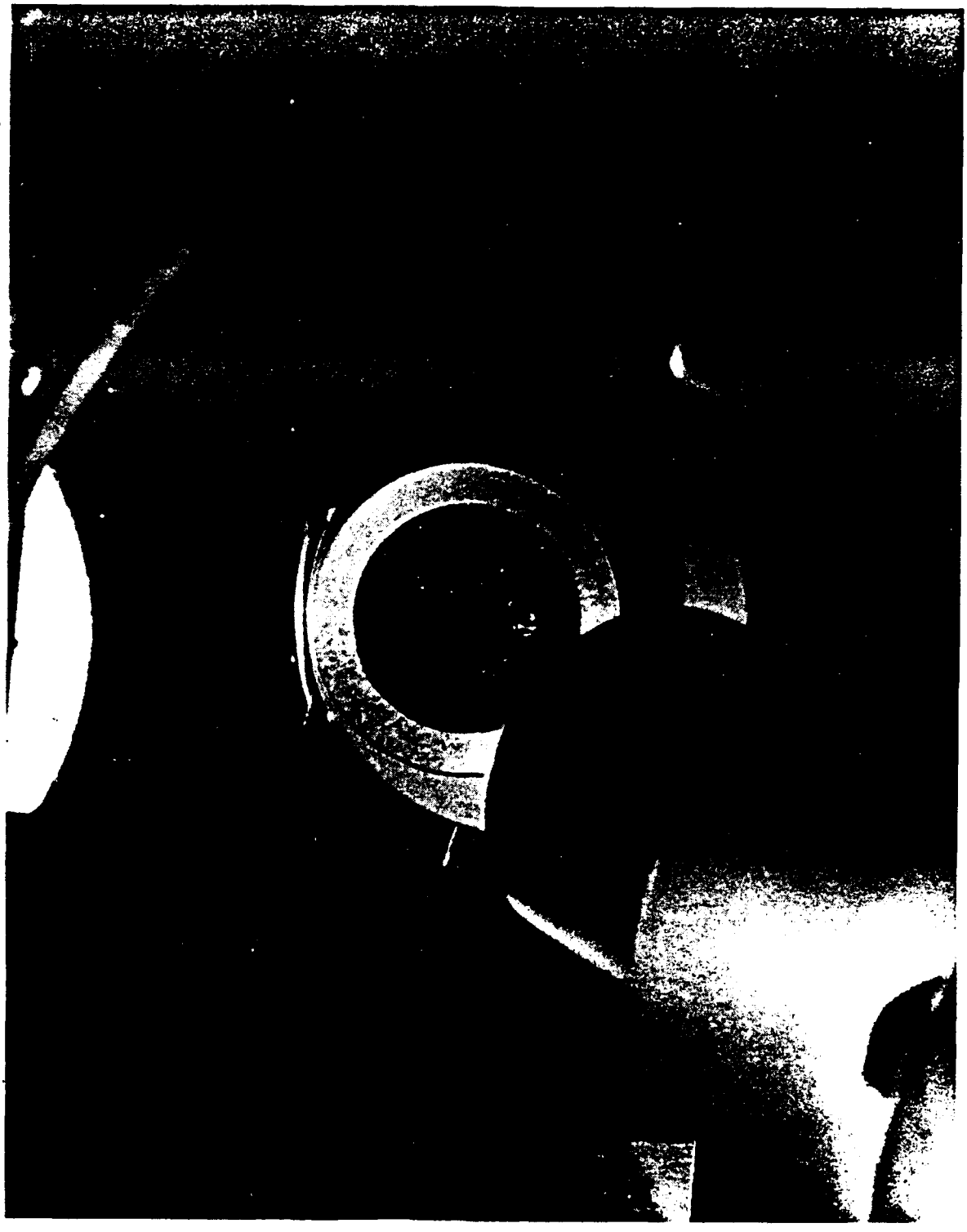

Figure 34. Photograph of Nozzle, Constrictor and Cathode After 573 Hours of Accumulated Run Time

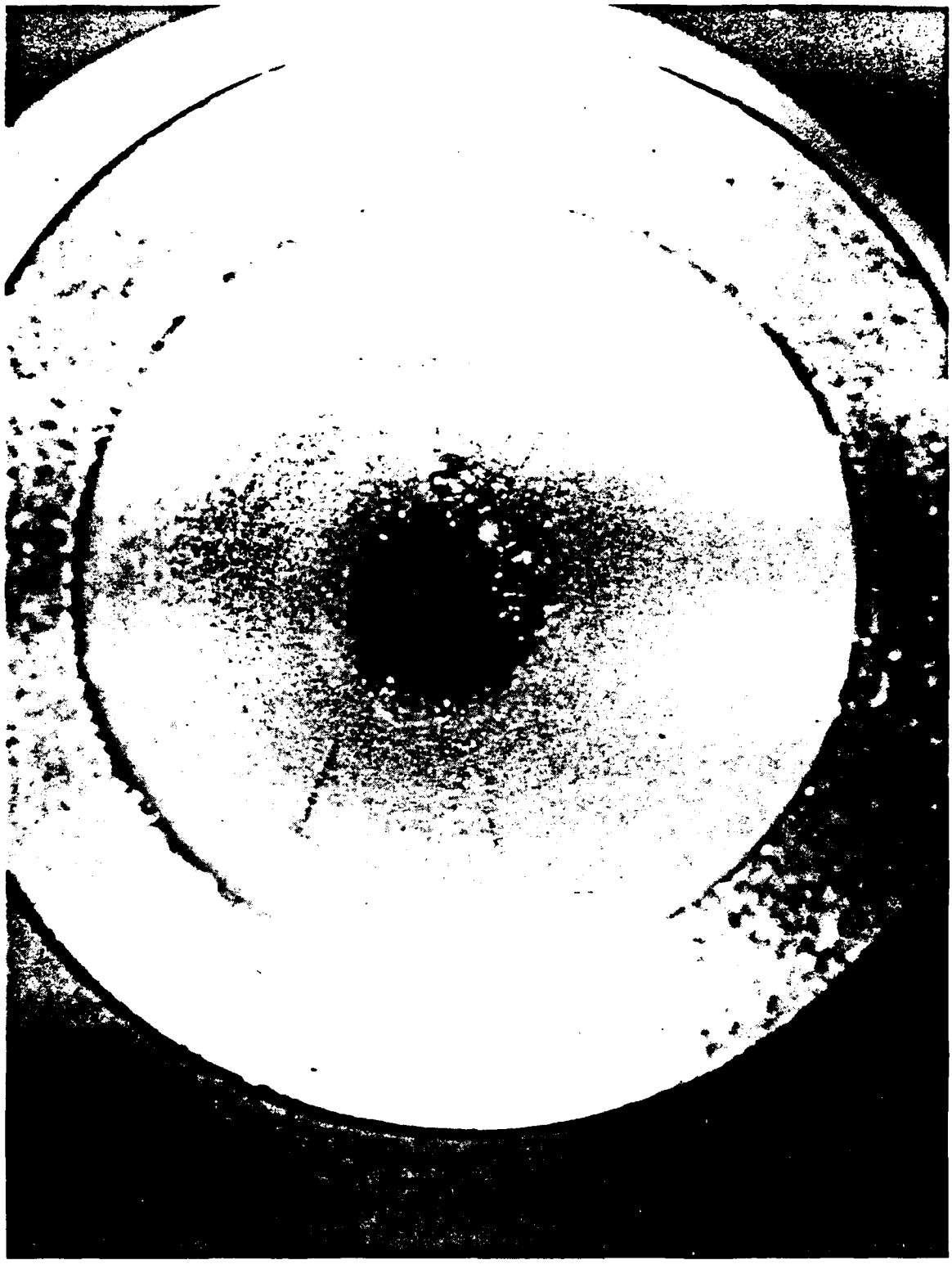

Figure 35. Close-up of Nozzle and Constrictor After Attempted Restart

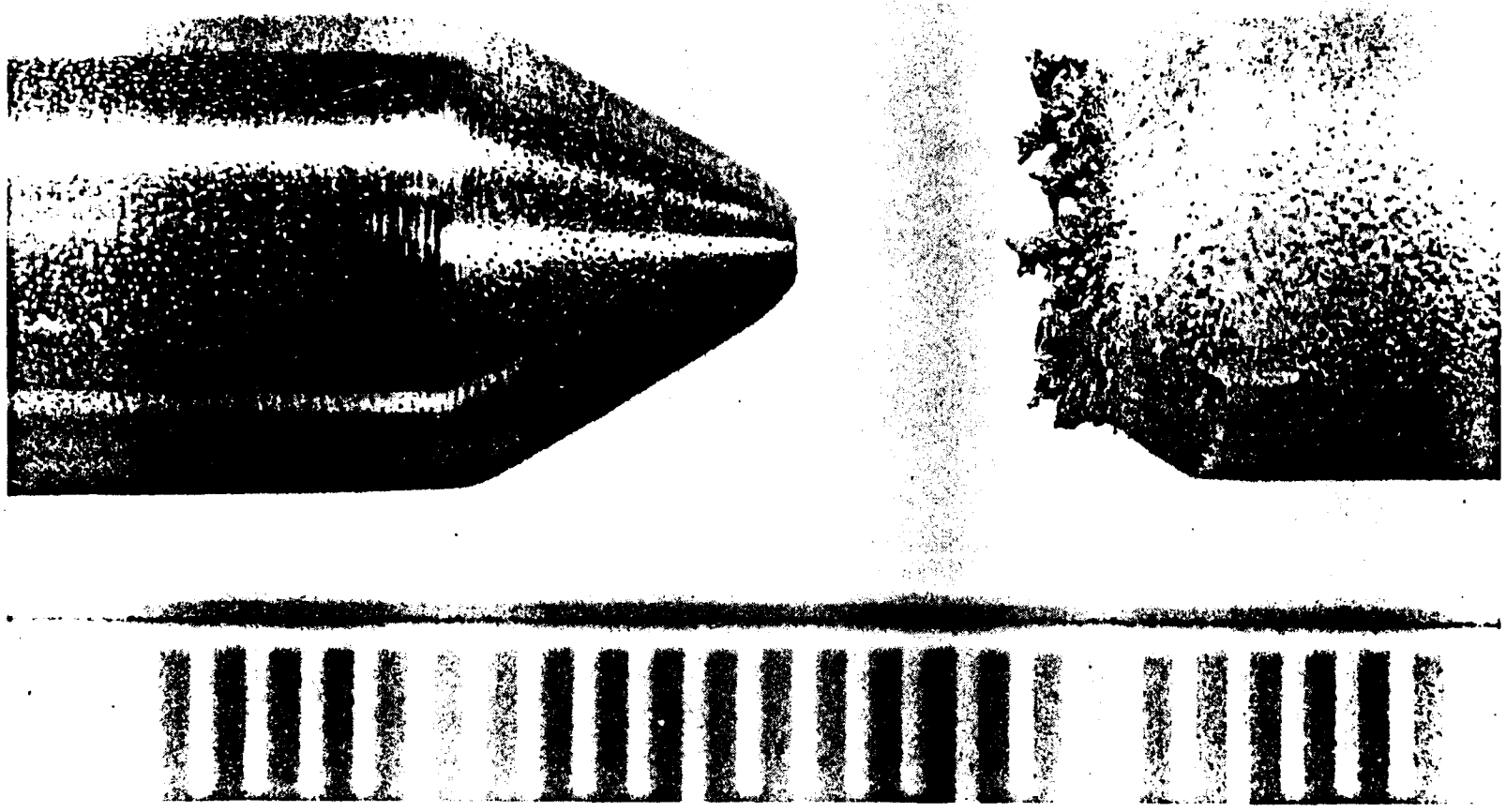

Figure 36. Close-up of Cathode Tip Before and After 573 Hours of Accumulated Run Time

enough to establish a high current arc between its tip and the anode. The rush of current melted the whisker and surface tension drew the molten tungsten into a ball and away from the anode. This ball can be seen in Figs. 37 and 38, which are an oblique and end-on picture of the cathode tip. At some point during this process the computer, which was monitoring the voltage once every eight seconds, noticed the voltage drop and terminated the test. The two small tracts of tungsten seen in Fig. 34 could have resulted from this source of molten tungsten.

During the attempt to re-establish the test and while at 16 kW the arc could have been attracted to a possible third particle of tungsten on the constrictor wall, not seen when the engine was inspected while on the thrust stand, or to a crack in the constrictor wall. A picture of the sectioned nozzle is shown in Fig. 39. Note that the pit, melted into the constrictor wall during the attempted restart, does appear to start at a crack. These cracks have been seen before and probably are the result of compression of the metal at the hotter inner surface of the nozzle due to thermal expansion forces. These cracks, most likely, would be tightly closed during high temperature operation, but during startup when the engine is relatively cold, they could still be open and with sharp edges.

The extent of this cracking is shown in Fig. 40, which is a picture of the plenum chamber side of the constrictor. This picture also shows the damage sustained by the constrictor wall during the attempted re-start. A more extensive pattern of cracks is shown in Fig. 41. This figure is a picture of the constrictor entrance of an engine used for engine development testing. This engine sustained many starts and shut-downs over a variety of conditions, resulting in the much more extensive cracking.

Section 7

RESULTS AND DISCUSSION OF MATERIAL ANALYSIS

7.1 Cathode

In the process of creating the crater and growing whiskers the cathode lost 1.95 $\pm$ 0.15 gms of tungsten over the entire 573-hour test, or about 3.4 mg per hour. The volume loss was about 0.1 cm^3. This lost material came from the tip, as can be seen in Figs. 36, 37 and 38, although some of the material removed from the tip was redeposited in the form of whiskers on the rim of the crater. Scanning Electron Microscope (SEM) pictures of the cathode tip were taken and a side view is shown in Fig. 42. Note that the whisker length, and presumably growth rate, decreases quickly away from the crater rim. These whiskers must have grown from the tungsten vapor, generated in the central crater, while it was flowing radially outward along the cathode surface and in the fluid boundary layer. A close-up of some large rim whiskers is shown in Fig. 43 and one of the small whiskers is shown in Fig. 44.

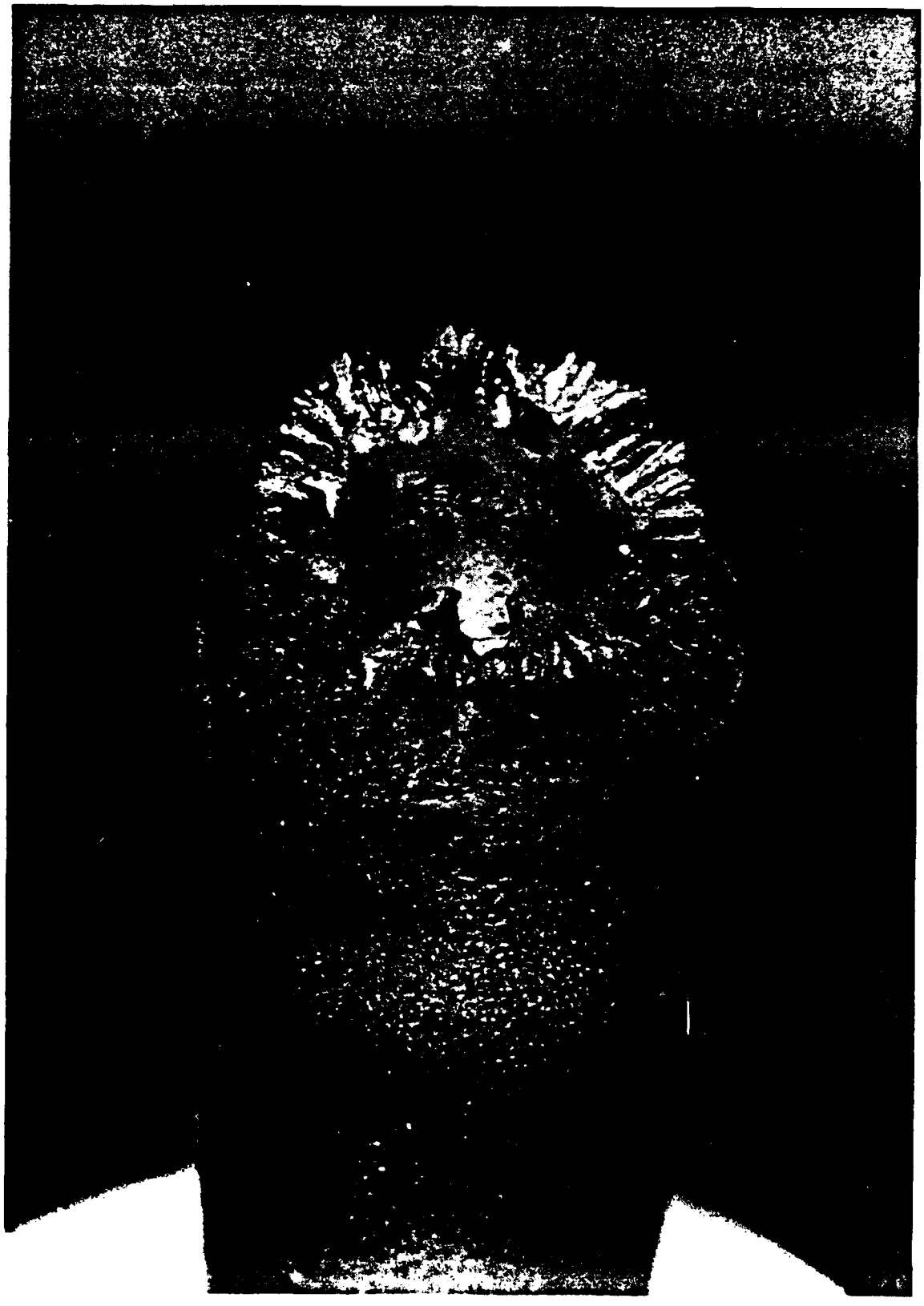

Figure 37. Oblique View of Cathode Tip After 573 Hours of Accumulated Run Time

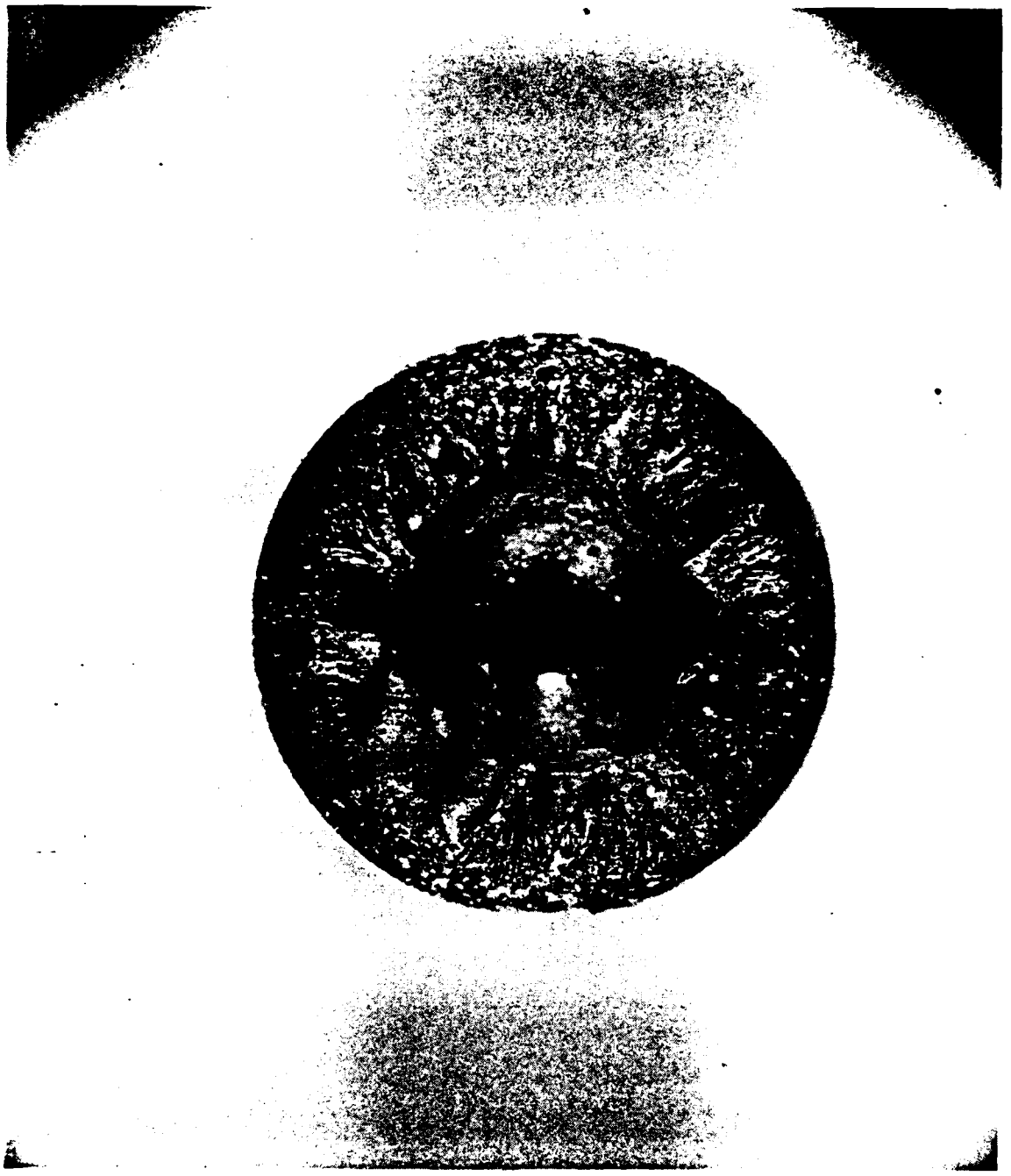

Figure 38. End-on View of Cathode Tip After 573 Hours of Accumulated Run Time

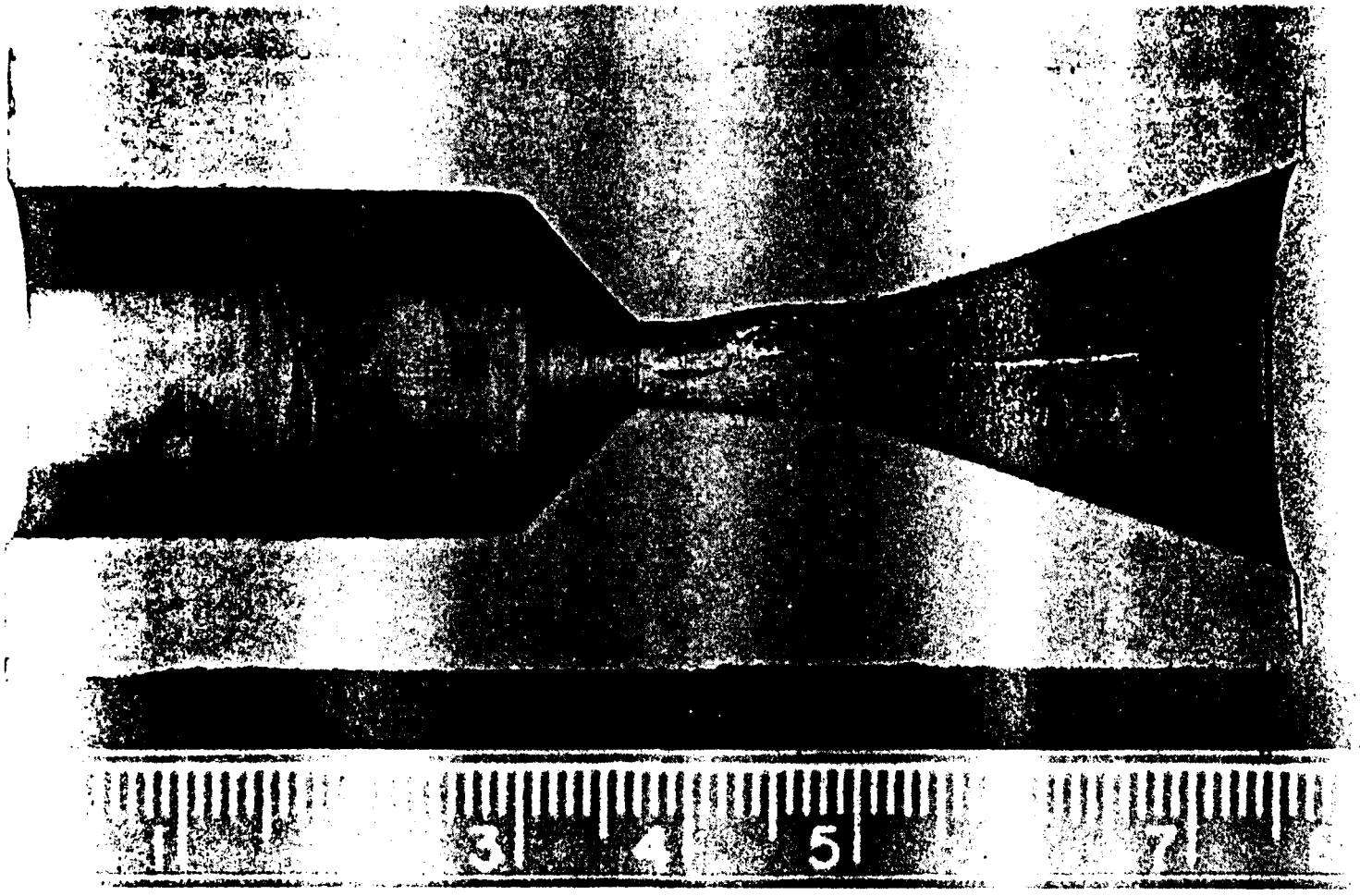

Figure 39. Sectional Anode Block After 573 Hours of Accumulated Run Time. This is the Least Damaged Half

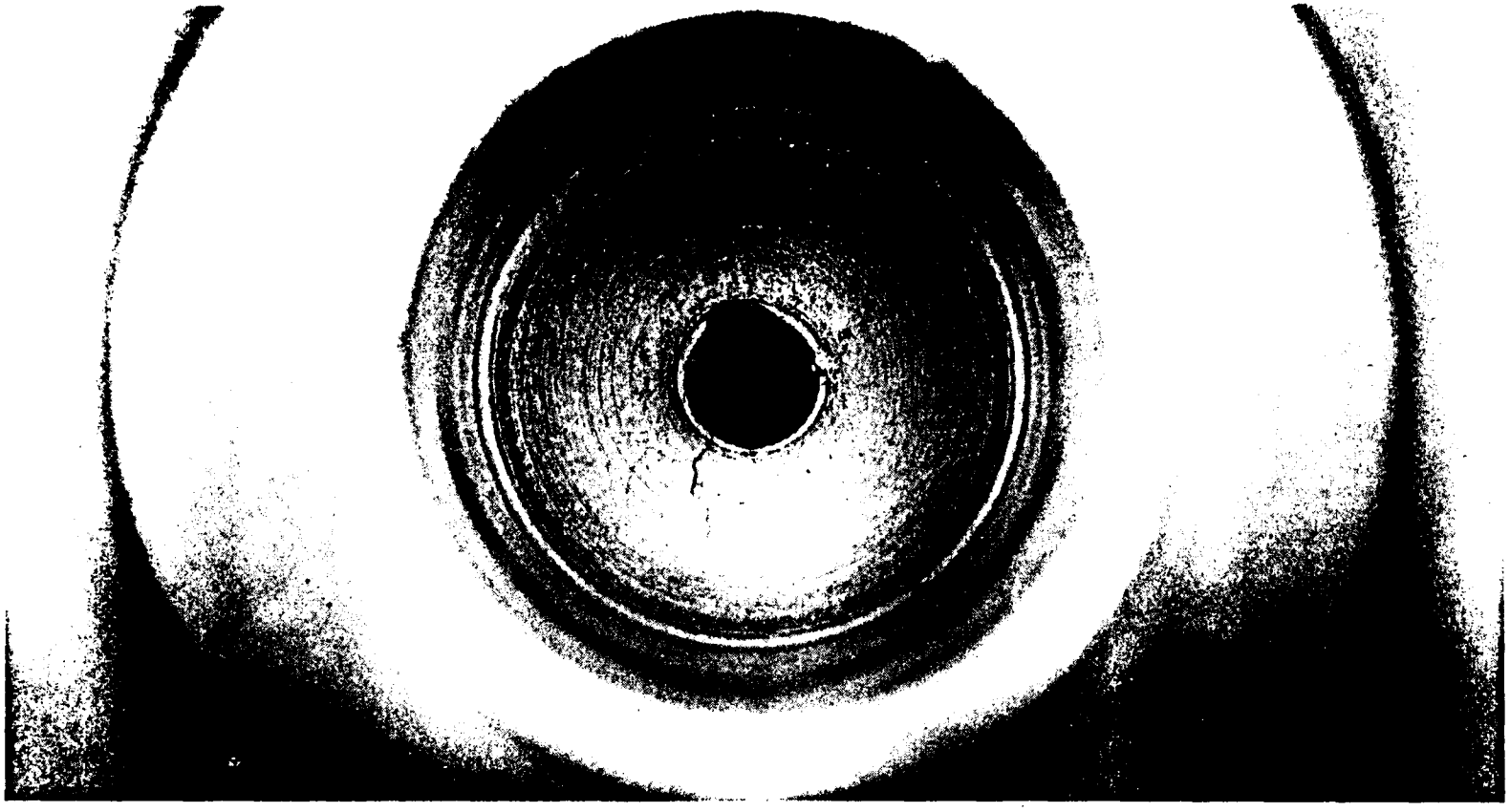

Figure 40. Photograph of Plenum Chamber End and Constrictor Entrance After 573 Hours of Accumulated Run Time

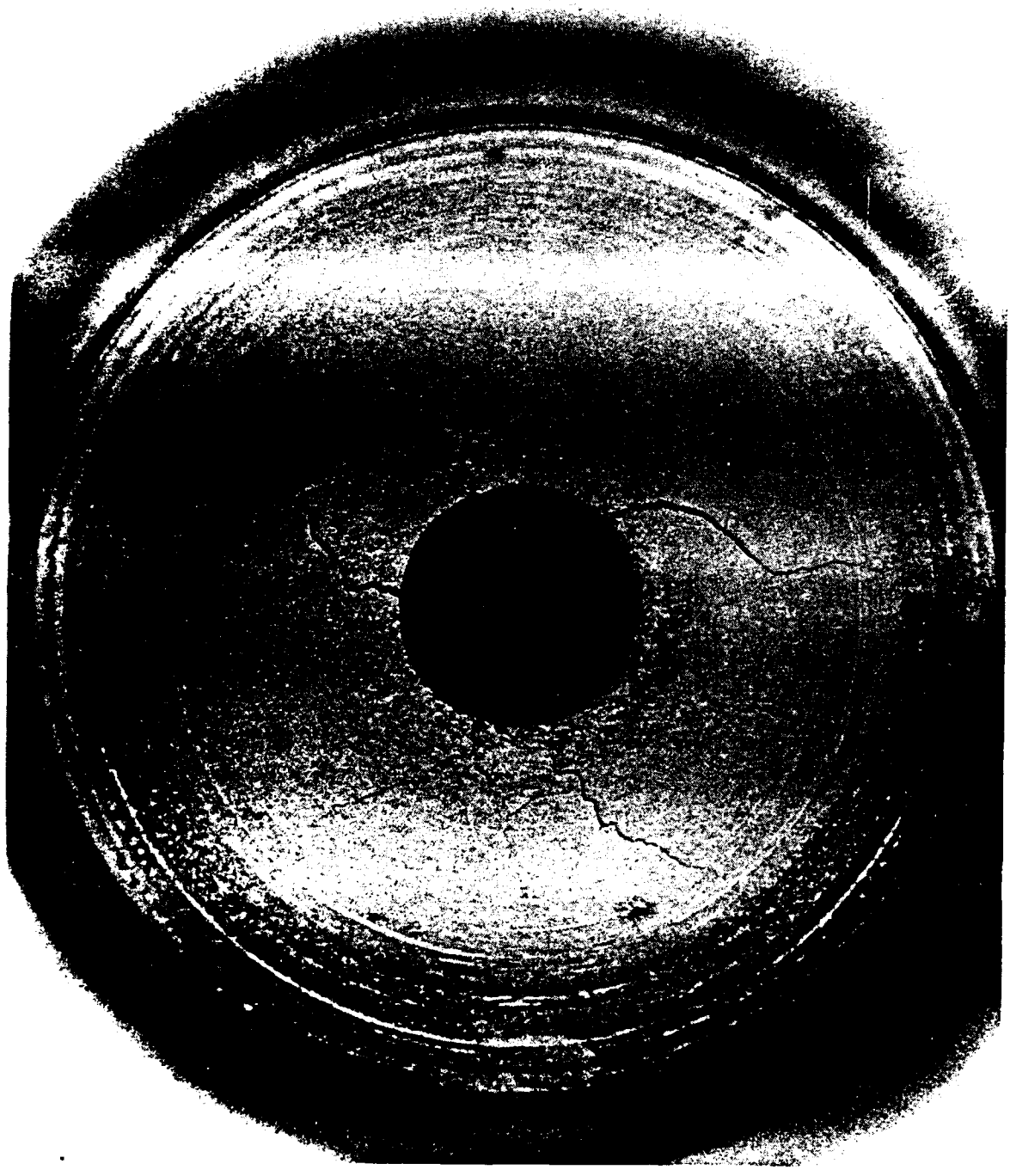

Figure 41. Photograph of Plenum Chamber End and Constrictor Entrance of Developmental Engine After Many Starts

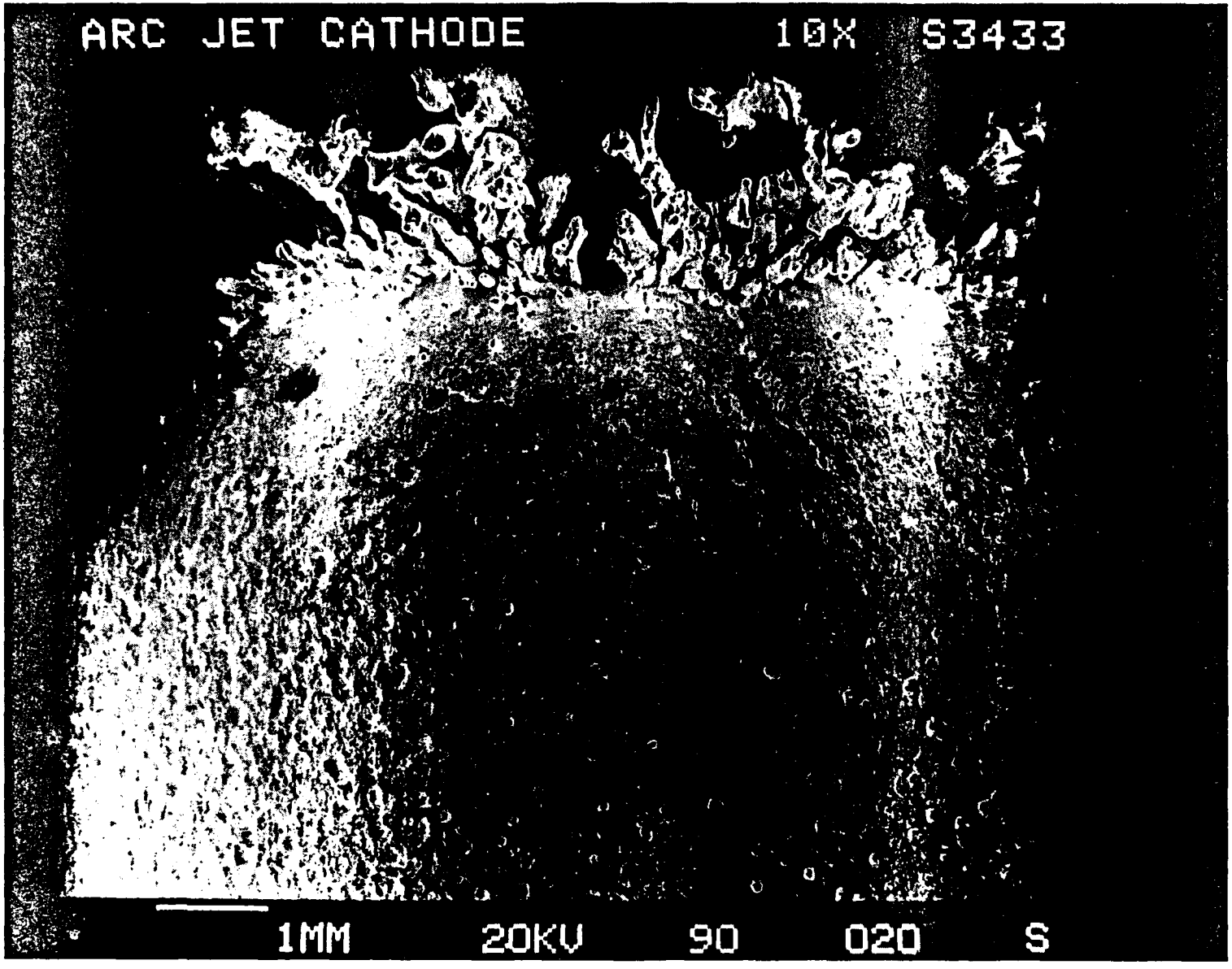

Figure 42. SEM Side View of Cathode Tip After 573 Hours of Accumulated Run Time

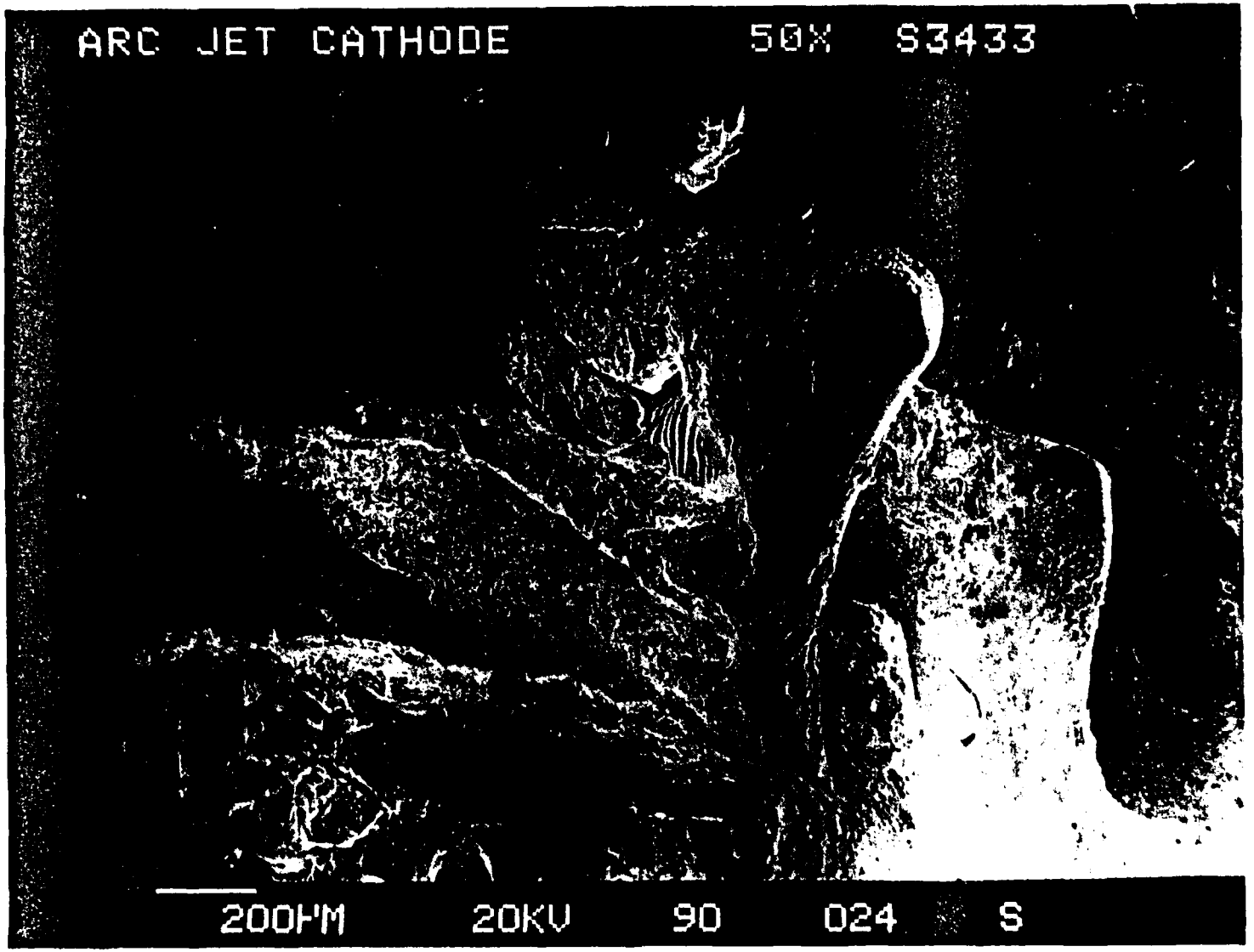

Figure 43. SEM Close-up of Whiskers on Crater Rim of Cathode

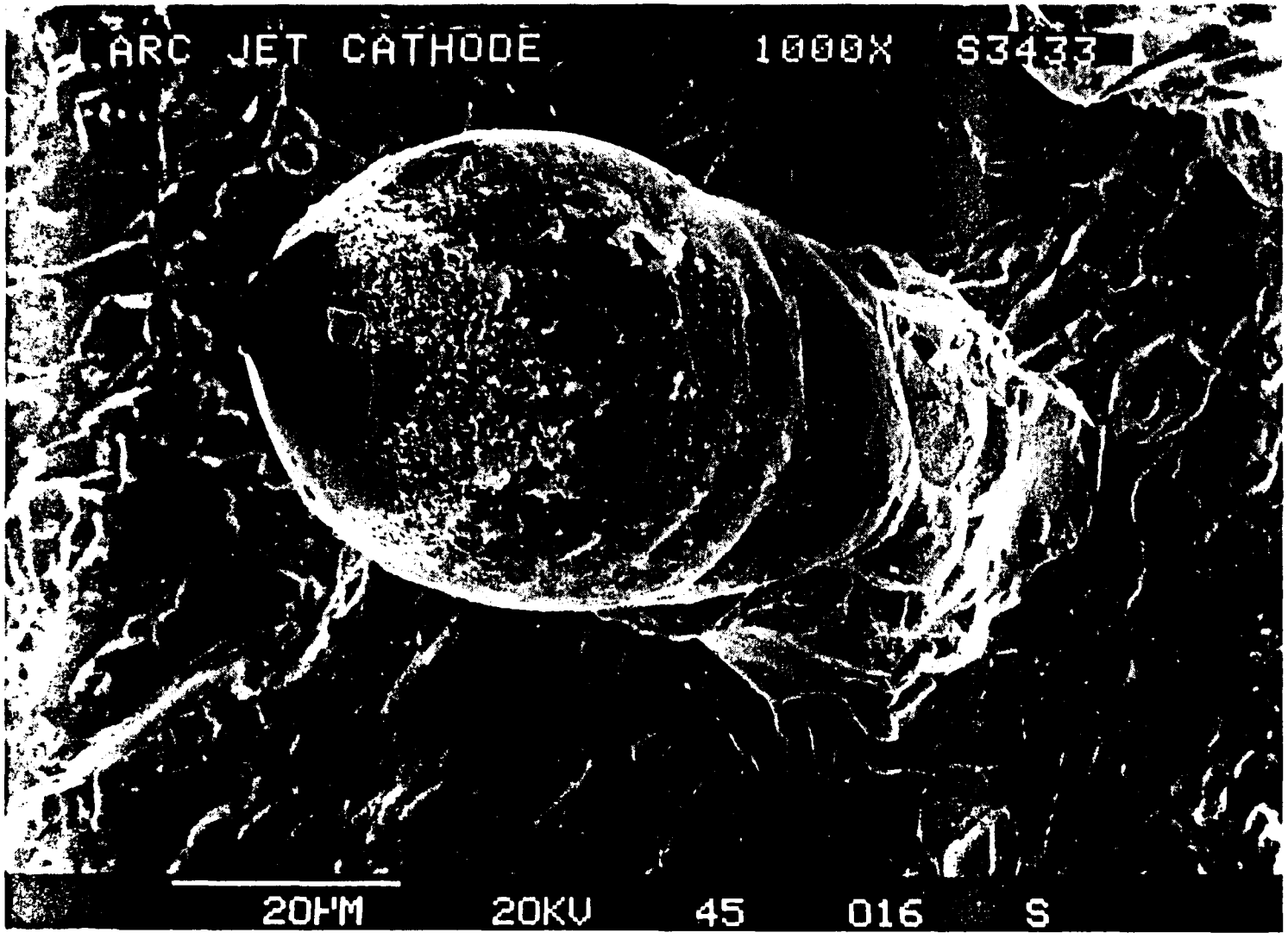

Figure 44. SEM Close-up of Whisker on Cone Surface of Cathode

The very tip of a large rim whisker is shown in Fig. 45 and clearly shows the sharp corners of crystal growth as opposed to forms created by splashed liquid metal as will be demonstrated below.

An end-on view of the cathode tip is shown in Fig. 46. Notice that the shining ball of Fig. 38 is at the bottom (6 o'clock) and seems to have a dimple at its center. A second ball, with a rough surface and a central dimple, can also be seen at about 10 o'clock. A close-up of the dimples is shown in Figs. 47 and 48 for the shining and rough balls, respectively. Both appear to be vent holes for escaping gases. Notice that the rough ball surface is covered with arc micro-spots, indicating that this ball was formed some time before the test was terminated. Arc micro-spots were also found over most of the surface of the central crater as can be seen in Figs. 49 and 50. Notice that the whiskers created by splashed molten tungsten, out of the micro-spots, are much smaller in diameter than the crystal whiskers and that the micro-spots are of order 20 to 40 μm in diameter.

While most of the central crater surface was covered with arc micro-spots, indicating intense thermionic electron emission from this surface, the cathode outer cylindrical surface had none. Instead, this surface was found to be covered with approximately 50 μm diameter pits and with crystal facets, as can be seen in Figs. 51 and 52. The thermionic electron emission current density from this surface was probably much lower than that of the crater but there may have been substantial field emission from the sharp crystal edges. Where this surface was covered with the boron nitride insulator, see Fig. 9, the surface was smooth, unpitted and still showed machining marks. The cathode tip cone surface also was covered with pits and crystal facets but no micro-spots.

The cathode tip was next sectioned axially and a quantitative microprobe analysis, for thorium, was performed at seven points using a scanning electron microscope. The seven points were (1) at the cold end of the cathode for a reference determination of thorium content, (2) inside a sectioned rim whisker, (3) the new tungsten ball surface, (4) at the edge of the crater on the cathode centerline, (5) one mm back from the edge and along the cathode centerline, (6) two mm back from the edge and along the cathode centerline, and (7) at the edge of the cylindrical outer surface of the cathode about 4 mm aft of the crater rim. The results of this analysis are given in Table 4.

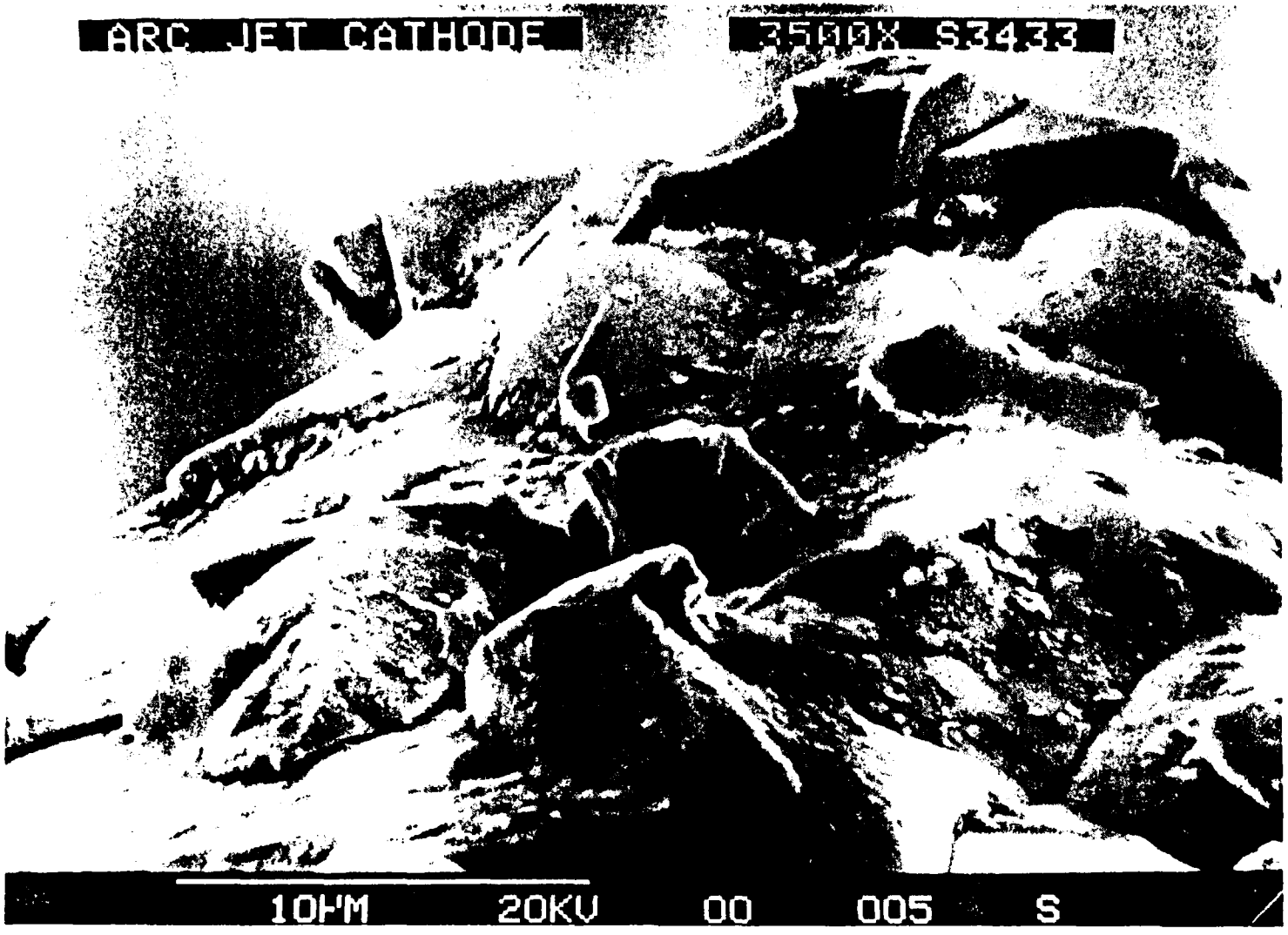

Figure 45. SEM Close-up of Very Tip of One Whisker on Crater Rim of Cathode

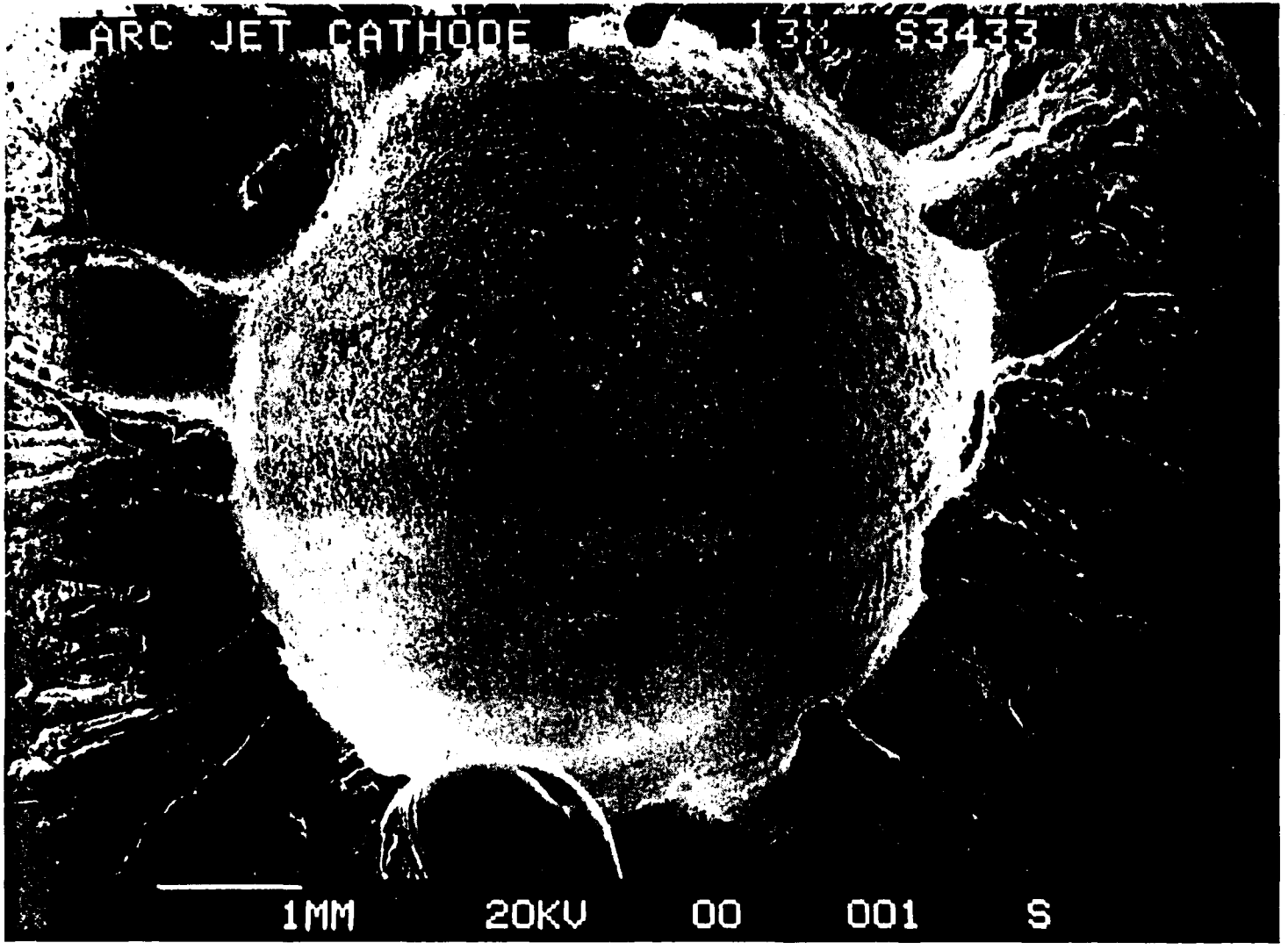

Figure 46. SEM Overall View of Cathode Tip Crater, Whiskers and Tungsten Balls

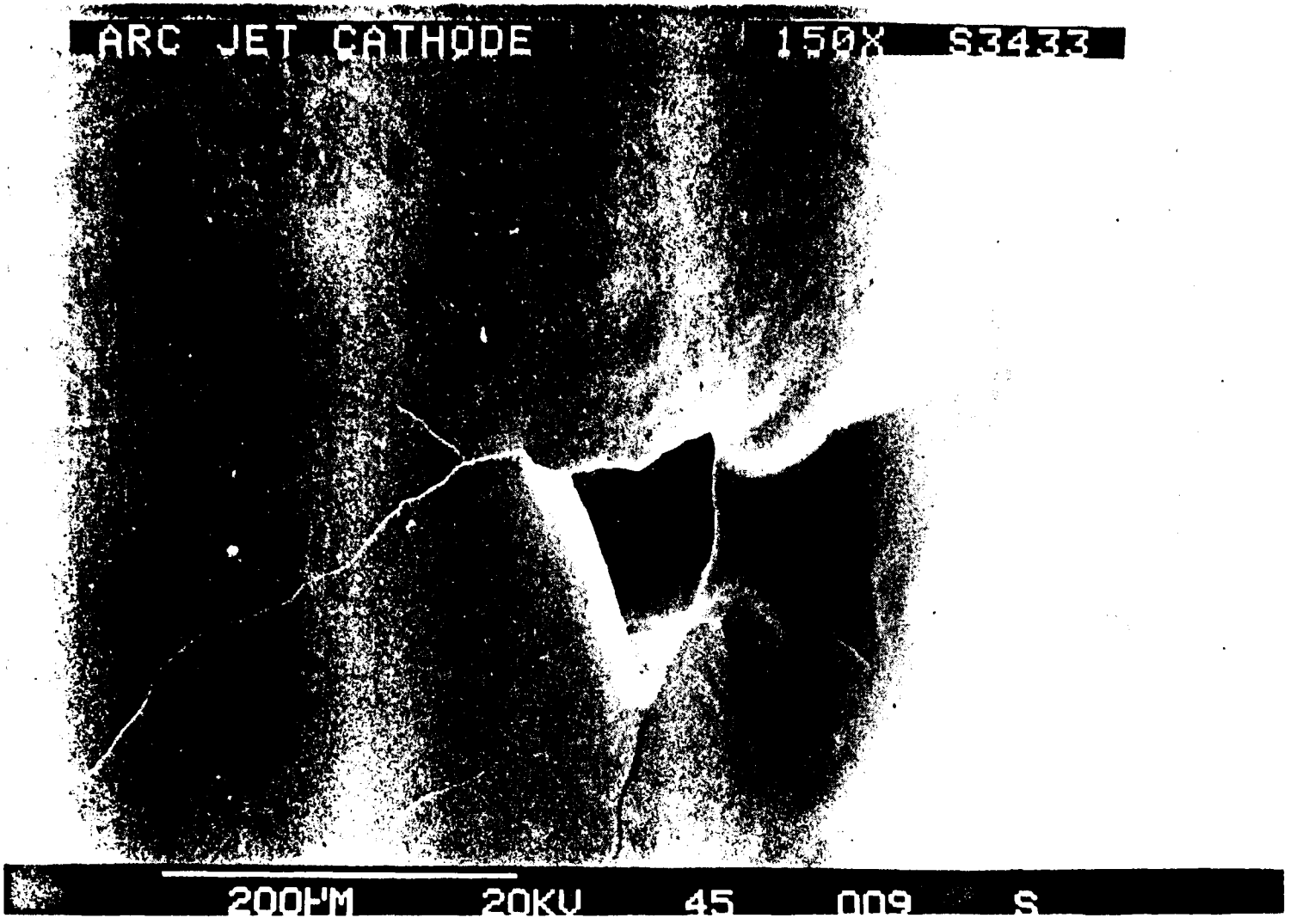

Figure 47. SEM Close-up of Shining New Tungsten Ball, Showing Hole at Center

Figure 48. SEM Close-up of Rough Old Tungsten Ball, Showing Hole at Center

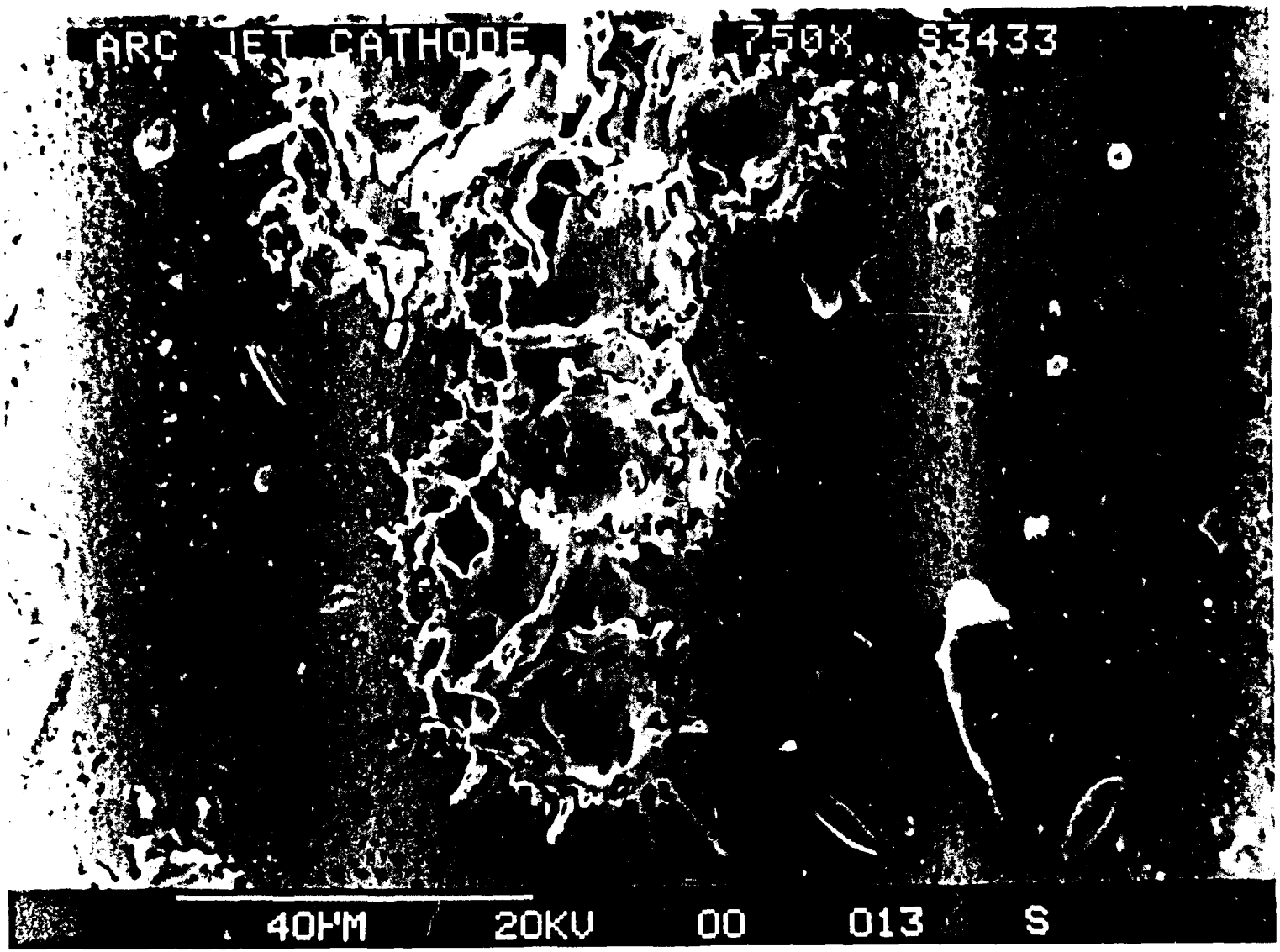

Figure 49. SEM Close-up of Cathode Crater Surface Showing Some Arc Microspots and Some Smooth Tunsten Surface

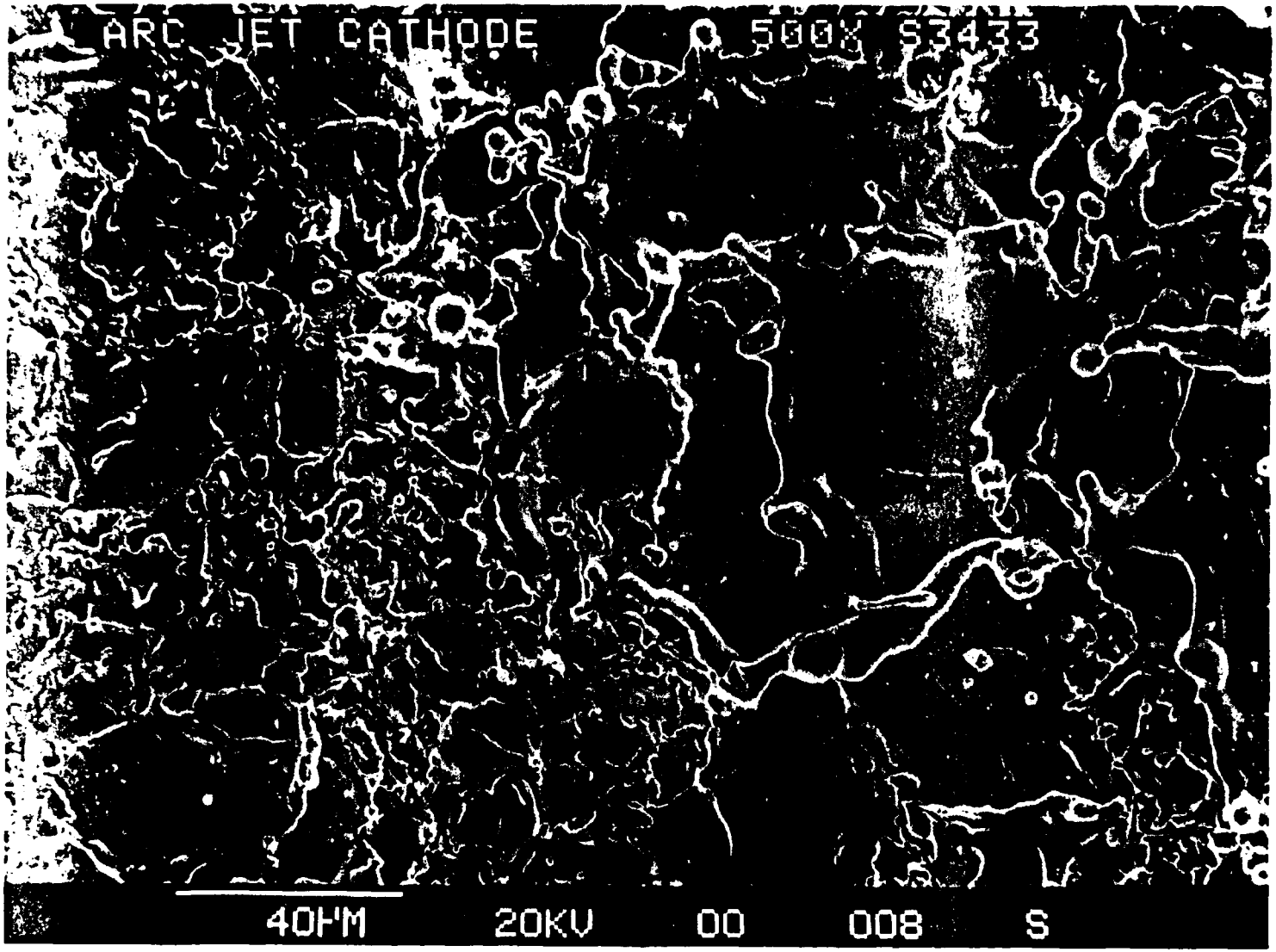

Figure 50. SEM Close-up of Cathode Crater Surface Completely Covered with Arc Microspots and Splashed Tungsten

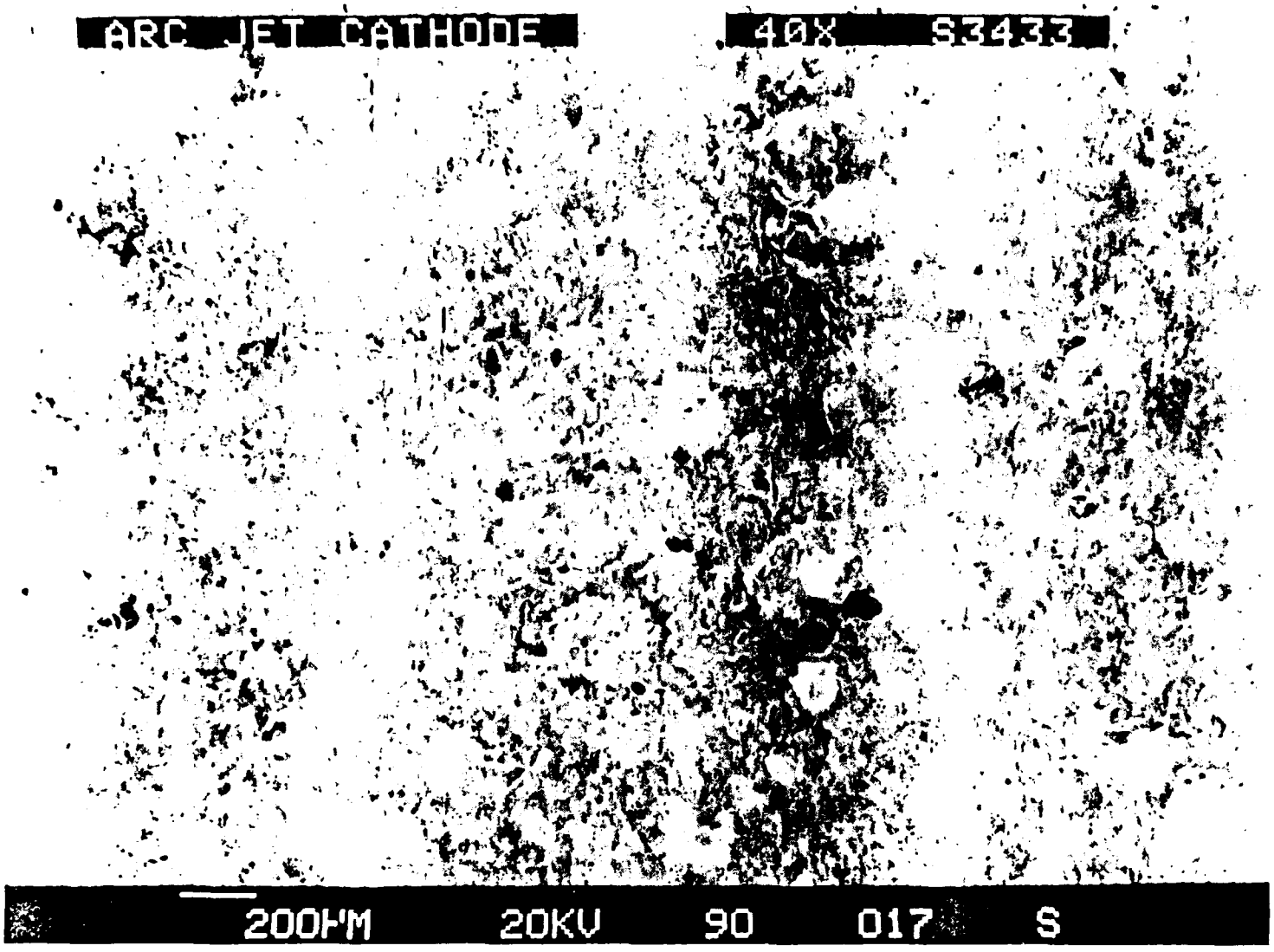

Figure 51. SEM View of Cathode Cylindrical Surface

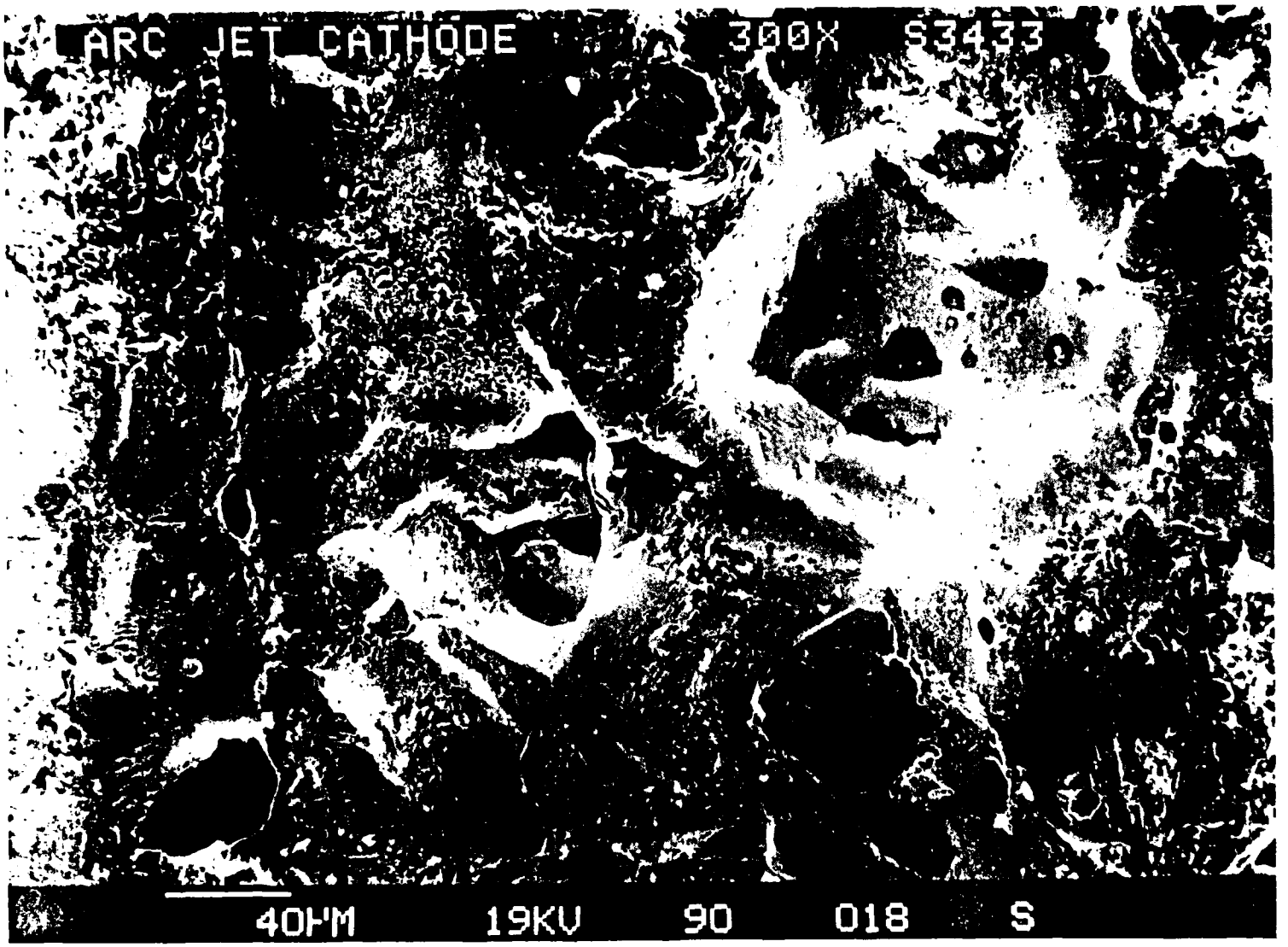

Figure 52. SEM Close-up of Pits and Crystal Facets on Cathode Cylindrical Surface

Table 4. Results of Cathode Tip Analysis

Location	Probe Area μm x μm	Atomic % Thorium	Statistical Error	Atomic % Tungsten	Statistical Error
Reference	300 x 300	1.98	5.12	98.02	0.23
Whisker	350 x 350	0.40	19.58	99.60	0.23
Shining Ball	12 x 12	0.44	17.93	99.56	0.23
Crater Edge	12 x 12	0.17	46.11	99.83	0.23
One mm Back From Edge	12 x 12	1.16	7.29	98.84	0.23
Two mm Back From Edge	12 x 12	1.71	4.62	98.29	0.23
Cylindrical Surface Edge	12 x 12	0.46	17.40	99.54	0.23

It appears that the thorium content near and at all emitting surfaces of this cathode is very low and possibly zero. Hence, an arcjet cathode, although starting out as a thoriated cathode, at some point becomes essentially a pure tungsten cathode. This situation could be corrected by providing a thorium reservoir inside the cathode. If the thorium is primarily at grain boundaries and if the grains are much bigger than a 12 μ m square the results in Table IV could be in error. Further analysis will be needed to clear up this point.

7.2 Anode-Nozzle

After completion of the long duration test and subsequent attempt at a restart the anode-nozzle was sectioned and the least damaged half was ground flat and smooth. A picture of this half is shown in Fig. 39. The lower contour of the constrictor was undamaged and clearly shows the erosion pattern caused by the long duration test. This contour was carefully measured and the results plotted on a large scale and compared with the original pre-test shape. As can be seen in Fig. 39, the erosion starts at about 1 mm into the constrictor. The constrictor radius then starts increasing at an ever-increasing rate for the next 6.5 mm, is then constant at 3.0 mm for the next 4.0 mm and then slowly blends into the 19^0 half angle cone. The erosion ends about 4 mm into the expansion nozzle. By performing a graphic integration on the data, the amount of tungsten eroded was determined to be 0.071 cm^3 or 1.37 gms. A careful inspection of the nozzle contour part of this plot indicates that material may have been deposited on the nozzle wall starting about 11 mm from the exit plane. The thickness of this deposited layer increased linearly and reached about 0.2 mm at the exit plane. The volume and mass of this layer was calculated to be 0.075 cm^3 and 1.45 g. Note that these determinations are at best an estimate since they involve very small changes in radius, 0.5 mm for the constrictor and 0.2 mm, maximum, for the nozzle. However, the results suggest that there is little net mass loss due to normal operation.

This result suggests that most of the material evaporated from the constrictor wall, flowed downstream in the laminar boundary layer and redeposited on the cooler downstream wall of the expansion nozzle.

By weighing the nozzle before and after the long duration test, and subsequent damage, a net loss of 2.4 g was found. This loss must have occurred, primarily, when the constrictor was damaged during the attempted restart. This damage can be seen as a pit in the constrictor wall in Fig. 39 and more clearly in the picture of the other half of the nozzle shown in Fig. 53. Note, in Fig. 39, that the pit appears to start on a crack in the tungsten wall. That pit may have occurred early in the restart, when the nozzle was still relatively cold. Note also that the plenum chamber walls, though stained, were not affected by the long test duration. The machining marks are still visible on the 50^{o} half angle cone wall.

A quantitative microprobe analysis of the sectioned anode-nozzle was also performed. Ten points were selected along the inner edge of the 50^{o} cone, constrictor and expansion nozzle with a point spacing of approximately 5 mm. A reference point was taken at the very back of the anode nozzle piece. The reference point indicated a thorium content of 1.88 atomic percent with a statistical error of 5.49 percent. Interestingly, about 2 percent molybdenum was also found at this point. Apparently the molybdenum diffused into the tungsten from the engine body during the long duration test. For the rest of the data, the thorium content was 1.2 atomic percent + 0.2 - 0.4 and this data had a statistical error of 6.4% + 2.8 - 1.0. Therefore, a significant amount of thorium was still found in the anode/nozzle surface material. A low concentration of 0.85 atomic percent was found about 5 mm downstream of the end of the constrictor and this is about where the arc is expected to attach to the nozzle, causing increased heating.

7.3 Propellant Injector

The propellant injector was badly eroded during the long duration test. This was entirely unexpected since the injector used in a continuous 168-hour test was unaffected. The eroded injector, and a similar but unused injector are shown in Fig. 54. The diameter of each of the four injection nozzles has increased from the original 1.6 mm to about 2.4 mm; an area increase of 2.25. It also appears that if the test had continued much longer, the tangential injection would have stopped and the propellant would have been injected axially. The effect of this change on engine performance is unknown at this time.

The eroded end of this propellant injector has been analyzed with an x-ray beam having a 600 μ spot size, and with a scanning electron microscope. The spots analyzed with the x-ray beam were composed of the black deposits that can be seen in Fig. 54 plus the boron nitride just below the deposit. The results of this analysis are given in Table 5.

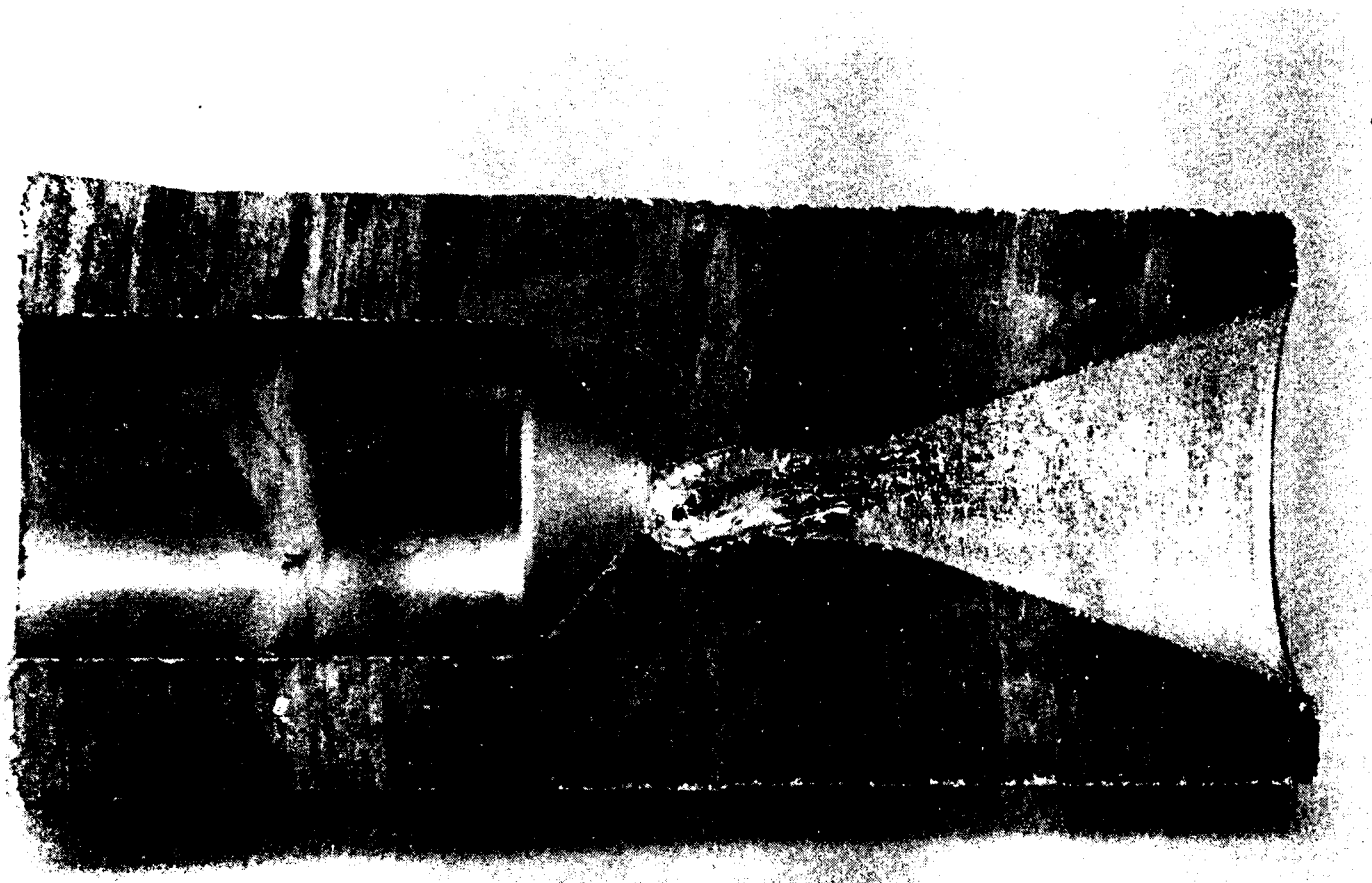

Figure 53. Sectional Anode Block After 573 Hours of Accumulated Run Time. This is the Most Damaged Half

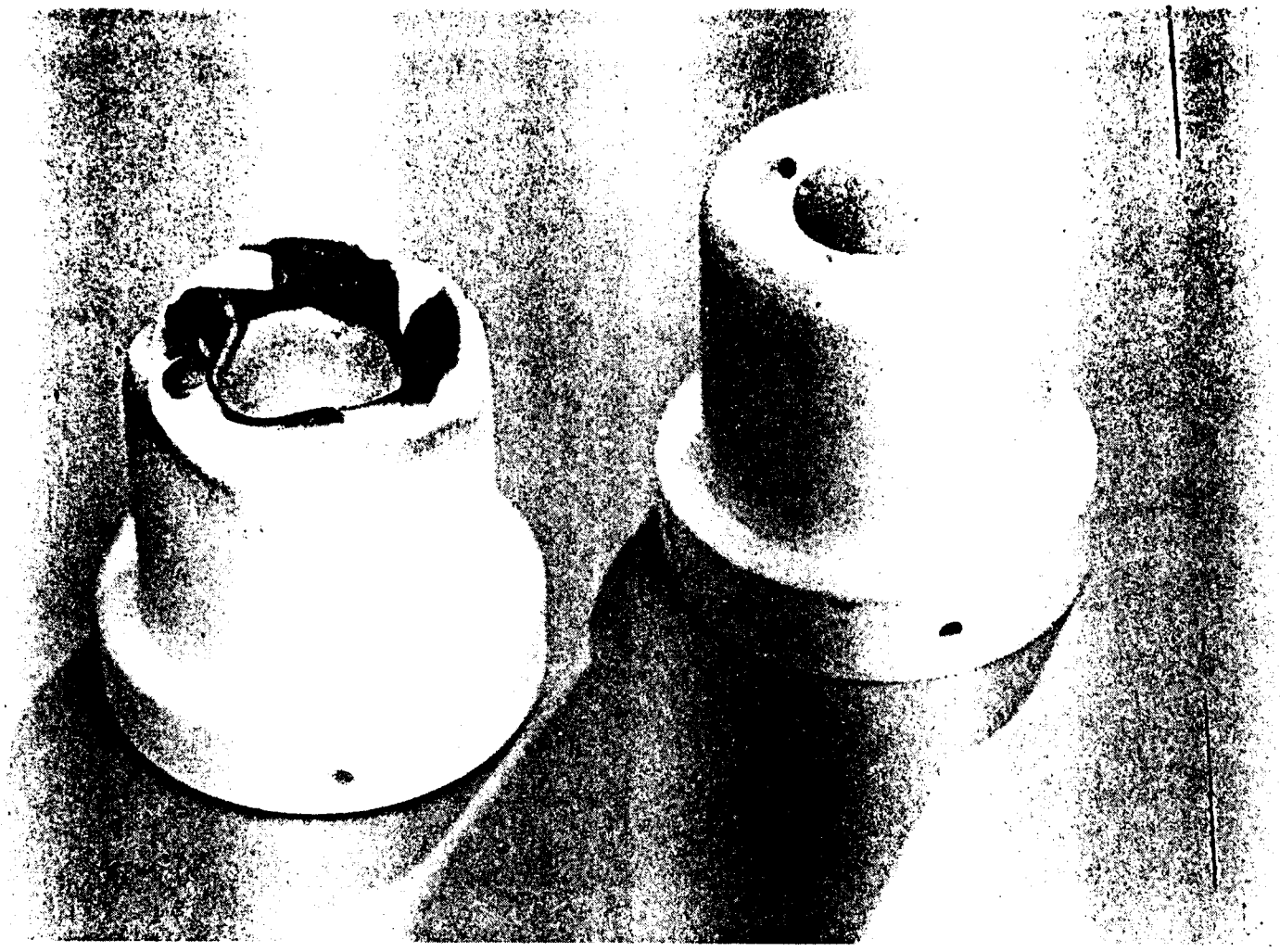

Figure 54. Propellant Injector Before and After 573 Hours of Accumulated Run Time

Table 5. Results of Propellant Injector Analysis

Element	Atomic %
Boron	30.47
Nitrogen	27.78
Tungsten	6.73
Thorium	0.49
Carbon	17.66
Oxygen	16.45
Sodium	0.41
Total	100.00

The fact that the boron nitride content of this analytical sample dominates suggests that the black deposit thickness was less than 10 Å since the total sample depth was 20 Å at most. The black deposit appears to be tungsten with a high percentage (7%) of thorium and these must have been evaporated or sputtered from the adjacent cathode surface. The carbon, oxygen and sodium probably came from deposits introduced while handling the injector.

The SEM analysis of the eroded areas revealed nothing unusual about the surface. These surfaces are made up of 10 μ m, striated, particles arranged randomly, as would be expected of hot-pressed boron nitride. No machine marks were present since the surfaces were eroded. Since the injector used in a continuous 168-hour test showed no sign of erosion, it is tentatively concluded that the erosion was due to a material defect.

Section 8

CONCLUSIONS AND RECOMMENDATIONS

8.1 Facility

Except for the four discrete facility failures noted in this report the JPL/AFRPL Arcjet Life Test facility performed well. The diffuser had a material effect on vacuum tank pressure and helped, along with the indispensable high-capacity pumps, to keep the vacuum tank pressure low enough to prevent serious effects on thrust measurements. However, larger diameter diffusers should be tested since an optimum diameter has not yet been found.

The thrust stand developed for this facility is simple, reliable and performed well. It can be adapted to a large variety of engine sizes by merely changing the thrust beam diameter and/or wall thickness. The device developed to calibrate this thrust stand, remotely, also worked well. However, the flexural pivot is very delicate and needs to

be protected. Several of these pivots were damaged by excess force on the sheave during handling.

The coaxial current feed system worked well and completely eliminated the possibility of having the thrust measurements effected by the heavy power cables. However, to eliminate the effect of magnetic forces on the thrust measurements the electrodes should be made of a non-magnetic material such as copper or stainless steel. In our program the magnetic effects were minimized by carefully centering the electrodes. With non-magnetic electrodes this requirement would be eliminated. Also, the buoyancy force of the mercury on the electrodes was important and care must be exercised to keep it a constant.

The Autonomous Control system performed flawlessly, recording and displaying raw, corrected and calculated data and being constantly alert to engine and/or facility failures. When failures did occur, as noted in this report, the control system shut down the test and facility in an orderly and safe manner, and each time it minimized damage to engine and facility. This system greatly increases the efficiency and reduces the cost of long-term testing and relieves personnel of a great deal of anxiety. With further understanding of engine and facility operation we should be able to program the system so as to allow it to anticipate failures and modify or interrupt the test before failure. This might be affected by noting rates-of-change of various parameters.

8.2 Arcjet Engines

8.2.1 Performance Verification

The first object of this program was to verify the performance results obtained on ammonia arcjets in previous arcjet development programs. Since the AVCO Corporation R3 engine (see Fig. 6 and Reference 3), designed specifically for ammonia, achieved a run duration of 50 hours at a specific impulse of 978 sec. it was chosen to be duplicated. The plenum chamber, constrictor, expansion nozzle and cathode configuration and size were duplicated. However, the R3 engine had some problems with seals so the back end of the engine was redesigned to take advantage of a different approach to sealing at high temperatures. The resulting engine is shown in Figs. 9, 10, 11 and 12.

The R3 engine was tested at a power of 30 kW and an ammonia mass flow rate of 0.25 g/s. The JPL duplicate engine was run at a maximum power of 28 kW with a mass flow rate of 0.25 g/s. Hence a slight extrapolation of the data in Figs. 15, 16a, 16b, 18a and 18b was required before a comparison could be made. These extrapolations are shown in the above-mentioned figures and the results of the comparison are given in Table 6.

Table 6. Performance Comparison Between the JPL/RPL and AVCO Engines

	JPL/RPL Results	AVCO R3 Results
Voltage, V	107	106
Current, A	285	283
Thrust, gm_f	240	245
Specific Impulse, sec	967	978
Thrust Efficiency	37	38

A review of Table 6 clearly shows that the performance of the two engines was essentially identical.

8.2.2 Long Duration Test Results

The Avco R3 engine was operated for 50 hours and at that point the test was voluntarily terminated. Hence, the question of ultimate life-time for these engines was left unanswered. The engine developed for this program ran for 573 hours before it failed. It is believed that the failure was caused by one of the whiskers (see Fig. 38), on the cathode tip, growing long enough to touch the anode or at least had gotten close enough to establish a high current arc between the whisker tip and the anode. The rush of current would have quickly melted the whisker and surface tension would have drawn the molten tungsten into a ball. If the whisker had not quite touched the anode this ball would be on the cathode. Indeed, such a ball was found on the cathode tip (see Figs. 37 and 38, at about 4 o'clock) and its surface was shining, indicated that it was formed shortly before the engine was shut down. A second, almost identical, ball can be seen at about 8 o'clock in Figs. 37 and 38. However, the surface of this ball was found to be covered by arc micro-spots (see Fig. 48). A close-up of both the new, shining and the old, rough balls can be seen in Fig. 46 with the new ball at 6 o'clock and the old ball at 10 o'clock. The presence of the micro-spots suggests that the rough ball was created long before the test was terminated.

The test was terminated at 573 hours because the computer noticed a voltage drop from about 110 V to 99.9 V, 0.1 V below the lower voltage tolerance. The existence of the rough, but otherwise identical ball, suggests that this type of engine failure occurred at least once before; but, possibly, it did not result in an engine shutdown because it occurred between computer voltage scans, once every 8 seconds. Hence, it

might be possible that these engines could survive this type of malfunction. Also, if the material for whisker growth came from creating the crater at the cathode tip, starting with a cratered tip might slow whisker growth and dramatically increase engine life.

The downstream portion of the constrictor was also eroded, probably because of excess temperature. This area of the anode needs to be cooled better and this can be done by increasing the radiating surface emissivity, by regeneratively cooling and/or by applying heat pipes to this area.

The boron nitride insulator/propellant injector (See Figs. 9, 10, 11, and 54) was badly eroded during the 573-hour test but not in a previous 168-hour test at higher power (28 kW). Hence, the erosion problem may have been due to a material defect. However, shortening this insulator, inside the plenum chamber, should reduce the thermal load on the insulator face. Also, by a slight change in engine design, the propellant could be injected tangentially into the plenum chamber through the tungsten walls.

Section 9

PUBLICATIONS

1. T. J. Pivirotto and D. Q. King, "Thermal Arcjet Technology for Space Propulsion," 1985 JANNAF Propulsion Meeting, San Diego, CA, Paper 3R-3, April 9 - 12, 1985.

2. J. R. Brophy, T. J. Pivirotto and D. Q. King, "Investigation of Arcjet Nozzle Performance," 18th International Electric Propulsion Conference, Alexandria, VA, AIAA 85-2016, Sept. 30 - Oct. 2, 1985.

3. T. J. Pivirotto, D. Q. King and J. R. Brophy, "Development and Life-Testing of 10-kW Class Thermal Arcjet Engines," 18th International Electric Propulsion Conference, Alexandria, VA, AIAA-85-2031, Sept. 30 - Oct. 2, 1985.

4. T. J. Pivirotto, D. Q. King, W. D. Deininger, and J. R. Brophy, "The Design and Operating Characteristics of a 30-kW Thermal Arcjet Engine for Space Propulsion," 22nd Joint Propulsion Conference, Huntsville, AL, AIAA-86-1508, June 16 - 18, 1986.

5. T. J. Pivirotto, D. Q. King and W. D. Deininger, "Long Duration Test of a 30-kW Class Thermal Arcjet Engine," 23rd Joint Propulsion Conference, San Diego, CA, AIAA 87-1947, June 29 - July 2, 1987.

SECTION 10

REFERENCES

1. Thirty Kilowatt Plasmajet Rocket-Engine Development/Second Year Development Program; Second Quarterly Progress Report, 15 August through 15 November 1962, RAD SR-62-255, Research and Advanced Development Division, Avco Corporation, Wilmington, Massachusetts for National Aeronautics and Space Administration, Lewis Research Center, Cleveland, Ohio, X64-10449, Contract Number NAS-5-600, 21 December 1962.

2. Development of a Thermal Arc Engine, Technical Documentary Report ASD-TDR-62-749, Plasmadyne Corporation, Santa Ana, California under Contract No. AF30(S16)-8367 for Electric and Advanced Propulsion Branch, Propulsion Laboratory, Aeronautical Systems Division, Air Force Systems Command, Wright-Patterson Air Force Base, Ohio, July 1962.

3. R. R. John, Thirty Kilowatt Plasmajet Rocket-Engine Development, Report No. RAD-TR-64-6, Avco Corporation, 15 July 1964.

4. James P. Todd, 30 kW Arcjet Thruster Research, Technical Documentary Report No. APL-TDR-64-58, prepared under Contract No. AF33(657)-10338 by Giannini Scientific Corporation, Santa Ana, California for Air Force Aero Propulsion Laboratory, Research and Technology Division, Air Force Systems Command, Wright-Patterson Air Force Base, Ohio, Project No. 3141, Task No. 314101, March 1964.

5. "Arcjet Thruster for Space Propulsion," NASA Technical Note TN D-2868, Lewis W. Wallner and Joseph Czika, Jr., Lewis Research Center, Cleveland, Ohio, June 1965.

6. Thomas J. Pivirotto, "Pressure and Current Effects on the Thermal Efficiency of an MPD Arc Used as a Plasma Source," AIAA Journal, Vol. II., No. 1, pp. 12-13, January 1973.

7. Vapor Pressure of the Chemical Elements, edited by Robert Gary of the National Bureau of Standards, Washington, D.C., published by Elsevier Publishing Company, 1963.

SECTION 11

APPENDIX A

THRUST STAND CALIBRATION DEVICE

The device that was developed to calibrate the thrust stand, after the vacuum tank is closed and evacuated, is shown in Figure A1. The known calibration force was applied at the engine centerline by attaching to the tungsten cathode rod, where it protrudes from the engine (see Figures 9 and 12). A ceramic insulator was used to prevent cathode grounding. A fine chain was used to transmit the force to the engine and this chain was guided by a sheave which was suspended by a flexural pivot to minimize stray forces. For an applied force of 250 gm_f the engine was pulled back by about 1.3 mm, which resulted in a rotation of less than 2^o at the pivot.

The circular pan used to hold the calibration weights was suspended from the chain by three 1.5 mm diameter rods, as shown in Figure A1. The weights and pan were rings of various thicknesses and diameters and made of aluminum. The sizes and weights are listed in Table A1 where the weight of the pan includes the weight of the pan support structure.

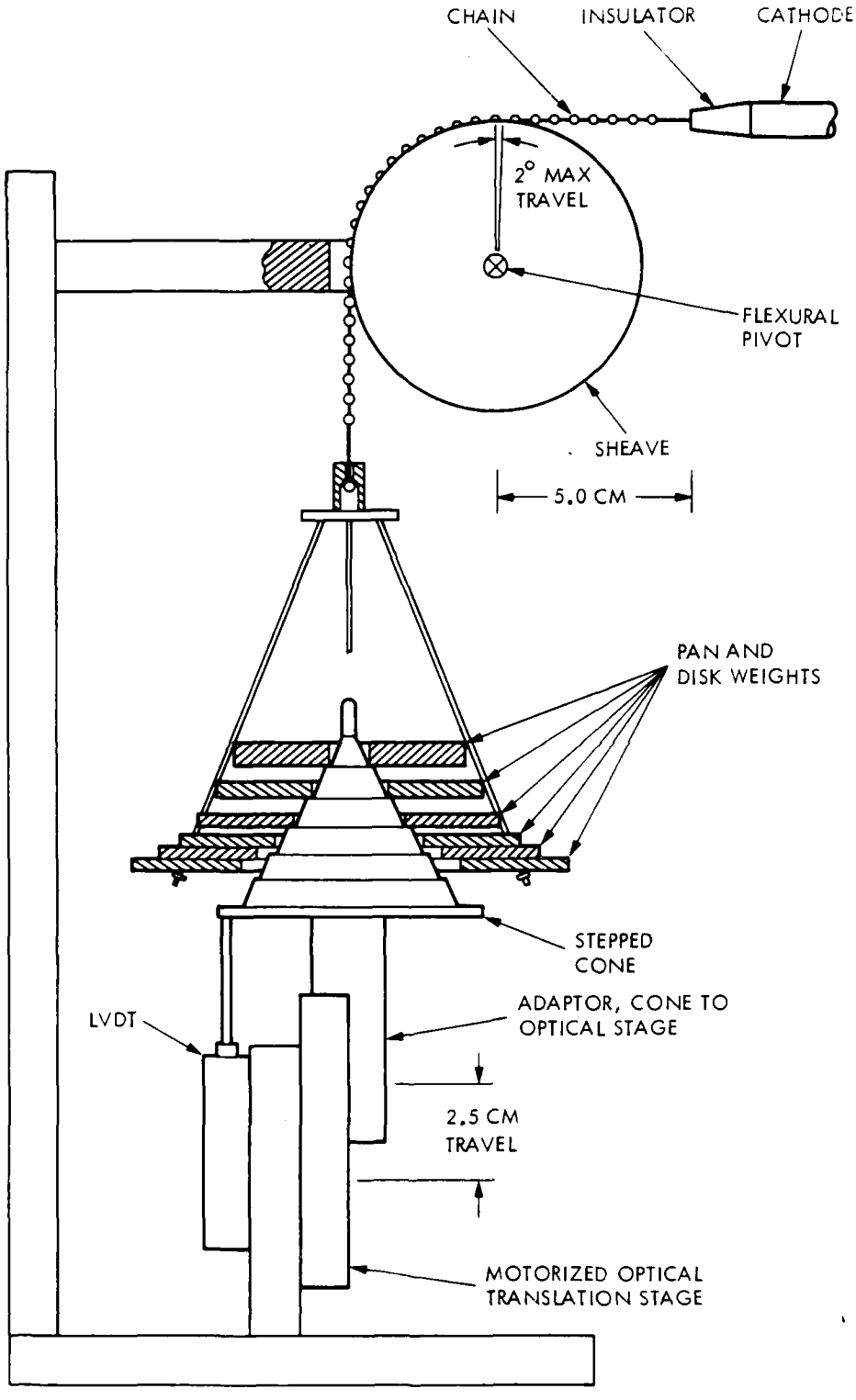

Figure A1. Thrust Stand Calibration Device

Table A1

Characteristics of the Calibration Weights

Weights	Thickness, cm	Outside Diameter, cm	Inside Diameter, cm	Weight, gm_f
PAN	0.33	11.43	5.72	69.4
FIRST	0.29	9.84	4.76	45.4
SECOND	0.33	8.89	3.81	45.3
THIRD	0.39	7.94	2.86	45.7
FOURTH	0.47	6.99	1.91	45.9
FIFTH	0.60	6.03	0.95	47.8

When this device was not being used to calibrate the thrust stand the pan and weights were supported by the stepped cone, in its uppermost position. When performing a calibration, the cone was lowered, in steps, in order to add weights to the engine for a six-point calibration. As shown in Figure A1, the pan and first two weights are pulling on the engine and the upper three weights are being supported by the stepped cone. The cone was remotely moved, up and down, with the aid of a motorized optical translation stage and the position of the stage and cone, at any given time, was determined by the output of the Linear-Variable-Differential-Transformer (LVDT), shown in Figure A1.

When calibrating the thrust stand, the applied weights and the thrust stand LVDT input voltage and output voltage were used by the computer to calculate, through a least-squares-fit, the calibration coefficients. These coefficients were then stored in the computer, and used to calculate thrust from the thrust stand LVDT output during a test. The results of a typical calibration are:

$$\text{Thrust, } gm_f = 0.011 + 3.590 \times 10^3 \left[\frac{out}{in} - \left(\frac{out}{in}\right)_{zero}\right]$$

and the least-squares-fit correlation coefficient was 0.99994. The out-to-in ratio refers to the thrust stand LVDT output to input voltage ratio.

SECTION 12

APPENDIX B

COAXIAL CURRENT FEED SYSTEM

The coaxial current feed system is shown in Figure B1. The electrodes (current carriers) were made of low carbon steel because of its low resistivity (13 $\mu\Omega$ cm) as compared to non-magnetic stainless steel (92 $\mu\Omega$ cm). The mercury did not wet the carbon steel electrodes; however, contact was still reasonably good since the total system resistance was measured to be only 3 mΩ . The contact surface of the negative electrode was 16 cm^2 and that of the positive electrode 189 cm^2. At a typical operating current of 200 amps the power dissipated in this system was 120 watts. This power was carried away by water cooling the bottom of each mercury pot as is shown in Figure B1. The copper bus bars were brazed to the carbon steel pots just above the water cooling jackets so that these high current carrying joints would be adequately cooled. The bus bars had a cross-sectioned area of 1.61 cm^2. Since the engine was constrained, by the stiffness of the thrust beam, to move only one to two mm, the gaps between the electrodes and pot walls were more than adequate to prevent binding. The upper ends of the two electrodes were mechanically attached to the engine as shown in Figures 11, 12 and 14. A double wall radiation shield was used to protect this system from the heat being radiated from the arcjet engine nozzle.

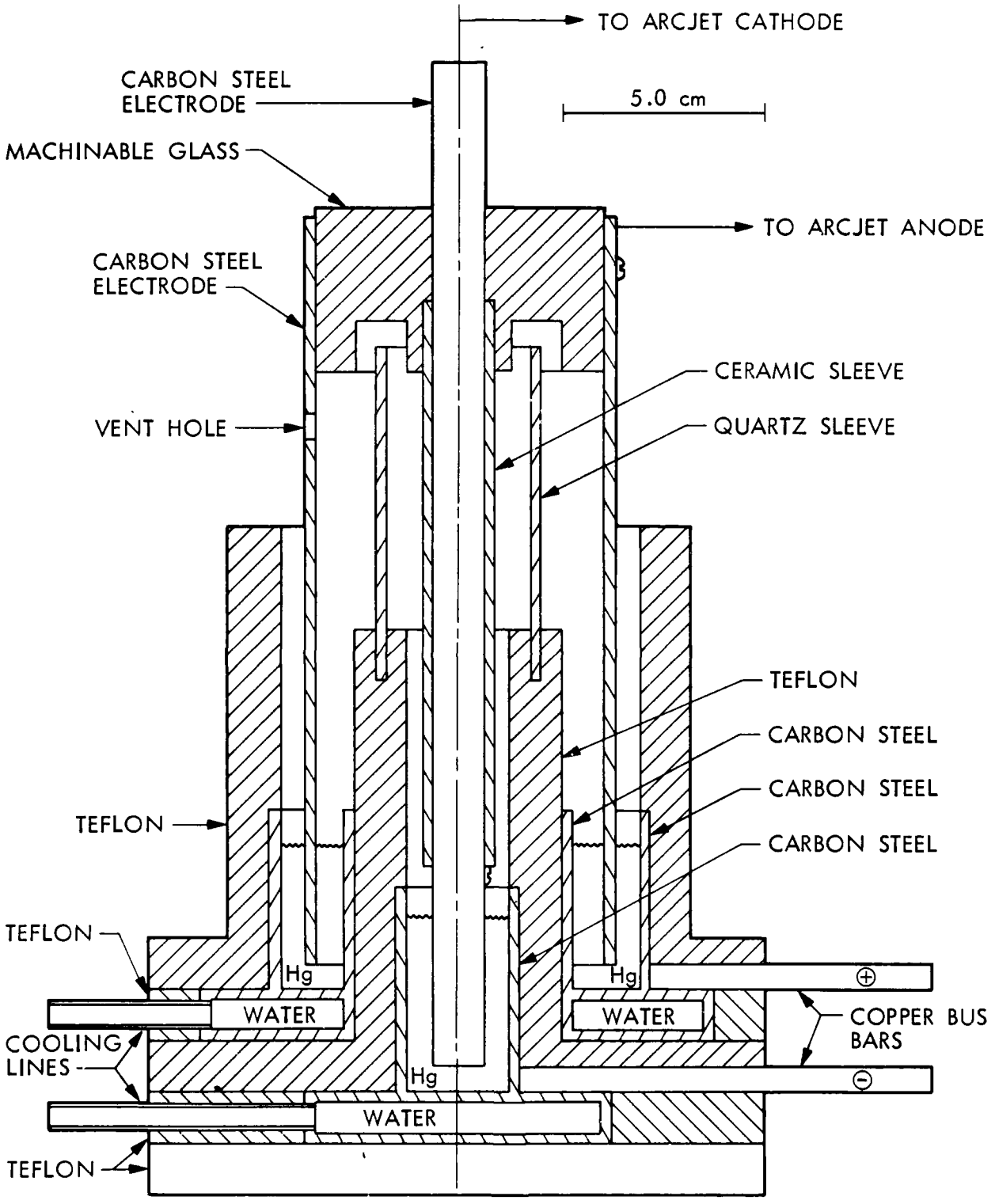

Figure B1. Schematic of Coaxial Current Feed System

SECTION 13

APPENDIX C

DATA ACQUISITION AND CONTROL SYSTEM

Introduction

A computer and data acquisition and control unit were used to record, monitor and shut down, if necessary, the arcjet life test facility. The computer was given veto control to simplify the implementation of an automatic monitoring system. The facility and arcjet engine were started manually.

Hardware

A slow-speed (30 sample/s, maximum), Hewlett-Packard 3421A data acquisition and control unit was connected to a Hewlett-Packard 9836 computer for purposes of measuring, storing, analyzing, and shut down control of the Arcjet Life Test facility. A total of 15 signals were measured and recorded in a period of 7 seconds. These signals were:

1. Arc Current
2. Arc Voltage
3. NH_3 Flow Rate
4. Propellant Pressure to Engine
5. Nozzle Temperature (Raytec Pyrometer)
6. Vacuum Tank Pressure
7. Thrust Stand Transducer Output Voltage
8. Thrust Stand Transducer Supply Voltage
9. Thrust Stand Transducer Temperature
10. Thrust Stand Beam Temperature
11. Thrust Stand Mounting Flange Temperature
12. Cooling Water Supply Temperature
13. Diffuser Cooling Water Outlet Temperature
14. Room Temperature
15. Outdoor Temperature

AD-A190 962 PERFORMANCE AND LONG DURATION TEST OF A 30 KW THERMAL ARCJET ENGINE(U) JET PROPULSION LAB PASADENA CA T J PIVIROTTO ET AL. NOV 87 JPL-D-4643 AFAL-TR-87-010 2/2

UNCLASSIFIED F/G 21/3 NL

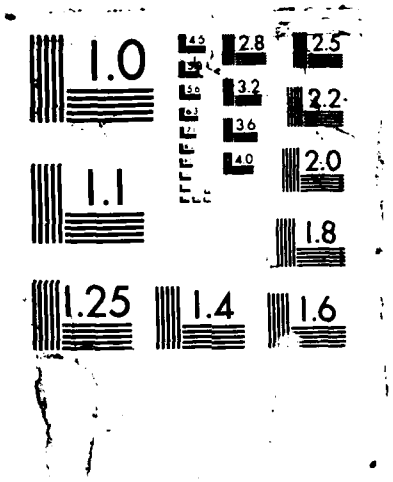
1.0
1.1
1.25
1.4
1.6
1.8
2.0
2.2
2.5
2.8
3.2
3.6
4.0

The arc voltage was sampled and checked continuously, while complete samples of the 15 measurements were taken every 15 seconds. This data was recorded once per minute on 5.25 inch diskettes.

The computer had authority to shut the system down if a critical parameter exceeded a preset tolerance. This was implemented through a relay output in the HP3421A, which cut power to the pumping plant, arc power supply, and solenoid valve in the propellant line.

Software

The program controlling the HP9836 had several functions. These were:

1. To sample the data listed above,
2. To compute thrust, power, specific impulse, and thrust efficiency,
3. To store the data once per minute,
4. To print the data once per minute,
5. To display the data on the CRT of the 9836 computer in alphanumeric and graphical form,
6. To display the data over a 300 baud modem and telephone line upon demand,
7. To permit manual changes to tolerance on current, voltage, nozzle temperature, water temperatures, propellant flow rate, and propellant and vacuum tank pressure, and
8. To shut the system down if a tolerance was exceeded.

Each of these processes was implemented in a rigorous way, such that if, for instance, a diskette became full, or the printer failed or ran out of paper, the program would continue to monitor the experiment, and be capable of shutting the system down if need be.

Since the system operated automatically and unattended for extended periods of time, a device that was appropriately described as a computer heartbeat was implemented to provide a fail-safe facility condition in the event that the computer itself failed. The rationale was that the computer was acting as the judge of whether the arcjet and facility were

functioning properly. A computer failure meant that there was no way to tell if the experiment was running properly. Thus, periodically the computer toggled a relay output. If the toggling, or heartbeat, stopped, a time delay relay would shut the system down in a safe manner. The computer operated flawlessly over the entire test period.

END

DATE

FILMED

5-88

DTIC